SAINT-PETERSBURG UNIVERSITY

Printed as a manuscript

Miroshnichenko Anna Sergeevna

RESEARCH AND DEVELOPMENT OF FUNCTIONAL SILICONE MATERIALS FOR FLEXIBLE INORGANIC LED DEVICES

Scientific speciality

1.4.7. High molecular weight compounds

A thesis submitted for the degree of candidate of chemical sciences

Translation from Russian

Academic supervisors:

Assoc.Prof, Dr. of Science in Chem., Regina M. Islamova

Assoc.Prof, Dr. of Science in Phys. and Math., Ivan S. Mukhin

Saint Petersburg — 2024

TABLE OF CONTENTS

INTRODUCTION AND GENERAL PROBLEM STATEMENT

Relevance of research. The development of flexible, mechanically stable and energy efficient light emitting diodes is one of the key milestones for the further flexible displays, RGB screens and wearable optoelectronics development. Currently, the manufacture of such devices is based mostly on OLED (Organic Light Emitting Diode) and AMOLED (Active-Matrix Organic Light Emitting Diode) technology. These devices have a complex architecture and characterized by a possible loss of brightness during long-term operation due to the degradation of pixels with blue electroluminescence. A possible alternative solution is LEDs based on inorganic lead halide perovskites $CsPbX_3$ (where X – Cl^-, Br^- or I^-). However, for these optoelectronic systems, the problems of perovskite stability under atmospheric conditions have not been completely solved. Another class of inorganic materials promising for flexible RGB screens fabrication, which devoid of the problems of low stability are A3B5 semiconductor compounds nanowires (NWs). NWs are structures with a high aspect ratio of length to diameter, with a diameter in the range of 100–200 nm, which ensures their mechanical strength and flexibility. Light emitting diodes based on A3B5 NW arrays are stable over time and do not require multilayer architecture compared to organic and perovskite LEDs. Fully flexible LEDs can be obtained by encapsulating an array of NWs in a polymer matrix, followed by exfoliation from a rigid growth substrate and application of flexible transparent electrical contacts. The material of the polymer matrix must: *i)* ensure complete transfer of the NW array from the growth substrate, which determines the uniformity and performance of the LED; *ii)* be mechanically strong and resistant to deformation when the membrane is separated from the growth substrate by mechanical shearing; *iii)* be optically transparent for efficient light extraction from the NW membrane.

It is also assumed that the combination of A3B5 semiconductor NWs with a given type of conductivity and light-emitting $CsPbX_3$ perovskites will make it possible to fabricate efficient and relatively easy-to-manufacture flexible LEDs.

Strong and transparent polymeric materials widely used in inorganic optoelectronic devices, such as polymethyl methacrylate, polystyrene, polyethylene oxide, and some others, have relatively low mechanical flexibility and can only be used to create fully flexible optoelectronic devices to a limited extent. Highly elastic (flexible), hydrophobic, bioinert, and transparent polysiloxanes are promising for use in flexible optoelectronics.

The commercially available silicone composition Sylgard 184 (Dow Corning) is widely used in flexible optoelectronics based on A3B5 NW arrays. However, the high adhesion of Sylgard 184 to the growth silicon (Si) substrate (most commonly used in the synthesis of NWs) hinders the efficiency of NWs transfer and can lead to inhomogeneity of the final optoelectronic structure and deterioration of its electrical characteristics. High adhesion is also a major obstacle to the manufacture of flexible LEDs

based on A3B5 NWs arrays /polymer matrices with a large area (3 inch sqr. or more). The solution to this problem is the development of transparent silicone materials with reduced adhesion to the silicon substrate by modification polysiloxane main chain with the appropriate functional groups.

In addition, one common approach for fully flexible RGB displays development is the use of flexible phosphors (photoluminophores). Currently, in flexible optoelectronics, as a rule, inorganic photoluminophores are used, which are integrated as fillers into the Sylgard 184 silicone matrix. However, this approach has a number of disadvantages: the fragility of the photoluminophor and low resistance to environmental influences (humidity, air oxygen, temperature) during operation. A promising alternative is flexible polymer-metal complexes (PMCs) basedon coordination compounds of lanthanides, which have a high photoluminescence quantum yield and narrow of spectral lines. The preparation of lanthanide-containing complexes of polysiloxanes (in which the polymer chains are coordinated by a metal atom) can not only achieve a high quantum yield of photoluminescence, but also impart flexibility, elasticity, and stability to the photoluminophor during long-term operation. The unique self-healing property of such modified polysiloxanes, that is, the ability to restore its structure and original characteristics after mechanical damage, will extend the service life of a flexible RGB device.

In this regard, this work was carried out in two directions:

The first direction involves the preparation of silicone materials with reduced adhesion to the growth silicon (Si) substrate by modifying polysiloxanes with introduction of functional groups (phenylethyl or 2-methyl-3-methoxy-3-oxopropyl substituents) into the main polymer chain via catalytic hydrosilylation. These functionalized silicone materials can be used as a support matrix for a flexible light emitting diode based on A3B5 NW arrays fabrication.

The second direction includes the preparation of PMCs based on 2,2'-bipyridine-6,6'-dicarboxamide-*co*-polydimethylsiloxane and lanthanides (Tb(III), Eu(III)), which have green and red photoluminescence, respectively and their employement as photoluminophores for inorganic LEDs based on NWs. According to the literature data [1], bipyridinedicarboxyamide seems to be one of the effective sensitizing ligands. In addition, the *O,N,N,O*-chelating fragments in the ligand structure provide the formation of coordinatively saturated lanthanide complexes, which makes it possible to obtain self-healing luminescent silicone materials with improved mechanical properties compared to described in the literature PMCs based on monopyridine-containing copolysiloxanes [2].

The applicability of the developed silicone materials was demonstrated in the creation of flexible LEDs based on arrays of NWs from A3B5 semiconductor compounds, as well as perovskites.

Purpose of the work: development of methods for obtaining transparent, relatively strong silicone materials with low adhesion to the Si substrate and their application as a flexible supporting

matrix for NW arrays; as well as the preparation of luminescent polymer metal complexes based on bipyridinedicarboxamide-*co*-polydimethylsiloxanes and Eu^{3+} or Tb^{3+}, which have self-healing properties, and their use as a photoluminescent layer in flexible LEDs based on NW arrays.

To achieve the goal, the following **tasks** were set:

1. Synthesis of phenylethyl-functionalized silicone rubbers (SSR) and 2-methyl-3-methoxy-3-oxopropyl-functionalized silicone rubbers (MSR)[1] by catalytic hydrosilylation reaction between polymethylhydrosiloxane and styrene or methyl methacrylate, respectively, and subsequent cross-linking with *α,ω*-di(trivinylsiloxy)polydimethylsiloxane. The content of phenylethyl and 2-methyl-3-methoxy-3-oxopropyl substituents in the resulting silicone rubbers was varied to control the adhesive properties.
2. Study of mechanical properties under uniaxial tension (tensile strength, elongation at break), degree of cross-linking, transparency, adhesion to Si obtained SSR and MSR. Comparison of mechanical and adhesive characteristics of obtained functionalized silicone rubbers depending on the type of substituent.
3. Development of a technique for encapsulating vertically oriented arrays of n-doped gallium phosphide (n-GaP) NWs on a Si substrate into a silicone matrix. Preparation of membranes based on SSR and MSR. Approbation of the obtained membranes based on SSR/NWs as part of a flexible hybrid light-emitting diode SSR25/n-GaP NWs/$CsPbBr_3$/SWCNT with transparent electrical contacts from layers of single-walled carbon nanotubes (SWCNTs). Investigation of electrophysical (current-voltage characteristics) and spectral (external quantum efficiency and electroluminescence spectrum) characteristics of the LED.
4. Synthesis of PMCs based on 2,2'-bipyridine-6,6'-dicarboxamide-*co*-polydimethylsiloxanes and Eu^{3+} (Eu–Bipy–PDMS) and Tb^{3+} (Tb–Bipy–PDMS) by polycondensation and complexation reactions. Selection of optimal conditions for the preparation of PMC: variation of the number-average molecular weight of the polymer ligand (M_n = 5000 and 25000) and temperature of the cross-linking process (25 and 100 °C), as well as the content of lanthanide (0.4–3.9 wt.%).
5. Study of self-healing properties (determination of self-healing efficiency) and mechanical characteristics in uniaxial tension (tensile strength, elongation at break) of Eu–Bipy–PDMS

[1]Analogously to styrene-butadiene rubbers [3] for convenience, the resulting materials are called “styrene-containing silicone rubbers” (SSR) and “methyl methacrylate-containing silicone rubbers”.

and Tb–Bipy–PDMS.

6. Study of the photoluminescent properties of the PMCs (study of the excitation and emission spectra, as well as the dependence of the quantum yield on the molecular weight of the polymer ligand). Analysis of the possibility of obtaining controlled luminescence spectra by stacking films based on various lanthanides. Approbation of the resulting luminescent films as part of flexible LEDs based on NW arrays.

Scientific novelty. Silicone rubbers with 25 and 50 mol.% content of phenylethyl or 2-methyl-3-methoxy-3-oxopropyl groups - SSR25, SSR50 and MSR25, respectively, with reduced adhesion to the Si substrate, have been synthesized. Functionalized silicone rubbers demonstrate relatively high tensile strength (σ) up to 1.5 MPa (SSR25) and relative elongation at break (ε) up to 130% (SSR50), have approximately 2 times reduced adhesion to the silicon substrate and higher Young's modulus (E = 3.4 MPa for SSR25) compared to with Sylgard 184, which allows to separate thin membranes based on them (3–4 μm thick) with encapsulated NWs without damage. For the first time, a flexible air-stable perovskite light-emitting diode (PLED) with the SSR25/n-GaP NWs/$CsPbBr_3$/SWCNT architecture was presented, demonstrating electroluminescence in the green region of the spectrum (538 nm) at an operating voltage of 5 V. The PLED continues to operate after 30 bending/relaxation cycles.

Luminescent polysiloxanes Eu–Bipy–PDMS and Tb–Bipy–PDMS, in which Tb^{3+} and Eu^{3+} act as the central atom, and 2,2'-bipyridine-6,6'-dicarboxamide-*co*-polydimethylsiloxanes (M_n = 5000 and 25000). It has been established that Eu–Bipy–PDMS and Tb–Bipy–PDMS have the property of non-autonomous self-healing at a temperature of 100°C (in the case of Eu–Bipy–PDMS with a molecular weight of the polysiloxane chain M_n = 25000, the efficiency of self-healing is 90%).

It has been shown that PMCs with a lower molecular weight of the polyloxane chain (M_n = 5000) and a higher content of lanthanide(III) (3.9 wt%) exhibit higher photoluminescence quantum yields compared to PMCs with M_n = 25000: 18.5% and 11.0% in the case of Tb–Bipy–PDMS, as well as 10.5% and 7.0% in the case of Eu–Bipy–PDMS, respectively. The relative narrow spectral lines in PMCs emission spectra allow to adjust the photoluminescence color from green to red through intermediate yellow and orange by superimposing thin films of the PMC of various compositions on top of each other.

The importance of this research and its application. Due to their high optical transparency, sufficient mechanical strength, and reduced adhesion to a growth silicon substrate, the obtained SSR25 can be used as a flexible supporting matrix for NW arrays in the creation of fully flexible, inorganic, light-emitting devices of various architectures. The SSR25/n-GaP NWs/$CsPbBr_3$/SWCNT architecture proposed in this work will make it possible to obtain fully flexible LEDs with green electroluminescence.

Luminescent Eu–Bipy–PDMS and Tb–Bipy–PDMS, which have relatively high photoluminescence quantum yields and non-autonomous self-healing properties, were used as

photoluminescent coatings for flexible ultraviolet (UV) LEDs based on GaN/AlGaN NW arrays. The obtained PMCs can also be used as self-healing protective coatings for the screens of smartphones, tablets, laptops and smart watches.

Research methods and methodology. To confirm the structure of the obtained polymer products, to study the processes of cross-linking of copolysiloxanes and the properties of the obtained silicone rubbers, the following modern research methods were used: liquid and solid-state nuclear magnetic resonance (NMR) spectroscopy (confirmation of the structure of the obtained copolysiloxanes, study of the mechanism of cross-linking of silicone rubbers); infrared spectroscopy (IR) with Fourier transform (confirmation of the structure of the obtained copolysiloxanes and the establishment of coordination cross-links in silicone rubbers); ultraviolet (UV) and visible spectroscopy (confirmation of the transparency of the obtained silicone rubbers); energy dispersive X-ray spectroscopy (determination of the content of lanthanides in PMC); mass spectrometry and X-ray diffraction analysis (analysis of model complexes); photoluminescence spectroscopy (study of the excitation and emission spectra of PMCs and low molecular weight model complexes), measurement of the photoluminescence quantum yield, voltammetry (study of the current-voltage characteristics (I-V curves) of a flexible LED), electroluminescence spectroscopy (study of the electroluminescence of a flexible LED); thermogravimetry (study of the thermal properties of PMC); mechanical tests on a tensile machine (study of the mechanical properties of silicone materials); swelling experiments (determination of the degree of cross-linking and segment mass between silicone rubber cross-links), atomic force microscopy (study of silicone rubber adhesion by analyzing the approach/retraction curves of a silicon AFM probe), scanning electron microscopy (study of the morphology of silicone rubber, study of the architecture of a flexible LED).

The structure and volume of the thesis. The work consists of an introduction, literature review, obtained results description and their discussion, experimental part, conclusion, acknowledgments, a list of abbreviations and symbols, a list of references, including 129 references to the literature. The materials are presented on 108 pages of typewritten text and contain 6 tables and 54 figures.

Approbation and publications. The results of the work were presented in the form of 3 oral and 1 poster presentations at international and all-Russian conferences: International workshop and school nanostructures for photonics 2021 (St. Petersburg, 2021), XI Congress of Young Scientists (St. Petersburg, 2022), 9th International school and conference on optoelectronics, photonics, engineering and nanostructures (St. Petersburg, 2022), XVIII International Scientific and Practical Conference "New Polymer Composite Materials" (Elbrus, 2022).

This work was supported by the Russian Science Foundation grant 20-19-00256 “Functional (*co*)polysiloxanes for flexible optoelectronic devices based on A3B5 semiconductor whisker nanocrystals” (2020–2022) and project of St. Petersburg State University No. 94124215 (2022–2023).

The main content of the work is presented in four **publications** indexed in the WoS and Scopus databases, of which three are in Q1 journals:

1. Miroshnichenko A.S. Flexible Perovskite $CsPbBr_3$ Light Emitting Devices Integrated with GaP Nanowire Arrays in Highly Transparent and Durable Functionalized Silicones / Miroshnichenko A.S., Deriabin K.V., Baeva M., Kochetkov F.M., Neplokh V., Fedorov V.V., Mozharov A.M., Koval’ O., Krasnikov D.V., Sharov V.A., Filatov N.A., Gets D.S., Nasibulin A.G., Makarov S.V., Mukhin I.S., Kukushkin V.Y., Islamova R.M. // ACS Journal of Physical Chemistry Letters — 2021. V. 12 – №39. – P. 9672–9676. DOI: 10.1021/acs.jpclett.1c02611.
2. Miroshnichenko A.S. Lanthanide(III)-Incorporating Polysiloxanes as Materials for Light-Emitting Devices. / Miroshnichenko A.S., Deriabin K.V., Baranov A.I., Neplokh V., Mitin D.M., Kolesnikov I.E., Mikhail D.V., Parshina E.K., Mukhin I.S., Islamova R.M. // ACS Applied Polymer Materials — 2022. V. 4. – №4. – P. 2683–2690. DOI: 10.1021/acsapm.2c00017.
3. Miroshnichenko A.S. Structural Features of Eu^{3+} and Tb^{3+}-Bipyridinedicarboxamide Complexes. / Miroshnichenko A.S., Deriabin K.V., Rashevskii A.A., Suslonov V.V., Novikov A.S., Mukhin I.S., Islamova R.M. // MDPI Polymers — 2022. V. 14. – №24. – P. 5540. DOI: 10.3390/polym14245540.
4. Miroshnichenko A.S. Low-Adhesive Silicone Rubbers For Flexible Light-Emitting Devices. // Miroshnichenko A.S., Deriabin K.V., Mukhin I.S., Islamova R.M. // St. Petersburg Polytechnical University Journal: Physics and Mathematics — 2022. – V. 15. – №3. – P. 320–325. DOI: 10.18721/JPM.153.363.

The author's personal contribution consisted in the collection and analysis of bibliographic data; participation in setting goals; direct experimental work: obtaining all the studied silicone rubbers and low molecular weight model complexes, optimizing the conditions for cross-linking reactions, studying the mechanical characteristics and self-healing properties of silicone rubbers, studying adhesive properties, studying photoluminescent properties, setting up swelling experiments; setting research objectives for resource centers of St Petersburg University; sample preparation for nuclear magnetic resonance spectroscopy, Fourier transform infrared spectroscopy, UV and visible spectroscopy, energy dispersive X-ray spectroscopy, luminescence spectroscopy and luminescence quantum yield measurements, thermogravimetry and differential

scanning calorimetry; data processing and interpretation; preparation of materials for publication; participation in writing articles; preparation of reports at scientific conferences on the topic of work.

Main scientific results:

1) Miroshnichenko A.S., Deriabin K.V., Baeva M., Kochetkov F.M., Neplokh V., Fedorov V.V., Mozharov A.M., Koval' O., Krasnikov D.V., Sharov V.A., Filatov N.A., Gets D.S., Nasibulin A.G., Makarov S.V., Mukhin I.S., Kukushkin V.Y., Islamova R.M. Flexible Perovskite CsPbBr3 Light Emitting Devices Integrated with GaP Nanowire Arrays in Highly Transparent and Durable Functionalized Silicones // ACS Journal of Physical Chemistry Letters — 2021. V. 12 – №39. – P. 9672–9676. DOI: 10.1021/acs.jpclett.1c02611.

A new transparent styrene-containing silicone rubbers (SSR), which have reduced adhesion to the growth silicon substrate, were obtained using catalytic hydrosilylation and dehydrocoupling reactions. The resulting silicone rubbers were employed as an encapsulating support matrix for arrays of vertically aligned GaP nanowiers (NWs). SSR25/GaP NW membranes were used as a flexible adderssed electrode to a light-emitting lead halide perovskite layer as part of a flexible light-emitting diode operating in the green spectral region at an opening voltage of 5 V.

The candidate collected and analyzed literature data; optimized the methodology for obtaining silicone rubbers and vulcanization conditions, studied the structure of cross-links and investigated the mechanical characteristics of silicone rubbers. The candidate optimized the technique of encapsulating NW arrays into a matrix of the resulting silicone rubbers. The candidate optimized a technique for depositing a layer of light-emitting perovskite on the surface of a silicone rubber membrane with NWs, analyzed and interpreted the results of a study of the electrophysical properties of a flexible light-emitting diode, as well as the morphological and adhesive properties of synthesized silicone rubbers. The candidate carried out sample preparation for spectroscopic studies (liquid and solid-state NMR, UV-vis), adhesion (analysis of AFM approach/retraction curves), morphological (SEM). The applicant interpreted the data obtained and prepared the text of the publication.

2) Miroshnichenko A.S., Deriabin K.V., Baranov A.I., Neplokh V., Mitin D.M., Kolesnikov I.E., Mikhail D.V., Parshina E.K., Mukhin I.S., Islamova R.M. Lanthanide(III)-incorporating polysiloxanes as materials for light-emitting devices. // ACS Applied Polymer Materials — 2022. V. 4. – №4. – P. 2683–2690. DOI: 10.1021/acsapm.2c00017.

New luminescent self-healing metal-polymer complexes were obtained by a complexation reaction, in which Tb^{3+} and Eu^{3+} act as the central atom, and 2,2-bipipridine-6,6'-dicarboxyamide-*co*-

polydimethylsiloxanes, obtained by the polycondensation reaction, act as polymer ligands. The possibility of regulating photoluminescence color by applying thin films (100 μm thick) containing different types of lanthanides has been demonstrated. The candidate collected and analyzed literature data; optimized the methodology for producing silicone rubber and vulcanization conditions, studied the structure of coordination cross-links, studied the luminescent, mechanical characteristics and self-healing properties of silicone rubber. The candidate has optimized a method for regulating the photoluminescence color of metal-polymer complexes and obtaining silicone materials with different photoluminescence colors - green, red and intermediate yellow and orange. The candidate carried out sample preparation for spectroscopic studies (NMR, IR and UV), thermogravimetry, studies of photoluminescence spectra and quantum yields. The applicant interpreted the data obtained and prepared the text of the publication.

3) Miroshnichenko A.S., Deriabin K.V., Rashevskii A.A., Suslonov V.V., Novikov A.S., Mukhin I.S., Islamova R.M. Structural features of Eu^{3+} and Tb^{3+}-bipyridinedicarboxamide complexes. // MDPI Polymers — 2022. V. 14. – №24. – P. 5540. DOI: 10.3390/polym14245540.

New low molecular weight coordination compounds in which the lanthanide ions Tb^{3+} and Eu^{3+} act as the central atom, and *N*⁶,*N*⁶–diisopropyl–2,2'-bipyridine–6,6'–dicarboxamide as the ligand were obtained. The structure of the synthesized *N*⁶,*N*⁶–diisopropyl–2,2'-bipyridine–6,6'–dicarboxamide dicarboxamide was confirmed by liquid NMR spectroscopy. The structure of the coordination center was studied by X-ray diffraction, IR, and HRESIMS methods. Lifetimes, quantum yields, and photoluminescence spectra were studied. The applicant carried out the synthesis of *N*⁶,*N*⁶–diisopropyl–2,2'-bipyridine–6,6'–dicarboxamide and its coordination compounds with Tb^{3+} and Eu^{3+}. The applicant carried out sample preparation for IR spectroscopy, XRD, HRESIMS and photoluminescent properties. The applicant interpreted the data obtained and prepared the text of the publication.

4) Miroshnichenko A.S. Low-adhesive silicone rubbers for flexible light-emitting devices. / Miroshnichenko A.S., Deriabin K.V., Mukhin I.S., Islamova R.M. // St. Petersburg Polytechnical University Journal: Physics and Mathematics — 2022. – V. 15. – №3. – P. 320–325. DOI: 10.18721/JPM.153.363.

The candidate has obtained new transparent methyl methacrylate-containing silicone rubbers (MSRs) with reduced adhesion to the growth silicon substrate. The candidate examined the structure of crosslinks and investigated the mechanical, adhesive and optical characteristics of silicone rubbers and conducted a comparative analysis with silicone rubbers presented in the literature. The candidate interpreted the data obtained and prepared the text of the publication.

Thesis outline:

1. The substitution of Si–H groups for phenylethyl or 2-methyl-3-methoxy-3-oxopropyl groups in SSR25 and MSR25, respectively, promotes a decrease in adhesion to the growth silicon substrate. The use of SSR25 as a flexible supporting matrix ensures the transfer of vertically oriented arrays of n-GaP semiconductor NWs into a silicone membrane and allows the formation of n-GaP NWs/ SSR25 membranes with a thickness of 4 μm.

2. n-GaP NW/SSR25 membranes serve as a flexible addressable electrode in a flexible green hybrid LED of the SSR25/n-GaP NW/$CsPbBr_3$/SWCNT composition with transparent SWCNT electrical contacts. The operating voltage of the LED is 5 V, and the electroluminescence peak at 538 nm corresponds to the $CsPbBr_3$ optical transition.

3. Synthesized Eu–Bipy–PDMS and Tb–Bipy–PDMS based on the polymeric ligand 2,2'-bipyridine-6,6'-dicarboxamide-*co*-polydimethylsiloxane and Eu(III) and Tb(III) chlorides, respectively, with non-autonomous self-healing properties (i.e., self-healing when heated) and characterized by improved mechanical characteristics (tensile strength σ up to 1.5 MPa) compared to PMCs based on monopyridyl ligands.

4. Eu–Bipy–PDMS and Tb–Bipy–PDMS have green and red photoluminescence, respectively. The selection of the optimal molecular weight (M_n = 5000) and lanthanide content (~3 wt %) makes it possible to increase the photoluminescence quantum yields, which are 10.5% and 18.5% for Eu–Bipy–PDMS and Tb–Bipy–PDMS, respectively.

5. Photoluminescence color tuning of the PMCs from green to red, through intermediate yellow and orange colors, is carried out by simply superimposing Eu–Bipy–PDMS and Tb–Bipy–PDMS films on each other. "Monolithic" silicone materials with desired photoluminescence colors due to the self-healing properties of Eu-Bipy-PDMS and Tb-Bipy-PDMS have been obtained. A flexible UV LED based on (GaN/AlGaN NWs)/Sylgard 184 with an emission wavelength of 340 nm provides excitation of photoluminescence of the PMC.

CHAPTER 1. LITERATURE REVIEW

INTRODUCTION

Polysiloxanes are polymers containing alternating silicon and oxygen atoms in the main chain, with side organic substituents R $(–R'R''SiO–)_n$, attached to each silicon atom, where R can be, for example, alkyl, aryl, vinyl, hydride and other groups [4,5].

Polysiloxanes and materials based on them (silicone materials) have a number of important properties, namely high thermal (decomposition start temperature 250°C frost- (glass transition temperature –123°C, crystallization temperature – 80°C [6]), weather, ozone and chemical resistance, and have found their application as sealants, insulators, protective coatings, etc. Due to their bioinertness, polysiloxanes are also used in the food industry (kitchen utensils), medicine (implants) and "lab on a chip" diagnostic devices [7,8]. In addition, polysiloxanes are of particular interest for optoelectronics. This is primarily due to their high flexibility, good film-forming properties and optical transparency.

The review paper of 2016 [9] describes in detail the possibilities of using polysiloxanes in liquid crystal devices [10], computer memory drives [11], OLED [12] and organic photovoltaic devices [13], including solar cells [14–16]. Also, polysiloxanes can be used in inkjet printing of flexible transistors and batteries [17].

However, the use of polysiloxanes in optoelectronics is not limited to the above mentioned applications. Due to the relative ease of preparation of (nano)composites based on polysiloxanes and various fillers, as well as the possibility of synthesizing copolymers with a wide range of functional side groups of the base chain and/or terminal functional groups, it is possible to obtain silicone materials with improved adhesion, semiconductor, photoluminescent, etc. properties [2,4,5,18].

Composites based on silicone materials with various electrically conductive fillers such as carbon nanotubes (CNTs), graphene, silver and copper nanowires are used as flexible electrodes and "skin electronics" [19–27]. Composites based on silicone materials with luminescent fillers are used as a light-emitting layer in flexible electroluminescent devices [28,29] and OLED.

Silicone materials can be used as protective layers to prevent degradation and destruction of metal halide perovskites upon contact with the environment conditions, which is extremely important in the case of perovskite light-emitting diodes (PLED) [30]. Due to their good film-forming properties and elasticity, silicone materials are used as membranes for encapsulating NWs arrays of A3B5 or Si semiconductor compounds. The deposition of flexible transparent SWCNT electrodes on such NWs- silicone membranes makes it possible to obtain flexible and extensible light-emitting devices with a relatively simple architecture. [31–35].

Thus, polysiloxanes and materials based on them are becoming gain attention in the field of flexible optoelectronics. In this regard, the purpose of literature review is to analyze the currently existing types of silicone materials and their key properties that are in demand in the creation of various flexible optoelectronic devices manufacture [36].

1.1 Silicone materials for optoelectronics

1.1.1 Transparency, morphology and adhesive properties of silicone materials

A typical representative of polysiloxanes is polydimethylsiloxane (PDMS). PDMS has a low refractive index of 1.41 (at a wavelength of $\lambda = 589$ nm) and is optically transparent in the UV-visible and near-IR spectral ranges. PDMS also has good film-forming properties and homogeneous morphology [37].

Optoelectronic devices mainly use the commercially available silicone composition Sylgard 184 from Dow Corning (USA) [37], which can form transparent silicone rubbers (cross-linked polysiloxanes) at room temperature and heating (60–100°C) [37].

Sylgard 184 is widely used in flexible optoelectronics, in particular, in LED devices based on A3B5 NWs arrays as a flexible supporting matrix due to its optical, mechanical and film-forming properties. A schematic diagram of such devices and a simplified manufacturing scheme are shown in **Figure 1**. A PDMS matrix encapsulates an array of NWs with a p-i-n structure (axial or radial), while opticaly transparent ohmic contacts to NW emitters of both types are deposited on the membrane surface. The separation of the polymeric membrane with NWs from the growth substrate can be organized both by selective etching of the substrate and by peeling-off with a razor blade.

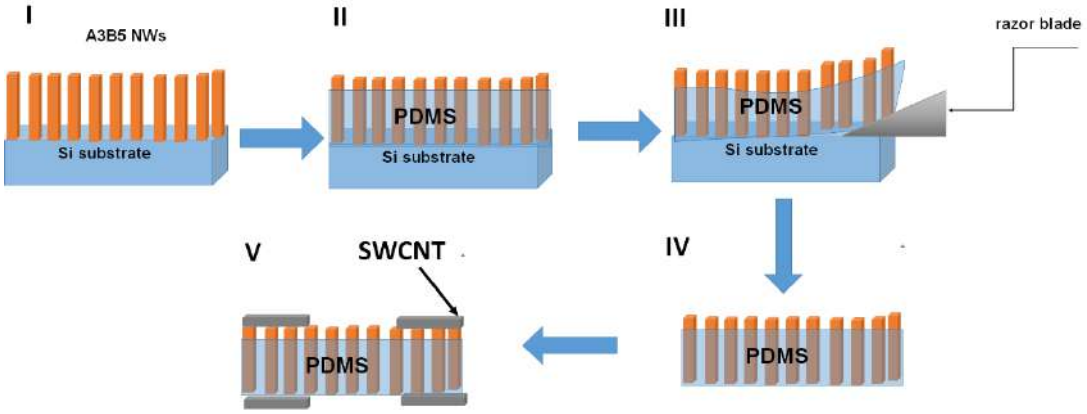

Figure 1 – Simplified fabrication scheme (I – IV) and schematic diagram (V) of LEDs based on NW arrays

However, a significant disadvantage of this silicone material (Sylgard 184) is high adhesion to the growth Si substrate (used for the synthesis of NW arrays) [31], which challeges the separation of NW arrays and can lead to damage to the integrity and deformation of the final optoelectronic device. This problem can be solved by using PDMS copolymers (modified analogues). As a rule, such copolymers have the flexibility typical of PDMS, for example, block copolymers PDMS-polyurethane [38], PDMS-polyester [39], but other characteristics are improved (decrease in adhesion, increase in strength, etc.). Thus, in 2020, the authors managed to reduce the adhesion to the growth Si substrate due to the grafting of polystyrene side chains to the main chain of PDMS [35]. The silicone composition based on the PDMS-*graft*-polystyrene obtained in the work (styrene loading was 40% wt.) showed adhesion values to the growth Si substrate of 0.66 from the value of Sylgard 184. However, PDMS-*graft*-polystyrene does not have optical transparency due to the formation of spherical supramolecular formations of side chains [40], which significantly limits its possible application in optoelectronic devices.

The homogeneity of PDMS copolymers morphology can also be disturbed due to the formation of so-called "blends" of one copolymer in another due to their differences in the structure of the main chain and molecular weights. The latter case is typical for PDMS-*block*-PMMA copolymers, the heterogeneity of the morphology of "blends " for which increases with an increase in the initial loading of PMMA [41] (**Figure 2**).

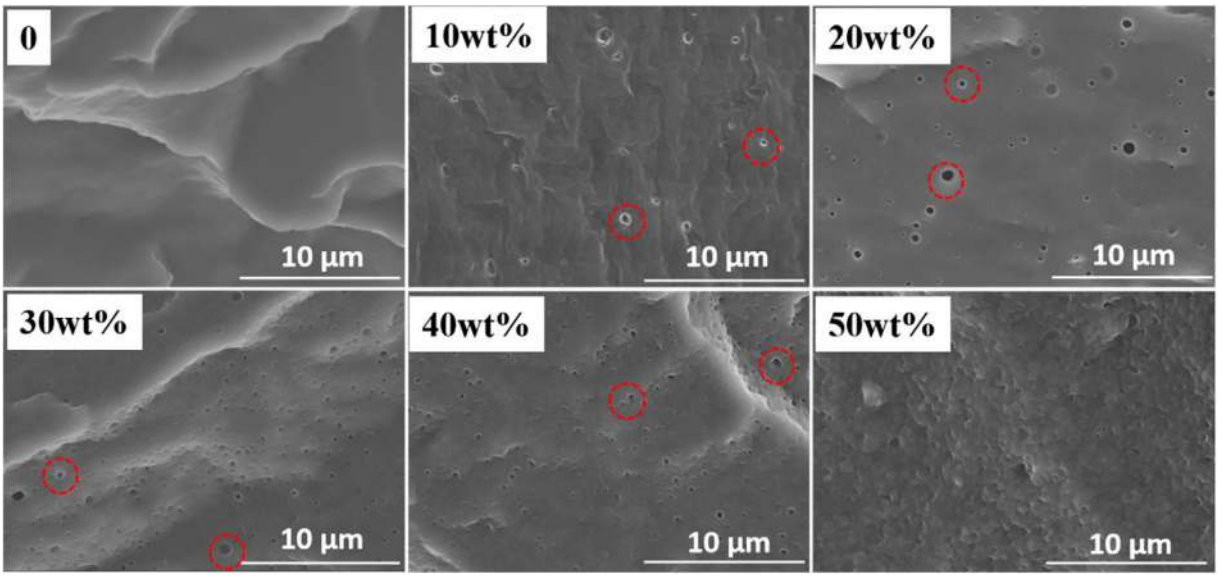

Figure 2 – Morphology images of PDMS-block-PMMA at different PMMA loading (wt% - mass percent) obtained by scanning electron microscopy (SEM) [41]

Nevertheless, for use in optoelectronic devices, it is desirable that the polymer material be optically transparent. In this regard, in 2012, a method was proposed for obtaining transparent copolymers based on PDMS and PMMA [42]. To obtain these materials, the authors synthesized PDMS

macromonomers functionalized with 2-(methacryloxy)ethyl isocyanate (MOI), SigUMAx, to which PMMA side chains were subsequently grafted. The transparency of the material was regulated by variation the molar ratio MOI (x) in SigUMAx. Despite the improved optical properties, PDMS-PMMA block copolymers have not yet become widely used in the field of optoelectronics, since their synthesis involves a relatively complex multi-stage process [41,42].

Modified polysiloxanes functionalized with imidazolium iodide [14] and cyclic sulfonium iodide [16] can be used to improve the optical transparency and thermal stability of electrolytes for dye-sensitized solar cells (DSSC). The use of poly[(3-N-methylimidazolium-propyl)methylsiloxane-co-dimethylsiloxane]iodides [43] for highly efficient DSSC electrolytes is also described in the literature.

1.1.2 Mechanical characteristics and self-healing silicone materials

For flexible optoelectronic devices fabrication it is important that the polymer material, along with transparency, has a relatively high elasticity and mechanical strength [37].

Silicone materials and composites based on the commercially available silicone composition Sylgard 184 are characterized by high (for applications in optoelectronics) elongation at break ε = 100 %, tensile strength σ = 2.4 MPa and Young's modulus E = 1.1 MPa [44]. Other silicone materials based on modified polysiloxanes are also used in optoelectronics, the main mechanical characteristics of which are presented in **Table 1**.

Obtaining *graft*- and *block*-copolymers enables the improvement of mechanical properties of PDMS (**Table 1**). For example, PDMS-*graft*-polystyrene, which is slightly inferior to Sylgard 184 in terms of σ, has a large Young's modulus E = 1.9 MPa. An increase in mechanical strength allows to separate the polymer membrane from the growth substrate without the risk of mechanical damage (PDMS-*graft*-polystyrene was used to create flexible optoelectronic membranes with a large area of 3 square inches [45]). Another example is PDMS–*block*–PMMA copolymers, whose mechanical properties can be controlled by varying the PMMA content. The mechanical strength values of PDMS–*block*–PMMA can be almost twice as high as those for Sylgard 184 (**Table 1**) which allowes to use them for flexible LEDs based on gallium nitride GaN fabrication [46]. PDMS and polyester-*block*-polyurethane copolymers achieve high σ values for polysiloxanes at relatively high elasticity ε (**Table 1**). In 2022, the preparation of an electrically conductive EFSR silicone material synthesized by catalytic hydrosilylation between ferrocenyl- and vinyl-containing PDMS was described. EFSR posseses almost 1.5 times tensile strength and almost twice higher elasticity compared to Sylgard 184 (**Table 1**). The paper [39] reports on the preparation of polyester-block-PDMS copolymers with extremely high values of ε = (778–815)% compared to the above-mentioned block copolymers of PDMS and PMMA.

Table 1 – Mechanical properties of silicone materials used in optoelectronics

Silicone material	*σ, MPa*	*ε*, %	*E*, *MPa*	*References*
Sylgard 184	2.4	92	1.1	[44]
EFSR	3.5	170	1.4	[39]
PDMS-*graft*-polystyrene	1.5	90	1.9	[35]
PDMS–*block*–PMMA (*w*t = 56%)	4.7	61	–	[47]
PDMS–*block*–PMMA (*w*t = 6%)	1.3	158	–	[47]
PDMS, polyester–*block*–polyurethane	14.3	92	–	[48]
Polyester-*block*-PDMS	0.5	815		[39]
$Zn(CF_3SO_3)_2$–PDMS	0.6	310	1.1	[49]
Cu–PDMS	0.39	171	–	[50]
Ni–Py–PDMS25000	0.04	2100	–	[51]
Co–Py–PDMS25000	0.05	1800	–	[52]
Ln–Py–PDMS	0.45	450	1.9	[2]
PDMS–*block*–dithiothreitol	0.43	1500		[53]

A number of polysiloxanes also have self-healing properties– the ability to partially or completely restore their original characteristics after mechanical damage, for example, cracks and ruptures formed. [54]. The self-healing property opens up new possibilities for flexible self-healing protective coatings, screens, electrodes and solar cells manufacturing. Self-healing silicone materials can be synthesized, for example, using covalent interactions, including reversible Diels-Alder interactions, [55–60], ester [61], imine [62], and disulfide bonds [63,64], metal-ligand coordination [51,52,65], as well as non-covalent ones, hydrogen bonds, π–π stacking, etc. (**Figure 3**).

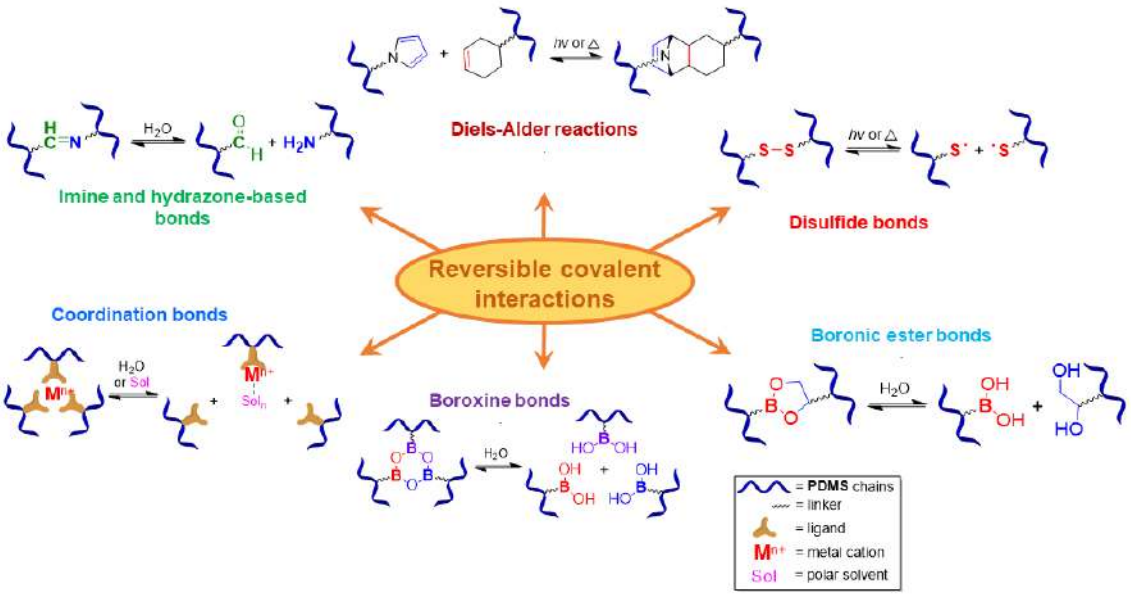

Figure 3 – Typical covalent internal self-healing mechanisms used in silicone materials [66]

In 2016 the preparation of a self-healing silicone material, which is an PMCs 2,2'-bipyridine-5,5'-dicarboxyamide-*co*-PDMS with Fe^{2+} and Zn^{2+} ions as a metal center and Cl^{-}, BF_4^{-}, ClO_4^{-}, $CF_3SO_3^{-}$ counterions was described. Zn-PDMS and Fe-PDMS are antistatic materials and, according to the authors [49], can be used in organic field-effect transistors (OFETs) as gate dielectrics and and as “skin electronics”. The self-healing efficiency of $Zn(CF_3SO_3)_2$-ПДМС reaches 76% at room temperature.

In 2017, Yu D. et al. [50] demonstrated a self-healing PMC with Cu^{2+} as a metal center (Cu-PDMS), achieving a self-healing efficiency of 87% at 30°C for 1 hour. Later, in 2021, self-healing PMCs based on pyridine-2,6-dicarboxamide-*co*-polydimethylsiloxanes (Py-PDMS) with Co^{2+} and Ni^{2+} metal centers [51,52], with self-healing efficiency at room temperature was from 92% (Ni-Py-PDMS25000) up to 96% (Co-Py-PDMS25000). The elongation at break for these silicone materials was 2100% and 1800%, respectively. The authors have shown that the mechanical characteristics and self-healing properties of Ni^{2+} and Co^{2+} based PMCs can be controlled by changing the ratio of metal and ligand, by varying the number average molecular weight of the polymer ligand (M_n: 850–900, 5000 or 25000 g/mol) and the amount of metal (0.09–2.41 wt.%, respectively).

Further development of self-healing materials based on Py–PDMS PMCs was demonstrated in 2021 [2]. The use of $Eu^{3+}$and Tb^{3+} as metal centers made it possible to achieve not only an elongation at break of 450% and a self-healing efficiency of 80% for 36 h at room temperature, but also impart photoluminescent properties to the material. Py–PDMS have relatively low tensile strength $\sigma = 0.45$ MPa, which hinders their application in flexible optoelectronic devices.

In 2022, Tang M. and colleagues obtained flexible self-healing silicone materials based on PDMS–*block*–dithiothreitol copolymers with satisfactory mechanical strength $\sigma = 0.43$ MPa and very

high elasticity $\varepsilon = 1500\%$ [53]. The self-healing efficiency of these materials reaches 100% at room temperature in as little as 30 seconds after damage, making this block copolymer one of the fastest self-healing elastomers available today. On the basis of this material, a flexible stretchable self-healing electrode was created and demonstrated, which opens up prospects for its application in flexible and stretchable light-emitting devices.

Thus, for the use of polymers in optoelectronics, their mechanical characteristics (high elasticity and sufficient mechanical strength) are important. Widely used in various optoelectronic devices, Sylgard 184 has relatively high ε and σ values, which can be improved by using, for example, PDMS-based copolymers. However, for optoelectronics, it is also important to have a set of properties, namely, improved tensile characteristics, but while maintaining the optical transparency of the material. In addition, self-healing silicone materials, which are able to restore their integrity and self-repair mechanical damage, open up special prospects for use as part of optoelectronic devices.

1.1.3 Luminescent silicone materials

Luminescent silicone materials are of great interest for optoelectronics as photoluminophores in the creation of flexible displays and devices. There are two fundamentally different ways to obtain luminescent silicone materials: *i)* the introduction of various phosphors as fillers into liquid silicone compositions (for example, Sylgard 184) (**Figure 3 a**) and, after curing, obtaining solid luminescent composites (cross-linked silicone rubber), *ii)* chemical modification of the polysiloxane chain and obtaining luminescent copolysiloxanes and/or materials based on them (**Figure 3 b, c**) [67].

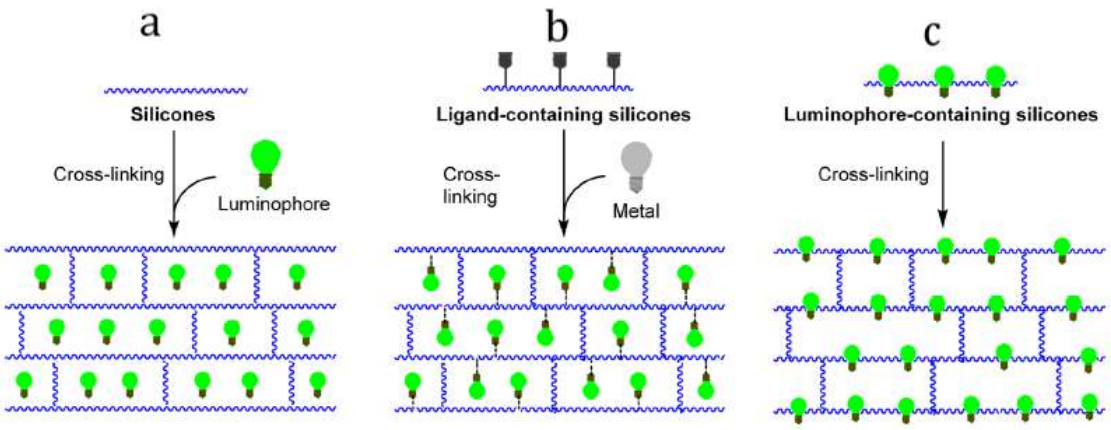

Figure 4 – General approaches to luminescent silicone rubbers: use of fillers **(a)**, metal binding **(b)**, and copolymers **(c)** [67]

The simplest way to obtain luminescent silicone materials is the introduction of fillers. This allows the use of a wide range of organic and inorganic fillers. Inorganic luminescent fillers include quantum dots of doped graphene [68,69] or semiconductors CdSe, CdS, ZnS, [29,70], as well as lanthanide-containing organometallic frameworks [71].

Mechanochromic photoluminescent silicone materials with fillers such as 1,1,2,3,4,5-heptaphenyl-1-hydrosilol (HPS) and other organic phosphors are known in the literature [74]. Coordination compounds of rare earth metals can also act as luminescent fillers. [74–77]. For example, luminescent materials obtained by incorporating $[Eu(tta)_3(H_2O)_2]$ during the hydrosilylation reaction between tetramethyl-tetravinyl-cyclotetrasiloxane (D_4Vi) and tetramethyl-tetrahydro-cyclotetrasiloxane (D_4H) are described in [77]. The photoluminescence quantum yield of the obtained silicone materials reaches 33%.

Another approach for luminescent silicone materials fabrication is the introduction of luminescent complexes into a polysiloxane matrix, which simultaneously perform a dual function - a catalyst for cross-linking by the hydrosilylation reaction and a phosphor [67,78]. In a 2021 paper, platinum(II) 2-phenylpyridinato-triphenylphosphine-chloride $[Pt(ppy)Cl(PPh_3)]$ was used as a luminescent filler and catalyst for the cross-linking of vinyl-terminated polydimethylsiloxane and polymethylhydrosiloxane [67]. The quantum yield of photoluminescence for the obtained silicone material was 12.5%.

Later, in [78] were presented silicone rubbers obtained by cross-linking *α,ω*-divinylpolydimethylsiloxane and poly(dimethylsiloxane-*co*-methylhydrosiloxane) by the hydrosilylation reaction, where C,N-chelate deprotonated diaminocarbene complexes of platinum(II) acted as a catalys. Silicone rubbers obtained with the aminoisoquinoline-containing complex *cis*-$[PtCl_2(CNXyl)_2]$, exhibit temperature-dependent luminescence. The photoluminescence emission of these silicone materials changes irreversibly when heated from 80–100 °C (green radiation) to 120°C or more (blue radiation) (**Figure 4)**.

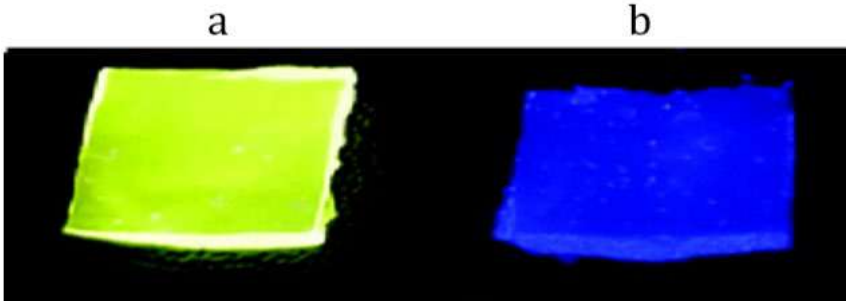

Figure 5 – Optical photographs of thermo-photoluminescent silicone rubbers at 80 **(a)** and 120°C **(b)** [78]

Despite the simplicity of the first approach, luminescent fillers can be washed out of the silicone material upon prolonged contact with organic solvents [67], the problem of their inhomogeneous distribution in the silicone matrix is also possible. As mentioned above, another approach to obtaining luminescent silicone materials is the modification of the polysiloxane chain by various chemical reactions, including using click chemistry, which allows solving the problem of uniform distribution of luminophores in the polymer matrix, and also eliminates their washing out upon contact with organic solvents.

The preparation of silicone luminescent materials by the reaction of azido-alkyne cycloaddition (CuAAC) catalyzed by copper (I) is described in the work [79]. Scheme for the preparation of rhenium-containing PMC (Re-PDMS) $[Re(CO)_3(MeCN)(5\text{-}(4\text{-ethylphenyl})\text{-}2,2'\text{-bipyridine})]OTf$ (Re^1) and $Re(CO)_3Cl(5,5'\text{-diethynyl-}2,2'\text{-bipyridine})]$ (Re^2) is shown in **Figure 5**. Re-PDMS have weak luminescence in the orange region of the spectrum with quantum yields of 0.5%.

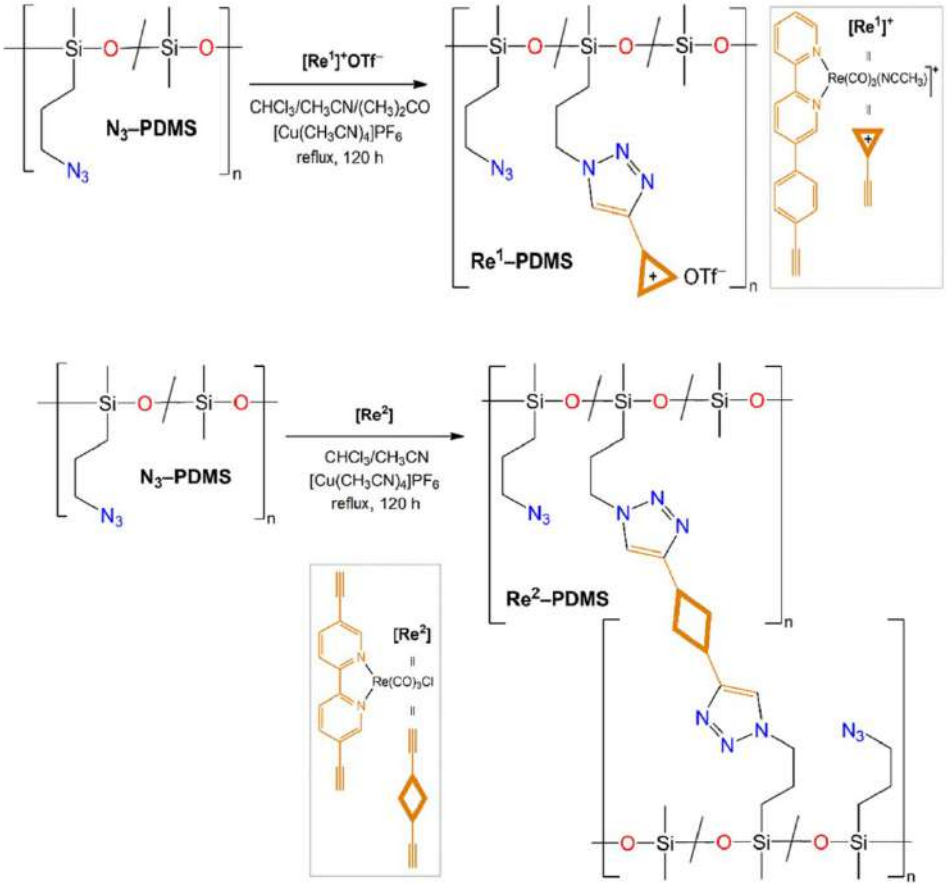

Figure 6 – Scheme of Re^1-PDMS and Re^2-PDMS synthesis [79]

To obtain silicone materials with a higher photoluminescence quantum yield, lanthanide coordination compounds can be used. Due to the forbidden nature of the characteristic 4f–4f electronic transitions, lanthanide ions have a long photoluminescence lifetime and narrow spectral lines [80].

In [81] preparation of branched photoluminescent PMC of polysiloxanes (P1-Ln with Eu^{3+} and Tb^{3+}) by the thiol-ene "click" chemistry reaction (**Figure 6**) were reported. The photoluminescence spectra exhibit characteristic signals of energy transitions $^5D_0 \rightarrow {}^7F_2$ (621 nm) for Eu^{3+} and $^5D_4 \rightarrow {}^7F_J$ (J = 6 – 3) for Tb^{3+}. However, the quantum yields were only 0.3%.

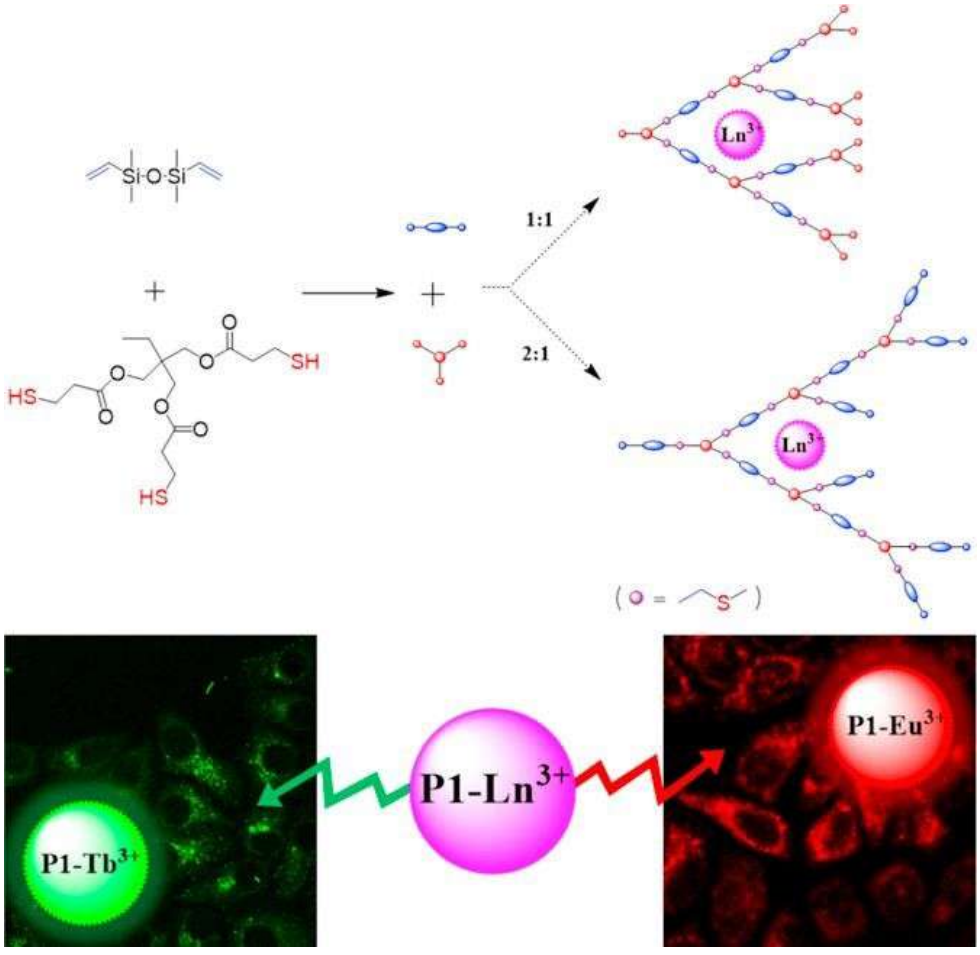

Figure 7 – Scheme of P1-Ln synthesis [81]

To achieve a high photoluminescence quantum yield, it is necessary to use a ligand that is a sensitizer for the so-called "antenna effect" [78]. One such sensitizer is pyridine (Py). In 2020, Li H. and colleagues reported on the preparation of photoluminescent self-healing terbium- and europium-containing PMCs based on pyridinecarboxydiamide-co-polydimethylsiloxane (Tb–Py–PDMS and Eu–Py–PDMS, respectively) [2]. The quantum yields for these PMCs were 40% and 30%, respectively. Narrow spectral lines of lanthanides allows PDMS photoluminescence color tuning by varying the Eu^{3+}:Tb^{3+} ratio. Thanks to this approach, the authors managed to obtain a silicone material whose

emission color is close to white light and which can be used as a phosphor to create white LEDs (**Figure 7**). However, the described PMCs have relatively low tensile strength σ = 0.45 MPa, which makes them difficult to use in flexible optoelectronic devices.

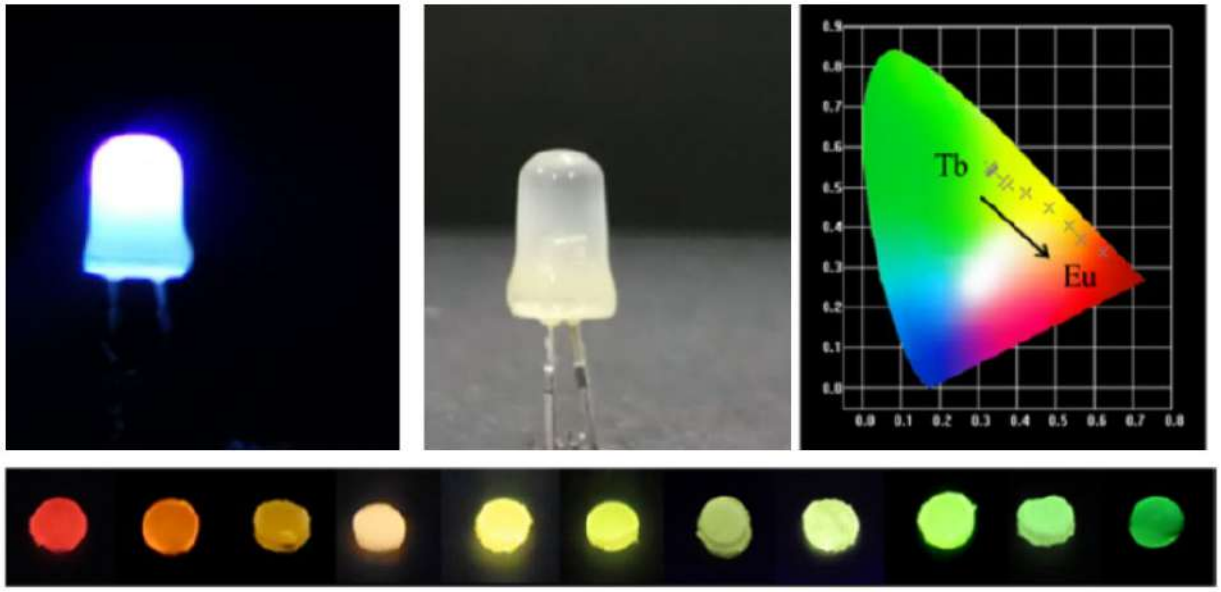

Figure 8 – Optical photographs of Tb–Py–PDMS and Eu–Py–PDMS based phosphors and CIE 1931 color space [2]

Later, in 2022, the photoluminescence color tuning was shown for lanthanide-containing polysiloxanes with the terpyridine ligand Ln–Tpy–PDMS [83]. The quantum yields of both terbium- and europium-containing PMCs were about 28%. The photoluminescence color tuning in the case of Ln–Tpy–PDMS is carried out not only by changing the Eu^{3+}:Tb^{3+}ratio, but also by choosing the excitation wavelength This is due to the shape of the Eu–Tpy–PDMS excitation spectrum as it presents a broad absorption peak in the range of 250 to 400 nm and centered around 331 nm from the terpyridine ligands along with a weaker and sharper peak at 395 nm from the internal 4f6 transition of Eu^{3+}. Despite the high quantum yield and the ability to tune photoluminescence, Ln–Tpy–PDMS posess poor self-healing efficiency 30%, which limits their applicability for flexible and stretchable RGB displays.

Thus, luminescent silicone materials are mainly obtained by introducing luminescent fillers into the silicone composition or photoactive centers into the backbone of the polysiloxane. Luminescent silicone materials filled with semiconductor quantum dots [28,29,70,84] and graphene [24] are used as light emitting layers in ACEL electroluminescent displays. Silicone matrices containing molecules of organic complexes are used as light emitting layers in OLED [12]. Chemical modification of the polysiloxane chain makes it possible to solve the problem of uniform distribution of luminophores in the polymer matrix, and also excludes their leaching upon possible contact with solvents. Using this approach, lanthanide-containing Ln-Py-PDMS copolysiloxanes [2], were obtained, which have not only

relatively high photoluminescence quantum yields and a long lifetime [80] but also self-healing properties. However, luminescent lanthanide-containing copolysiloxanes presented in the literature have relatively low mechanical strength and require additional synthesis steps to obtain materials with different luminescence colors. In this regard, there is a problem in obtaining lanthanide-containing PMCs with improved tensile properties and simple control of photoluminescence color without resorting to additional synthetic steps.

1.1.4 Electrically conductive silicone materials

As in the case of luminescent materials, there are two main methods for obtaining electrically conductive silicone materials: *i)* introducing various electrically conductive fillers into liquid silicone compositions (for example, Sylgard 184) and obtaining solid electrically conductive composites, *ii)* chemical modification of the polysiloxane chain and obtaining electrically conductive composites and/or materials based on them.

In a 2019 paper by the Guo C.F. presented a flexible tensile electrode obtained by functionalizing the surface of PDMS with a layer of conductive poly(3,4-ethylenedioxythiophene)-polystyrenesulfonate (PEDOT:PSS)-graft-PDMS. The resistivity of the PEDOT:PSS-graft-PDMS flexible electrode is 90 Ω·cm [85]. At the same time, the change in resistance during deformation up to 100% was insignificant and did not change during 10,000 cyclic stretches up to 100% strain.

In a 2019 paper, conducting ferrocenyl-functionalized polymethylhydrosiloxanes and their composites with CNTs were used as electrodes for flexible Schottky barrier diodes [35]. Later, in 2022, EFSR rubbers were demonstrated, which had a specific electrical conductivity of $9.5 \cdot 10^{-12}$ S·cm^{-1} at an applied electric current frequency of 1 Hz, which corresponds to antistatic materials [86–88]. The authors showed that ferrocenyl units contribute to the achievement of a high charge injection capacity without changing the microelectrode area (EFSR) in the neuronal implant, which makes it possible to avoid damage to neuronal tissues during electrical stimulation. The introduction of carbon nanotubes into EFSR in an amount of 5% by weight makes it possible to achieve a specific electrical conductivity of $7 \cdot 10^{-5}$ S·cm^{-1}. Such electrical conductivity values are comparable with the electrical conductivity of a number of semiconductors. Due to their electrically conductive properties, EFSR-CNT composites have been used as neuroimplants [89].

The potential of using modified electrically conductive polysiloxanes has not been fully disclosed. Only a few cases of transformation of a typical dielectric PDMS into antistatic and semiconductor materials due to chemical transformations are presented in the literature [89].

In turn, electrically conductive PDMS composites with graphene, CNTs, silver (AgNWs), and copper nanowires (CuNWs) can be considered as typical semiconductors. Thus, electrically conductive PDMS composites have become widespread as flexible tensile electrodes for optoelectronic devices and "skin electronics" [19,21,22,26,27,33].

Thus, as in the case of luminescent silicone materials, two approaches are used to obtain electrically conductive polysiloxanes: the introduction of conductive fillers into PDMS and the chemical introduction of electroactive centers into the polysiloxane chain as side substituents. The literature presents electrically conductive ferrocenyl-containing polysiloxanes and materials based on them, which were used as flexible electrodes for a Schottky diode [35] and as neuronal implants [89]. However, these materials are not widely used in the field of flexible optoelectronics due to their opacity.

1.2 Application of polysiloxanes in optoelectronic devices

The direction of development of stretchable and flexible light-emitting devices and RGB displays has been actively developing since 2009, and stretchable displays based on various technologies are currently known [90]. Typically, PDMS in such devices serves as a mechanical support material that allows the light-emitting device to stretch without losing its electrical properties. However, further development of the field of flexible optoelectronics requires the development of new efficient flexible stretchable electrodes.

In 2014, a flexible piezoelement based on Sylgard 184 / AgNWs was presented [25,91]. The resistivity of the Sylgard 184 / AgNWs composites was 210 Ω [91]. Sylgard 184/AgNWs composites can have a piezoelectric effect, i.e., under the action of deformation, induce an electric charge on their surface (direct piezoelectric effect), and deform under the influence of an external electric field (reverse piezoelectric effect).) [92]. In this case, the nanowiers inside the silicone material are arranged in a random order (**Figure 9**). Mathematical modeling has shown three possible options for the arrangement of nanofilaments relative to each other in a silicone material: (I) complete connection without contact resistance, when the distance between the axial lines of adjacent nanofilaments is less than the diameter of a single filament, (II) disconnected nanofilaments, when the distance between the axial lines of nanofilaments exceeds the limit distance and (III) tunnel junction if the distance from the center of two adjacent nanowires is between the diameter and the cut-off distance (~150.5 nm) so that electrons can tunnel through the PDMS matrix [92].

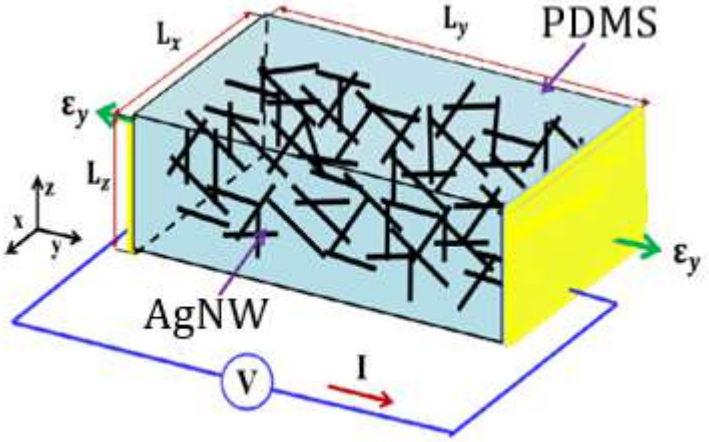

Figure 9 – Arrangement of AgNWs in a flexible electrode based on PDMS [92]

In 2016, J. Sun et al demonstrated a flexible tensile electrode based on PDMS and copper nanowires (CuNWs) [27]. Further, in the work of 2019, the K. Suganuma group presented an extensible CuNWs/PDMS electrode with a surface resistance of $4.65 \cdot 10^9$ Ω/□ and an optical transmittance of 78%. Electrode resistance increased about 3 times after 1000 bending cycles at 10% strain [93]. In 2022, flexible self-healing electrodes based on AgNWs/PDMS-*block*-dithiothreitol (**Figure 10**) composites were obtained, which were used in flexible optoelectronics and "skin electronics" [53]. Self-healing of the material occurred due to the interaction of hydroxyl groups in the chain of the PDMS-block-dithiothreitol copolymer with boronate ester groups formed after condensation with boric acid.

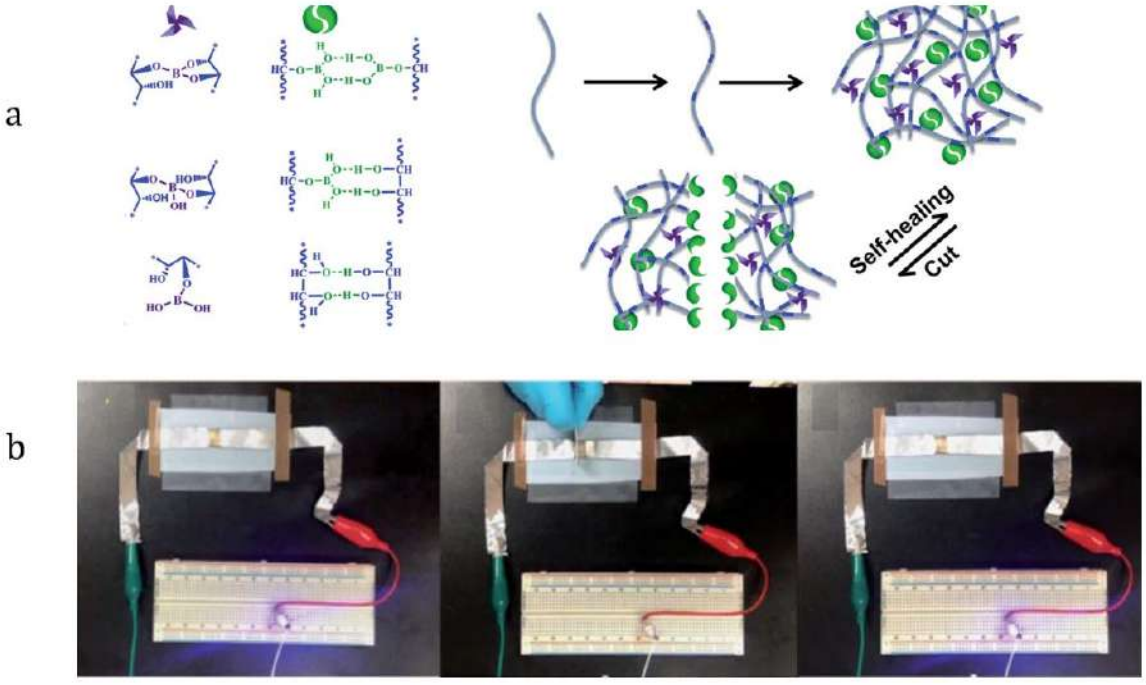

Figure 10 – Scheme of PDMS-block-dithiothreitol preparation **(a)** and optical image of working electrode **(b)** [53]

Thus, due to their flexibility, transparency, and the ability to maintain electrophysical properties during deformation, flexible and extensible electrodes based on Sylgard 184/AgNWs composites are used for extensible light emitting devices of various architectures: electroluminescent devices operating at high voltages (ACEL) [28,29], NWs/PDMS LEDs [33], stretchable organic light emitting diodes (OLED).

First of all, among the light-emitting devices in which polysiloxanes are used, it should be said about flexible and stretchable OLEDs, which have a thin-film layered architecture (**Figure 11**). As a rule, to achieve electroluminescence in a layer of light-emitting material, the OLED architecture assumes the presence of electron- and hole-transporting and injection layers. The The interface between the electrode and the active material has a key effect on the efficiency of charge carrier injection. Holes must overcome the energy barrier between the anode and the highest occupied molecular orbital (HOMO) of the organic electroluminescent material, while electrons must overcome the barrier between the cathode and the lowest unoccupied molecular orbital (LUMO), as shown in **Figure 11**. A hole injection layer (HIL) and an electron injection layer (EIL) must be inserted into the anode and cathode interfaces to facilitate charge injection. As a result of electron-hole recombination, excitons with a finite binding energy and lifetime are formed. To prevent exciton damping, hole-transporting layers (HTL) and electron-transporting layers (ETL) are added to the electrodes or injection layers. HTL and ETL help soften the interfacial energy barrier with a stepwise cascade of energy levels [90].

The light emitting layers are generally composed of organic conjugated molecules or light emitting polymers (LEPs). OLEDs that use LEP as the electroluminescent layer layer are also referred to as polymer OLEDs. Small molecule OLEDs are typically created by vacuum deposition of material by physical vapor deposition. Polymers are mechanically more stable than small molecules and therefore polymer LEDs are more promising candidates for stretchable electroluminescent devices.

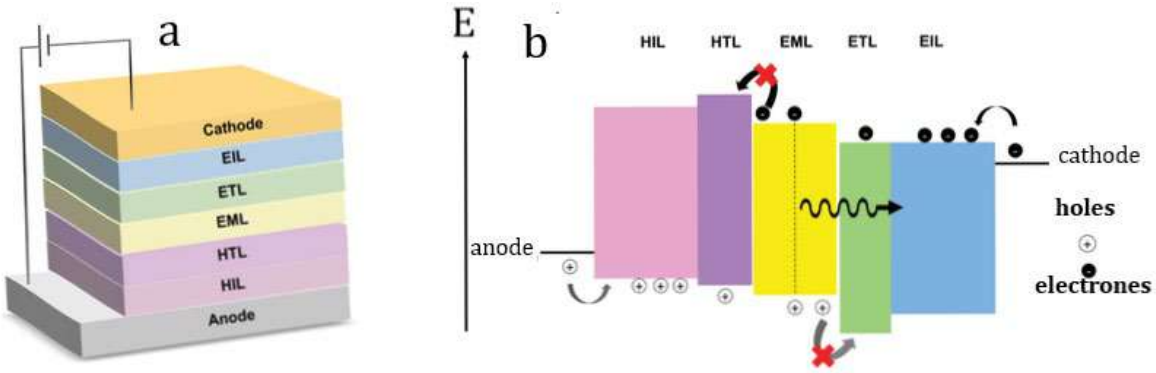

Figure 11 – Typical architecture **(a)** and power diagram **(b)** OLED [90]

In convetional OLEDs, polysiloxanes can perform several functions. One of their applications is the use of functional layers to improve the properties of injecting holes or as transport layers. [94]. Polysiloxanes can also be used as a matrix for electroluminescent molecules in flexible OLEDs. At the same time, polysiloxane derivatives can act as phosphorescent substances in the light-emitting layer. [95].

The most widely used PDMS is in ACEL light emitting devices. With a relatively simple architecture compared to OLED, PLED and LEC devices, flexible and stretchable ACEL devices have many applications: wearable health monitoring systems [96], “skin electronics” [97], humidity sensors [98], wearable displays [99], self-healing [100] and electrocromic displays [101], portable flexible lamps [99], e-textile [102] and pixel displays [103].

A typical flexible ACEL architecture is shown in **Figure 12**. In a thin film ACEL device, the light emitting layer consists of a semiconductor phosphor in a dielectric matrix, typically PDMS, sandwiched between two PDMS/AgNWs electrodes, both of which are transparent to light. [99].

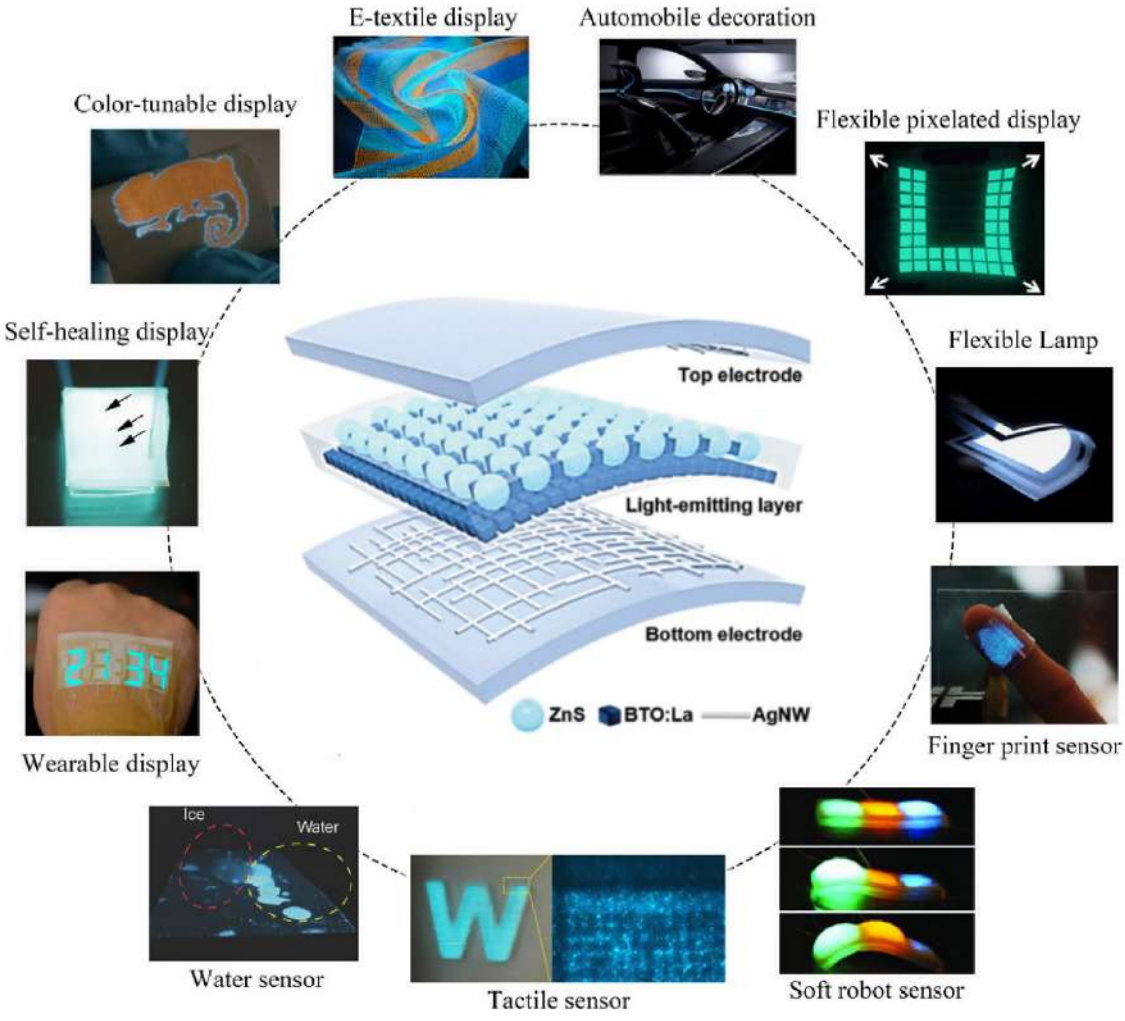

Figure 12 – Stretchable ACEL architecture [95] and their applications [99]

The excitation of luminescent centers in ACEL is usually described by the theory of impact ionization or impact excitation [104]. In the impact ionization model, a strong electric field of more than 106 V/cm creates and accelerates hot electrons that collide with the phosphor lattice, resulting in the generation of electron-hole pairs. Luminescence occurs as a result of the recombination of electrons and holes (**Figure 13**). Impact excitation is associated with the direct collision of hot electrons with localized luminescent centers. Electrons in the ground state will be excited to higher energy levels, resulting in luminescence.

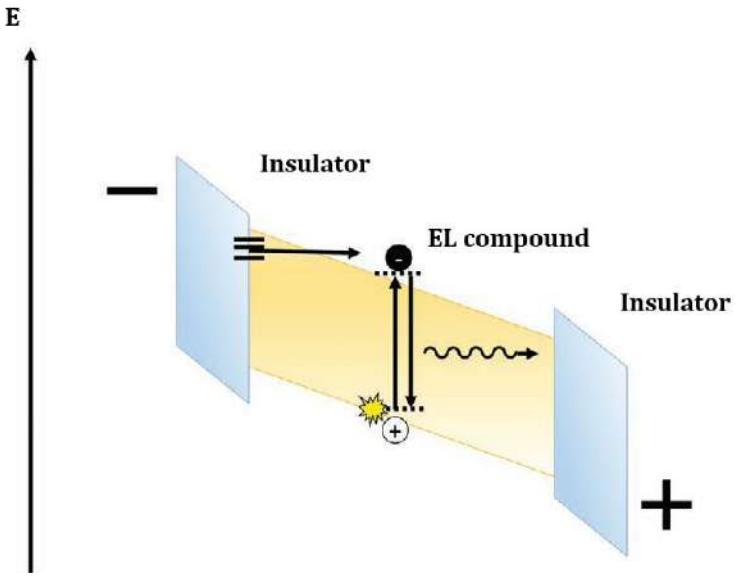

Figure 13 – ACEL energy diagram [90]

Luminescent silicone composites based on PDMS and semiconductor phosphors of zinc sulfide ZnS as a filler exhibit electroluminescent properties when a high voltage of up to 200 V is applied at a layer thickness of 60 μm. Based on this principle, flexible and stretchable ACELs in blue were created [28]. Doping of ZnS with copper (ZnS:Cu) and manganese (ZnS:Cu,Mn) atoms made it possible to achieve electroluminescence in the green and orange spectral ranges, respectively, and their combination – intermediate yellow and violet colors, which was shown by the example of strecheble ACEL (**Figure 14**) [29,68]. In this case, the electroluminescence intensity of ZnS/PDMS remains at the same level even after the device is stretched up to 100%.

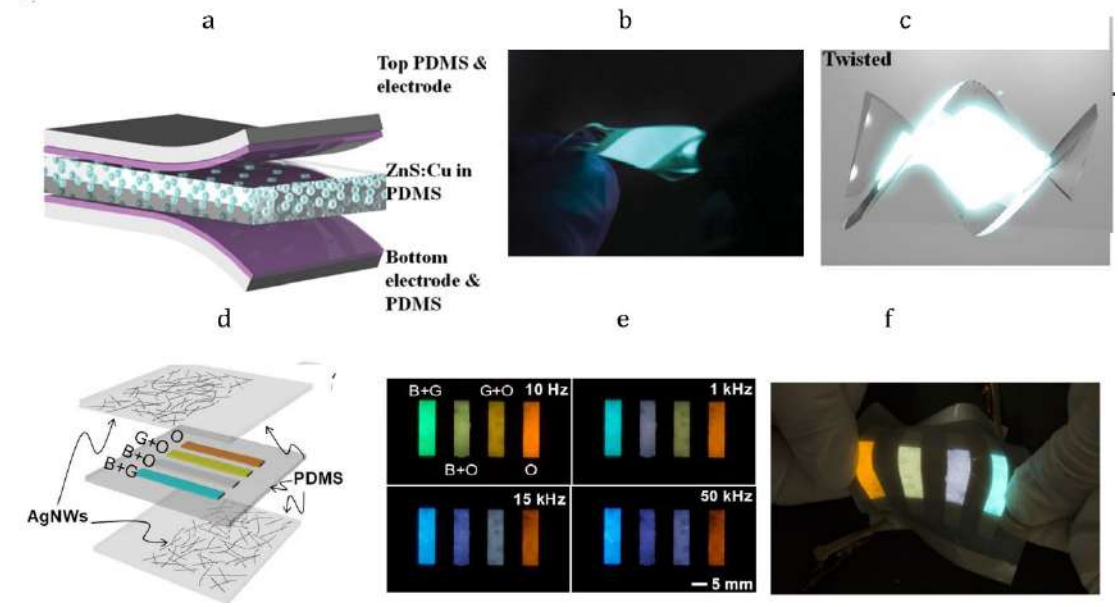

Figure 14 – Blue ACEL Architecture **(a)**, optical photographs of a bent blue ACEL under applied voltage **(b)** and a 3D model of a twisted device **(c)** [28]. Multicolored ACEL architecture **(d)**, optical photographs of a multi-colored ACEL under applied voltage **(e)** and stretching **(f)** [29]

With a simple architecture, ACEL devices can easily be not only flexible (able to bend and withstand deformations along the z axis), but also extensible, which contributes to the preservation of the electroluminescent properties of the device during elastic deformations along the x and y axes. To achieve the extensibility of the device, additional supporting layers of PDMS are used, which are applied over the top and bottom electrodes. Extensible ACEL displays can also be pixelated by applying contact-addressable strechable electrodes. In [103] an extensible ACEL pixel display based on an extensible AgNW:PEDOT:PSS patterned electrode and a light-emitting ZnS:Mn/PDMS layer was demonstrated (**Figure 15**). being bent, stretched and twisted. The brightness of the stretchable ACEL display reached ~80 cd/m^2 at a frequency of 10 kHz and was maintained when the device was stretched to 80%. The electroluminescence intensity remained at the same level after 200 bending cycles.

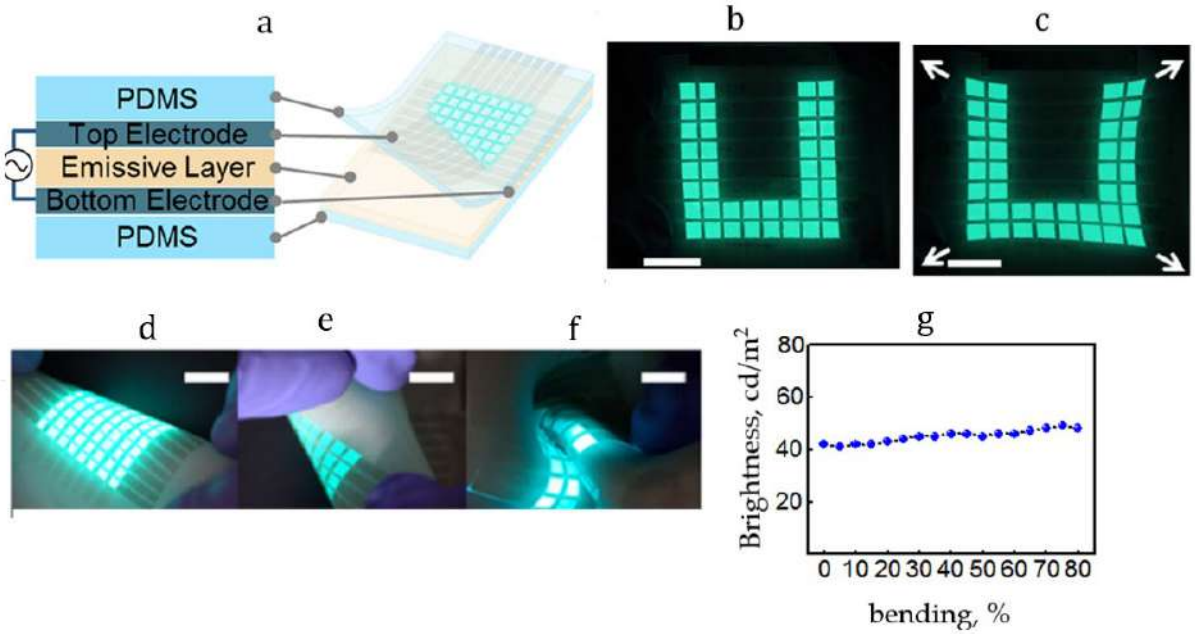

Figure 15 – Strachable ACEL architecture **(a)**, optical image of a pixel ACEL display in the initial state **(b)** and when stretched **(c)**, optical images of a pixel ACEL display when bending **(d-e)** and twisting **(e)**, ACEL display brightness dependence when stretched [103]

For nowadays, there are high-performance ACEL devices that have mechanical strength and resistance to deformation (more than 1000 cycles), characterized by the absence of electrical breakdown during operation.

Further development of tensile ACELs involves the fabrication of devices with the possibility of self-healing, as well as a long service life (> 50% of the original brightness for more than 3000 h) and safe operating conditions for wearable electronics (<36 V) with sufficient brightness (100–200 cd/m^2).

In particular, a new class of flexible and extensible inorganic LEDs based on arrays of whisker nanocrystals (NWss) A3B5 semiconductors encapsulated in a PDMS polymer matrix should be singled out. Light-emitting diodes based on A3B5 NWs arrays are stable over time and do not require multilayer architecture compared to perovskite and organic LEDs, however, they are difficult to manufacture. Due to the mechanical resistance of NWs to bending, fully flexible LEDs can be obtained by encapsulating an array of NWs in a polymer matrix, followed by separation from the growth silicon substrate and the deposition of flexible transparent electrical contacts. The process of creating flexible NW/PDMS LEDs consists in transferring a vertical NWs array into a silicone matrix (mainly Sylgard 184), while the upper and lower parts of the NW are opened to deposit flexible transparent electrodes, usually from SWCNTs [34]. The NWs contain an active region where radiative recombination of injected charge carriers occurs, while the base and top of the NW serve as p- and n-type emitters for the injection of carriers from the external electric circuit into the active region inside the NWs. NWs can have an axial geometry, with the active region being a disk of material with a narrower bandgap (compared to the emitter material) located

between p- and n-doped segments, or a core-shell geometry or a radial geometry, when the active region appears as an annular cylinder of material with a narrower bandgap between the conducting core and the n-/p-type shell material. In the latter case, the shell material in the upper part of the NW is in contact with an electrode of the same conductivity type, while the core material in the lower part of the NW is connected to the opposite polarity. NWs/PDMS membrane LEDs require at least one transparent electrode to output light, while the other electrode may be opaque. Therefore, one of the most effective methods for manufacturing such LED devices is based on the use of flexible copper tape, which serves as a mechanical support during separation and at the same time as an electrode to the upper parts of the NWs array [34,55]. After separation of the membrane from the substrate, the lower parts of the NW are exposed, which makes it possible to directly apply a face contact from a transparent conductive material.

The material of the polymeric encapsulating matrix for flexible LEDs based on NW should: *i)* ensure complete transfer of the NW array from the growth substrate, which determines the uniformity and performance of the LED; *ii)* be mechanically strong and resistant to deformation when the membrane is separated from the growth substrate; *iii)* be optically transparent for efficient light extraction from the NW membrane. Sylgard 184, a commercial silicone composition, has gained wide acceptance in the field of membrane LEDs.

The problem arises at the manufacturing stage, since the most common method for creating NW/PDMS membranes is mechanical separation from the growth substrate, which is a nontrivial task for a PDMS matrix. Sparse arrays of long (i.e., more than 15 μm in length) NWs can be easily separated from the epitaxial substrate, since in this case the PDMS membrane has sufficient thickness to withstand the deformation that occurs during the separation process. However, for dense arrays of short (less than 5 μm in length) NWs, the PDMS matrix becomes brittle; therefore, during mechanical separation, deformations of the PDMS membrane are inevitable, which manifest themselves in the form of ruptures and multiple micrometer-scale holes. As a rule, the reason for these tears and deformations is the high adhesion of the commonly used Sylgard 184 to the epitaxial substrate [38,56]. Nevertheless, for sapphire growth substrates and sparse arrays of long NWs (for example, those consisting of InGaN/GaN semiconductor materials), this adhesion is negligibly small, since the application of force is rarely required during separation, and the stress effectively relaxes at a membrane thickness of 15–20 μm.

The NWs/PDMS flexible LEDs developed to date are highly stable in the blue spectral region, since III-V semiconductors, especially nitrides, exhibit high stability even at high current densities. Compared to most commercially available OLEDs, NWs/PDMS LEDs can also maintain their performance after multiple bending and stretching cycles (up to 30 cycles) [10,57]. For the first time, flexible green and blue LEDs based on InGaN NW arrays in a Sylgard 184 matrix [34, 58] were demonstrated in 2015 by the group of M. Chernysheva. Later in 2016 [35] fabrication of white LEDs

was reported. A blue flexible LED based on arrays of NW nitride compounds is shown in **Figure 16 a** In this InGaN structure, NWs have a lower content of indium (In) compared to the green LED shown in **Figure 16 b**. The white LED shown in **Figure 16 c**, has yellow photophosphor particles in a Sylgard 184 membrane that downconverts the light emitted by the NWs.

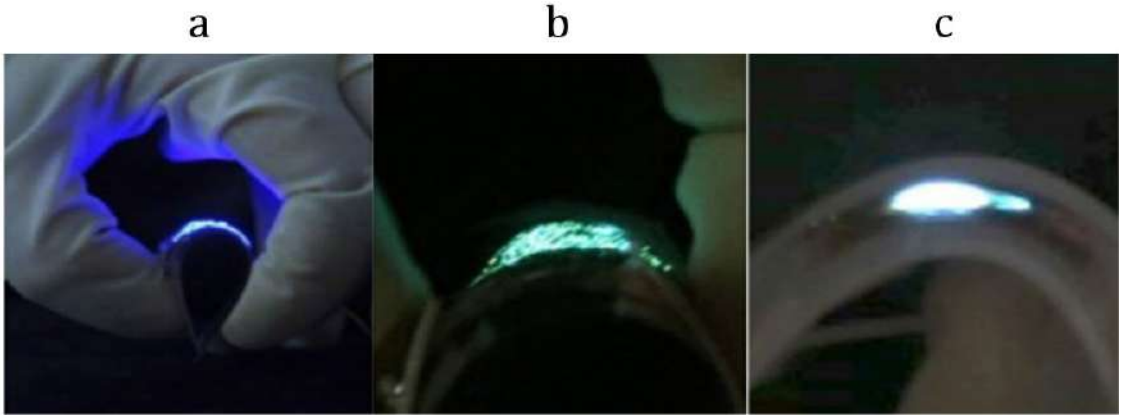

Figure 16 – Optical images of flexible blue **(a),** green **(b)**, and white **(c)** Sylgard/InGaN LEDs in operation [31,32,105]

A 2021 paper demonstrated a flexible and extensible LED based on InGaN/Sylgard 184 membranes with a flexible single-walled carbon nanotube (SWCNT) contact [33]. In the same year, the authors of [34] reported on the creation of a flexible red LED based on arrays of GaP/GaPAs NWs in a Sylgard 184 matrix.

A flexible Schottky barrier diode was introduced in a 2020 paper [35,45], where silicone composition based on PDMS-*graft*-polystyrene was used as a supporting encapsulating matrix for n-GaP NWs arrays (**Figure 17**). The reduced adhesion value (0.66 relative to the value for Sylgard 184) made it possible to efficiently transfer arrays of n-GaP NWs with a height of 8 μm into a membrane with a relatively large area (3 inch sqr) [45]. However, the application of PDMS–*graft*–polystyrene as a supporting matrix for flexible light-emitting devices based on NW arrays is limited due to its opacity.

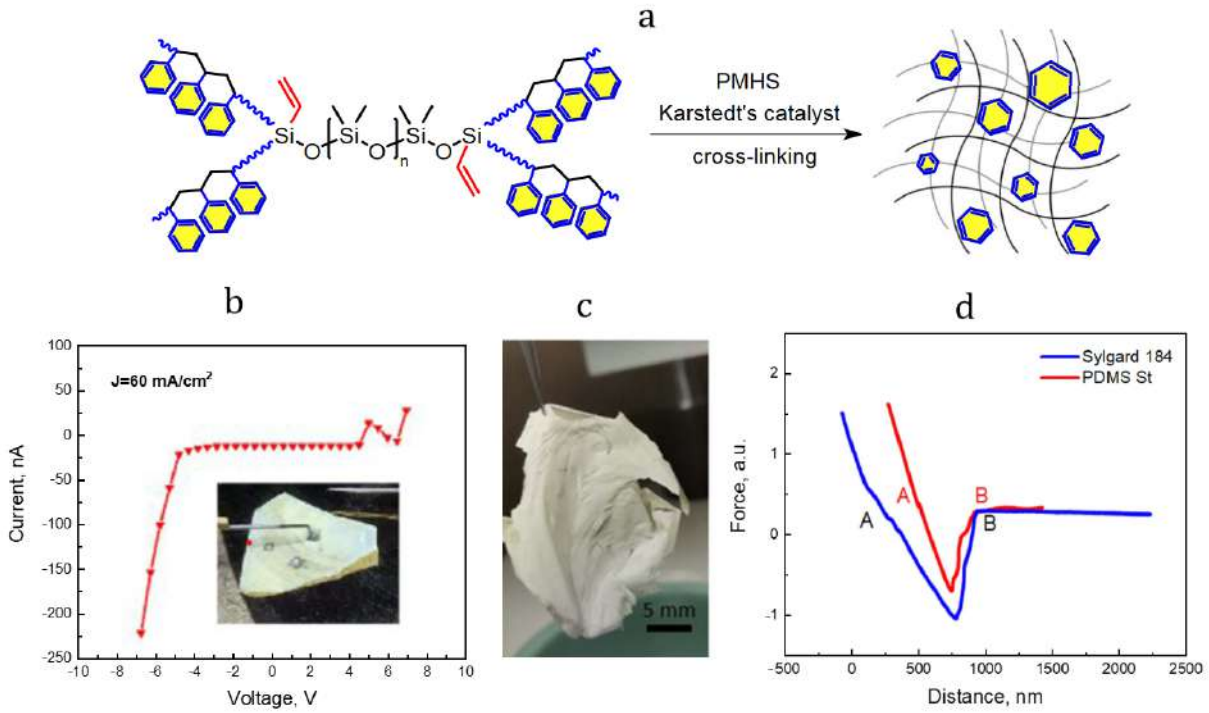

Figure 17 – Scheme of PDMS-*graft*-polystyrene cross-linking **(a)**, I-V curve **(b)** and optical image **(c)** of released PDMS-*graft*-polystyrene / n-GaP, approach/retraction curves of the silicon AFM probe to the layers of polymers under study **(d)** [35]

Thus, silicone materials and composites based on Sylgard 184 have become the most widely used in optoelectronics. Due to their transparency, these materials are used in OLEDs, flexible electrodes and piezoelectric elements, solar cells, and body-worn electronics. PDMS is also the main material of stretchable ACEL devices. Sylgard 184 has gained particular popularity as a flexible supporting matrix for flexible inorganic LEDs based on NW A3B5 arrays. PDMS-*graft*-polystyrene, which has reduced adhesion to a growth silicon substrate, was also used in a flexible Schottky barrier diode. However, the opacity of PDMS-*graft*-polystyrene makes it difficult to use it as a matrix for flexible light-emitting devices based on NW arrays.

Conclusion to the literature review

The optical transparency and homogeneity of the morphology of polysiloxanes and materials based on them contribute to their widespread use in optoelectronics. Thus, silicone materials based on the commercially available silicone composition Sylgard 184 are widely used in OLED devices as a matrix for organic emitters. Sylgard 184 is also used in flexible and stetchable ACELs as an electrode material, dielectric matrix of the light emitting layer, and mechanical support for tensile devices. Sylgard 184 has become widespread in the field of flexible optoelectronics based on A3B5 NW arrays as a flexible supporting matrix. At the moment, flexible LEDs based on Sylgard 184/NWs blue, green, red

and white are presented in the literature [31–34,105]. However, the high adhesion of Sylgard 184 to the silicon growth substrate makes it difficult to create effective large-area (3 inch sqr.) optoelectronic devices and RGB displays. The literature reports on the use of PDMS-*graft*-polystyrene copolymers [35], which have almost a twofold lower adhesion to a growth silicon substrate compared to Sylgard 184, for a flexible diode with a Schottky barrier fabrication. At the same time, the opacity of PDMS-*graft*-polystyrene makes it difficult to use it for flexible light-emitting diodes based on NW arrays. Thus, the problem of obtaining transparent silicone materials with low adhesion to a growth silicon substrate is still relevant. The development of methods for obtaining such silicone materials is a key point for scaling up the production of flexible inorganic LEDs based on A3B5 NWs.

Further development of flexible optoelectronics based on NW A3B5 arrays is to obtain bright and stretchable RGB displays. This requires effective luminescent silicone materials. Luminescent silicone materials filled with semiconductor quantum dots [28,29,70,84] and graphene [24] are already used as light emitting layers in ACEL displays. Silicone matrices containing molecules of organic complexes are used as light-emitting layers in OLED [12]. However, with this approach, there are problems associated with the washing out of luminescent fillers from silicone material when interacting with solvents, as well as their uneven distribution. An alternative to composite silicone materials are lanthanide-containing copolysiloxanes [2,106], possessing not only high photoluminescence quantum yields and long photoluminescence decay time, but also self-healing properties. The luminescent lanthanide-containing copolysiloxanes presented in the literature have relatively low mechanical strength and require additional synthesis steps to obtain materials with different luminescence colors. In this regard, there is a need to obtain coordinatively saturated lanthanide-containing copolysiloxanes with more effective sensitizers ("antenna effect"). This will make it possible to achieve narrowing of the Ln^{3+} energy transition lines in the photoluminescence spectra and, as a consequence, a high color rendering. Coordinatively saturated PMCs will also have improved mechanical properties. Optimization of the technique for obtaining self-healing yellow and orange photoluminophores layers from the initial red and green lanthanide-containing copolysiloxanes is of particular scientific interest.

Thus, to create flexible inorganic LEDs based on arrays of NWs and RGB displays of a new generation, it is necessary: *i*) to develop strong transparent silicone materials with low adhesion to a silicon substrate; *ii*) to develop luminescent self-healing silicone materials with a high quantum yield (≥10%) based on lanthanide-containing PMCs. This dissertation is aimed at solving these problems.

CHAPTER 2. RESULTS AND DISCUSSION

2.1 Styrene- and methyl methacrylate-containing silicone rubbers

2.1.1 S-PMHS, SSR, M-PMHS and MSR

Phenylethyl-functionalized silicone rubbers were prepared in two steps (**Figure 18**). At the first stage, poly(methylhydrosiloxane-co-methyl(2-phenylethyl)siloxane-co-methyl(1-phenylethyl)siloxanes) (S-PMHS) were synthesized by the catalytic hydrosilylation reaction between polymethylhydrosiloxane (PMHS) and styrene, previously distilled and purified from the inhibitor. A Karstedt complex (a complex of platinum(0) with 1,3 divinyl-1,1,3,3 tetramethyldisiloxane) was used as a catalyst for the hydrosilylation reaction. The mole ratios of Si–H groups (from PMHS) and vinyl groups of styrene (5:1) were chosen so that the content of phenylethyl units in S–PMHS was 50 (S–PMHS50) and 75 mol.% (S–PMHS75), respectively.

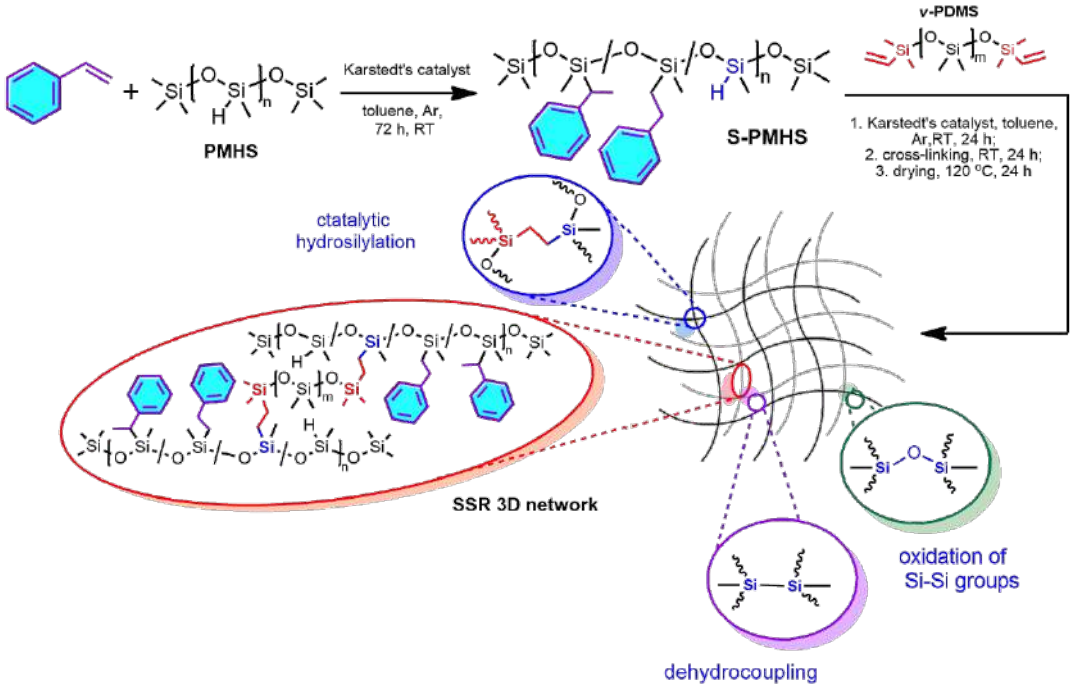

Figure 18 – Schemes for the production of S–PMHS and cross-linked materials based on them (SSR)

At the first stage, the completeness of catalytic hydrosilylation was monitored by analyzing the reaction products by ^{1}H NMR spectroscopy. Analysis of ^{1}H NMR spectra of S–PMHS50 showed that hydrosilylation between PMHS and styrene proceeds equally via anti-Markovnikov and Markovnikov routes [107] : two new signals were found at δ = 1.19–0.90 ppm (PhSiC***H₂***CH₂≡) and 2.01–2.44 ppm (PhSiCH₂C***H₂***≡), which correspons to –CH₂CH₂– linker. The signals of styrene vinyl groups (δ = 5.19,

5.76and 6.71) were not observed at ^{1}H NMR spectra (which indicates complete conversion of styrene). Self-crosslinking of S–PMHS50 occurred after removal of 2/3 of the solvent volume on a vacuum evaporator at a reduced pressure (0.267 bar) and a temperature of 60°C, followed by curing. Cross-linked S–PMHS50 is a fragile transparent silicone rubber that crumbles when deformed.

In order to increase the elasticity of phenylethyl-functionalized silicone rubber (SSR), at the next stage, carried out the reaction of catalytic hydrosilation of the synthesized S-PMHS50 and S-PMHS75 with *α,ω*-di(dimethylvinylsiloxy)polydimethylsiloxane (*v*-PDMS) using the same Karstedt catalyst in toluene solution, which led to the formation of a gel. SSR curing was first carried out at room temperature for 12 hours. Then, the resulting 500 μm thick film was separated with a scalpel, and the resulting rubber was dried at 120 °C for 12 hours in a vacuum oven. The SSR was a transparent, non-tacky, flexible silicone rubber. The content of phenylethyl groups in SSR was 50 (SSR50) and 25 (SSR25) mol.%, respectively.

In order to establish the mechanism of cross-linking, the SSR was studied using ^{1}H, ^{13}C and ^{29}Si SSNMR spectroscopy (**Figure 19**). At ^{29}Si SS NMR a broad signal was observed at δ = –22 ppm, which corresponds to several types of silicon atoms: phenylethyl-substituted silicon atom (–(PhCH$_2$CH$_2$)(CH$_3$)***Si***O–), polydimethylsiloxane unit (–(CH$_3$)$_2$***Si***O–) and silicon atoms next to the formed cross-links by catalytic hydrosilylation (≡Si***C***H$_2$***C***H$_2$Si≡) (**Figure 18**). Weak signals at ^{29}Si SSNMR were observed at δ = –35 ppm. (Si–H), as well as signals of *O*-trisubstituted silicon atoms at δ = –57 ppm. and –66 ppm., corresponding to the cross-linking of Si–H groups by the dehydrocoupling mechanism with the formation of Si–Si bonds and their subsequent autoxidation to Si–O–Si bonds [108,109]. The ^{1}H SSNMR spectrum turned out to be of little information due to extremely broad peaks.

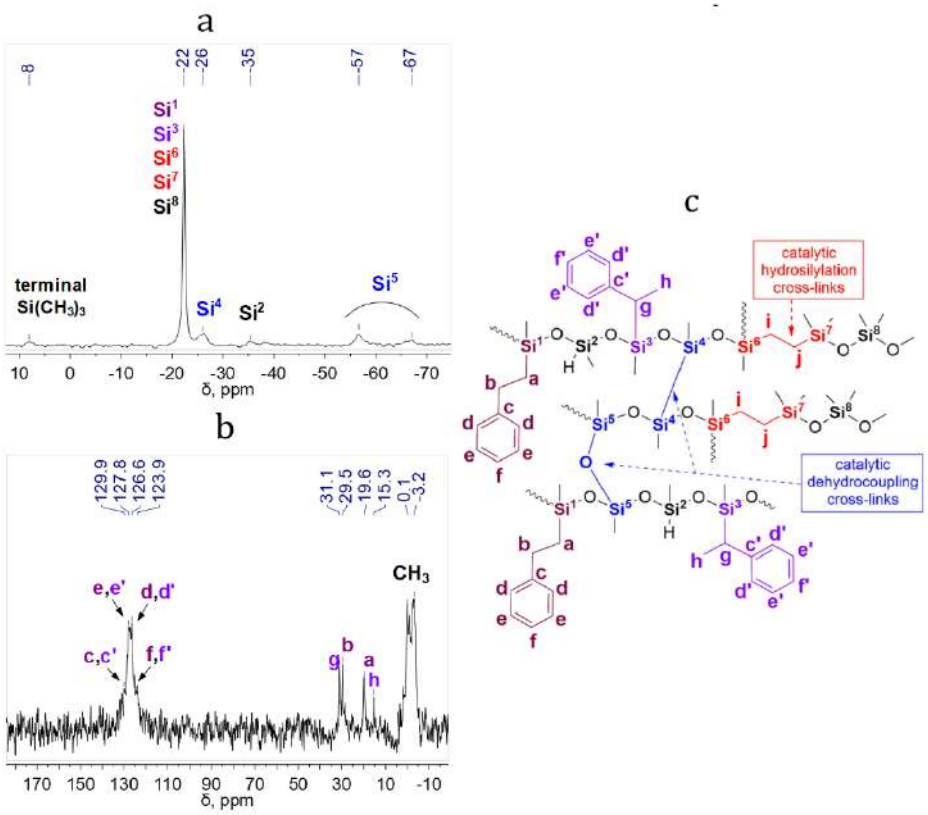

Figure 19 – ^{29}Si SS NMR **(a)**, ^{13}C SS NMR **(b)** and the structure of the 3D polymer network **(c)** SSR25

M-PMHS and MSR

To obtain 2-methyl-3-methoxy-3-oxopropyl-functionalized silicone rubber (MSR), poly(methyl(2-methyl-3-methoxy-3-oxopropyl)siloxane-co-methylhydrosiloxane) (M-PMHS) according to the catalytic hydrosylation reaction between PMHS and methyl methacrylate in a toluene solution (**Figure 20**). The molar ratio of Si–H and vinyl groups of methyl methacrylate was chosen so that methyl methacrylate reacted with only 50% of the Si–H groups of PMHS. In this case, the remaining hydride groups are consumed in the reaction with *v*-PDMS, and the molar ratio of Si–H groups of PMHS to vinyl groups of *v*-PDMS is 1:1.

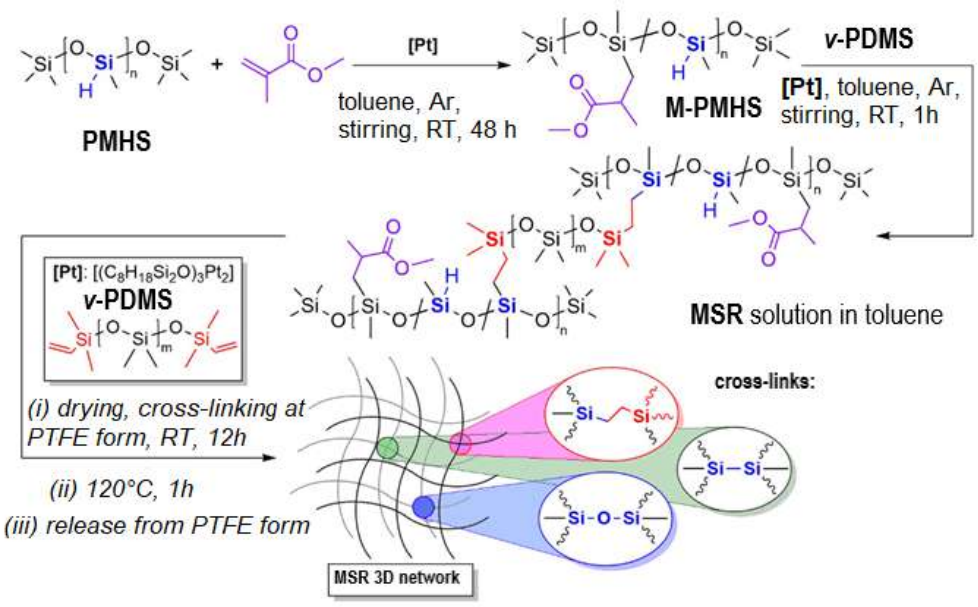

Figure 20 – Scheme of MSR synthesis

At the first stage, the completeness of the hydrosylation reaction was monitored using ^{1}H and ^{13}C NMR spectroscopy (**Figure 21**). Analysis of the ^{1}H NMR spectra of M-PMHS showed that hydrosylation between PMHS and methyl methacrylate proceeds predominantly against the Markovnikov rule (>99%): three new signals were found at δ = 0.78 ((COOCH$_3$)(CH$_3$)CHC***H***H'Si≡), 1.09 ppm. ((COOCH$_3$)(CH$_3$)CHCH***H'***Si≡) and 2.65 ppm. ((COOCH$_3$)(CH$_3$)C***H***CHH'Si≡), which corresponds to –CH$_2$CH– linker. The signals of the vinyl group of methyl methacrylate (δ = 5.55 and 6.10 ppm.) at ^{1}H NMR spectrum were not observed, which indicates complete methylmetacrylate conversion. According to ^{1}H NMR, the mole fraction of 2-methyl-3-methoxy-3-oxopropyl-containing units in M-PMHS was calculated from the ratios of the integral signal intensities δ = 4.75 ppm. (the remaining Si–***H*** groups) and 2.65 ppm. ((COOCH$_3$)(CH$_3$)C***H***CHH'Si≡) linker and amounted to approximately 44 mol.%.

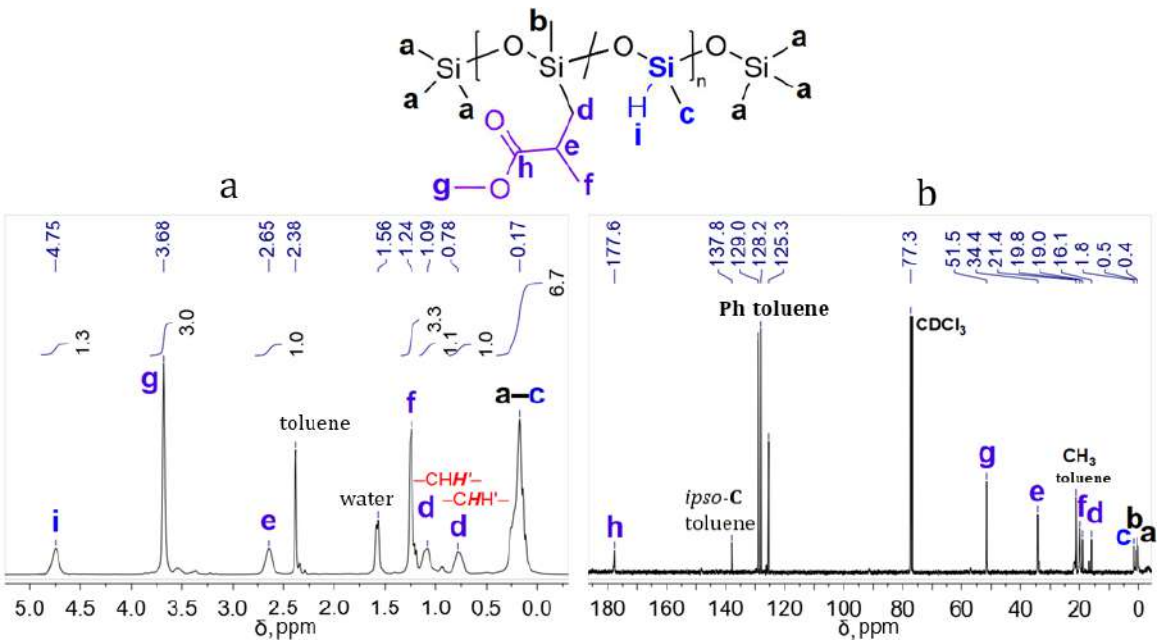

Figure 21 – M-PMHS ^{1}H NMR **(a)** and ^{13}C NMR **(b)** spectra

In order to obtain MSR at the next stage, the reaction of catalytic hydrosilation of the previously synthesized M-PMHS with *v*-PDMS was carried out using the same Karstedt catalyst in a toluene solution at RT, which led to the formation of a gel. The resulting gel was then poured onto a Teflon substrate. MSR curing was first carried out at room temperature 21°C for 12 hours. Then the mold was removed with a scalpel and the cured rubber was dried at 120°C for 12 hours. The resulting MSR were translucent, non-tacky, elastic silicone rubber.

Analogously to SSR [44], the cross-linking proceeds via the catalytic hydrosilylation reaction between the M-PMHS formed *in-situ* and the *v*-PDMS introduced into the reaction mixture **(Figure 20)**, as well as the catalytic dehydrocoupling of Si–H groups with the formation of Si –Si bonds followed by their oxidation in air to Si–O–Si [108,109].

Thus, SSR with a molar content of phenylethyl units of 25% and 50% (SSR25 and SSR50, respectively) and MSR with a molar content of 2-methyl-3-methoxy-3-oxopropyl units of 25% (MSR25) were obtained in two stages by the reaction of catalytic hydrosilation between PMHS and styrene/ methyl methacrylate followed by the addition of high molecular weight *v*-PDMS. In the case of MSR, the addition of methylmethacrylate proceeds via anti-Markovnikov route, since the hydrosylation reaction is characterized by the addition of a silyl radical to the carbon atom of the unsymmetrical C=C double bond bonded to a large number of hydrogen atoms [107]. In the case of SSR, the addition of styrene proceeds equally *via* anti-Markovnikov and Markovnikov routes [107]. The cross-linking of SSR and MSR proceeds by the catalytic hydrosilylation reaction alongwith catalytic dehydrocoupling reactions.

2.1.2 Optical and adhesive properties of SSR and MSR

For flexible inorganic LEDs with A3B5 NWs/PDMS (cross-linked silicone rubber) architecture, silicone materials must satisfy a number of characteristics. For efficient light output, the silicon supporting matrix encapsulating the array of NWs must be optically transparent in the visible spectral range, in which, as a rule, the luminescence of the used light-emitting NWs is observed. In this regard, a study of the optical and adhesive properties of the obtained SSR and MSR was carried out. A decrease in the adhesion of rubbers to Si is necessary to facilitate the separation of the membrane with NWs from the growth substrate.

Earlier in the literature, a method was proposed to reduce the adhesion of PDMS to a growth silicon substrate by grafting polystyrene side chains. Silicone compositions based on polydimethylsiloxane-*graft*-polystyrene (PDMS-*graft*-PSt) have adhesion almost two times lower than Sylgard 184 [35]. However, these materials are opaque due to the formation of spherical supramolecular structures of polystyrene side chains. [35,40,44].

Obtaining SSR and MSR by the reaction of catalytic hydrosilation involves introduction of side substituents in the main chain of the polysiloxane, which contributes to maintaining the uniformity of the morphology of the silicone material. Analysis of the surface morphology of SSR and MSR by SEM showed the absence of supramolecular formations in the form of spheres in SSR25 and MSR25 (), which are characteristic of PDMS–*graft*–PSt (**Figure 22 a, b)**. The homogeneity of the morphology contributes to the preservation of the optical transparency of the obtained silicone materials. Transparency has been proven by UV-visible spectroscopy - SSR25 and MSR25 do not absorb in the visible and near-IR region (**Figure 22 d**).

Adhesion to the growth silicon substrate was studied by analyzing the approach/retraction curves of the Si AFM probe. The value of the adhesion force is proportional to the width of the "beak" (the distance between points A and B on the curves – **Figure 22 c**) of the AFM approach/retraction curve corresponding to the bending of the silicon cantilever when interacting with a film of silicone material (160 and 200 nm for SSR25 and MSR25, respectively) . The adhesion values of silicone rubbers were determined relative to the adhesion value to Sylgard 184 (the beak width value on the AFM approach/retraction curve was 300 nm).

For MSR25 and SSR25, the adhesion values relative to Sylgard 184 were 0.67 and 0.53, respectively [110], while the adhesion value for Sylgard 184 is assumed to be 1.

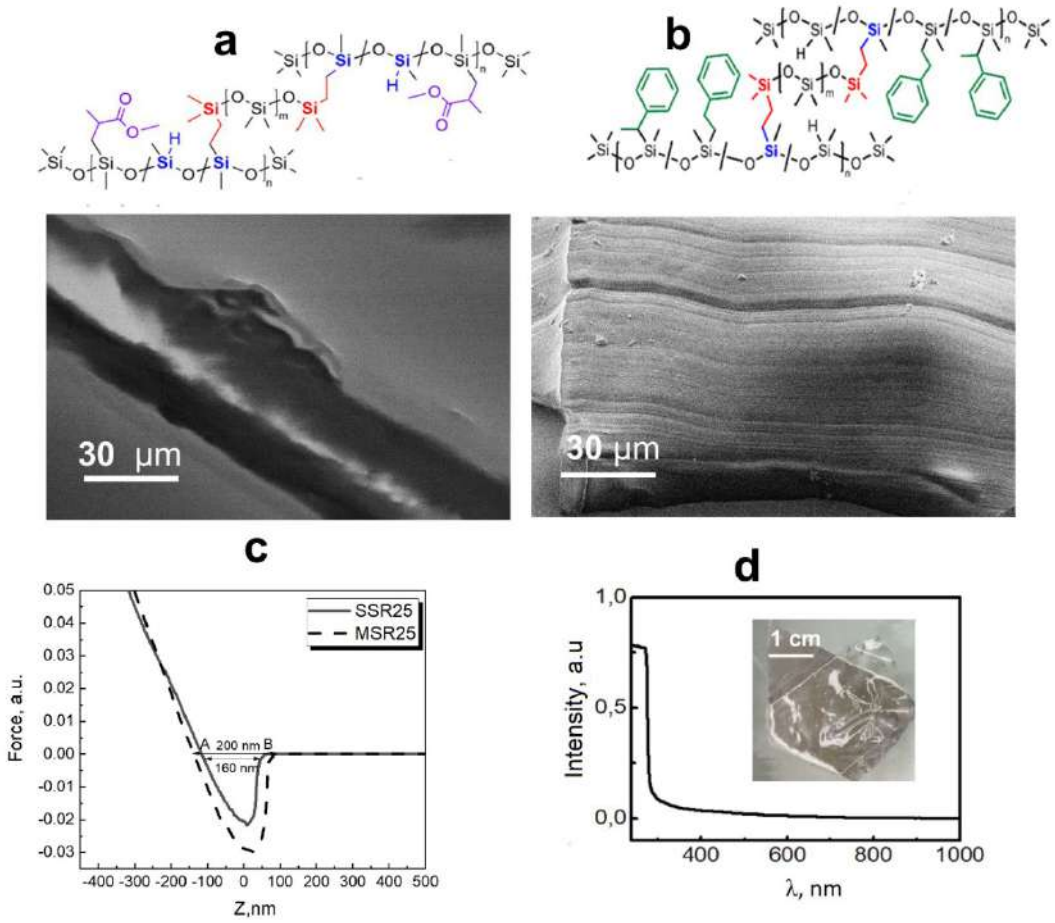

Figure 22 –Structural formulas and SEM images of MSR25 **(a)** and SSR25 **(b)** surfaces, AFM approach/retraction curves **(c)**, absorption spectra of SSR25 film (the inset in the figure shows an optical image of the released from substrate SSR25 membrane) **(d)**

Thus, the introduction of large hydrophobic phenylethyl and 2-methyl-3-methoxy-3-oxopropyl units into the main chain of PMHS by catalytic hydrosilylation reduces the adhesion of cross-linked silicone rubber to the surface of the growth silicon substrate, which is presumably due to the interaction of Si–H and Si–OH groups with the surface of crystalline silicon. due to the forces of van der Waals [111]. The use of the proposed synthesis method also makes it possible to avoid the formation of spherical supramolecular formations (microphase separation), which are observed in the case of graft copolymers [35,40]. Consequently, the transparency of the resulting silicone rubber is maintained.

2.1.3 Encapsulating properties of SSR and MSR

Polysiloxanes and silicone compositions based on them are known to have good film-forming properties [18]. Encapsulation efficiency and membrane thickness control can be monitored visually

during application, as well as by SEM methods. If the silicone material completely covers the height of the NWs, it can be removed in a controlled manner by etching in oxygen plasma.

SSR25 and MSR25 were employed as a flexible support matrix for gallium phosphide (GaP) NW arrays. The application of silicone films was carried out by the method of gravitational wrapping (G-coating) [35]. The method consists in using a centrifuge with suspended glasses (swinging bucket centrifuge), in which the centrifugal force G (in contrast to the standard spin-coating method) is directed perpendicular to the sample plane, which makes it possible to effectively encapsulate arrays of NWs), pressing the polymer matrix into the space between the NWs. (**Figure 23**).

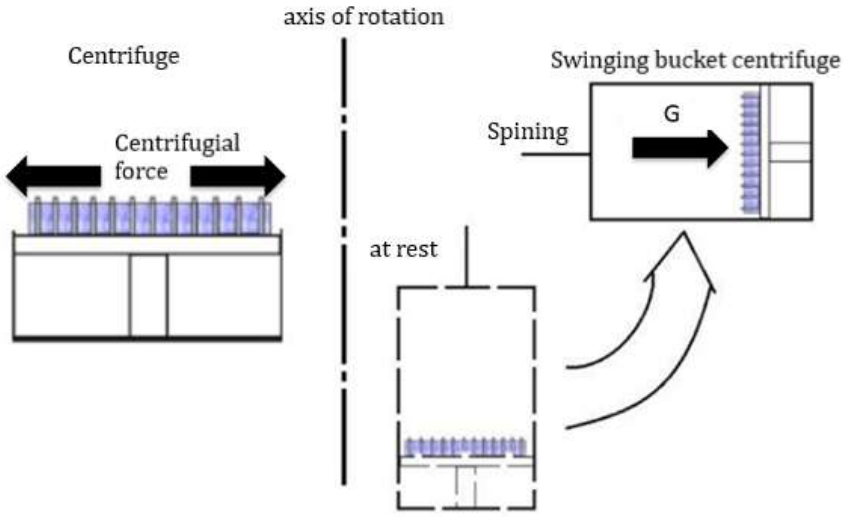

Figure 23 – Scheme of NW array encapsulation in SSR by centrifugation and G-coating [35]

The described method allows to effectively encapsulate arrays of NWs in a silicone matrix. When using this method, the orientation of the NWs is preserved, and the thickness of the polymer membrane corresponds to the length of the NWs (**Figure 24**). According to the analysis of the obtained SEM images, SSR25 and MSR25 completely cover the arrays of n-GaP NWs, leaving only the upper ends of the nanostructures uncovered, to which electrical contacts are further formed (**Figure 24**). Moreover, thickness of the encapsulating layer corresponds to the average height of the NW and is about 4 μm. This thickness is sufficient for further effective separation of the membrane from the growth substrate without mechanical damage to the membrane itself.

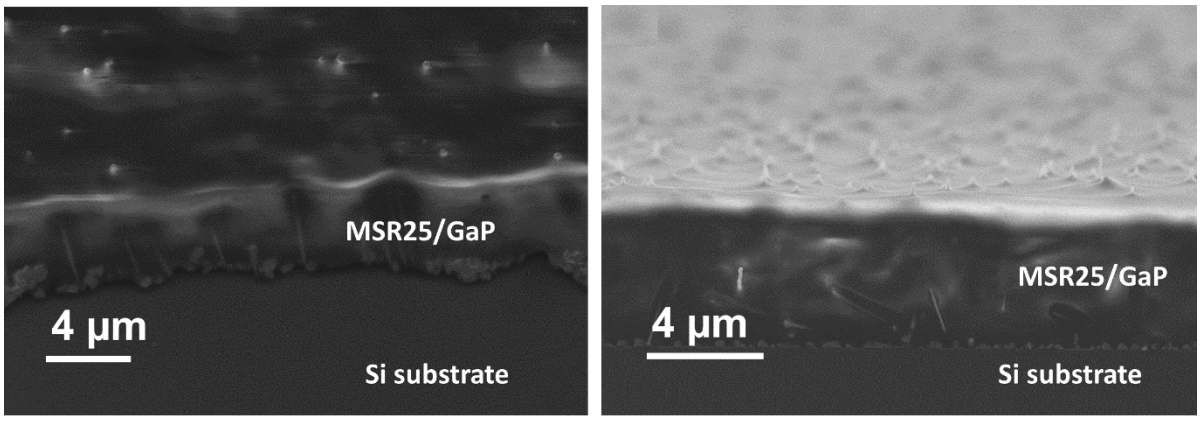

Figure 24 – SEM images of the cross section of MSR25 and SSR25 membranes with encapsulated arrays of n-GaP NWs on a Si substrate

Thus, it was shown that MSR25 and SSR25 have a high encapsulating ability and can be further used as supporting matrices for optoelectronic devices based on A3B5 NW arrays.

2.1.4 Swelling properties of SSR and MSR

SSR and MSR swell in organic solvents (benzene, toluene, dichloromethane), but do not dissolve in them. This makes it possible to determine the cross-linking parameters of SSR and MSR by swelling in a solvent, for which toluene was chosen. Swelling was carried out at 110°C in a Soxhlet extractor for 2 h. In this case, the density (ρ) of SSR and MSR was preliminarily estimated by pycnometry (**Table 2**).

Sylgard 184 silicone composition was chosen as a reference sample for studying the swelling parameters, which was pre-cured by the catalytic hydrosilylation reaction at 80 °C for 12 hours. Also, as a reference sample, an opaque silicone composition based on PDMS-*graft*-PSt[2], previously used in the literature for the encapsulation of arrays of NWs [35].

For the studied silicone rubbers, there is a regular direct relationship between the values of the swelling percentage (*s)* and soluble fraction content (w_{sol}), as well as an inverse relationship between the values of w_{sol} and the fraction of the polymer in the swollen sample (υ), υ and the average molecular weight of the segment between the cross-links (M_c) (**Table 2**). The cross-linking degree (ρ_{cross}) and M_c were calculated for each sample according to the Flory-Röner equations [112].

SSR25 has the highest values of υ and ρ_{cross} both in the SSR25-MSR25-SSR50 series and in comparison with Sylgard 184 and PDMS-graft-PSt. M_c values increase in the series: SSR25-MSR25-

[2]Measurements of the swelling parameters of PDMS-*graft*-PSt were carried out in the framework of the presented dissertation work.

SSR50. SSR25 has similar values of average molecular weight of the segment between the cross-links M_c and fraction of the polymer in the swollen sample υ with Sylgard 184.

Table 2 – Swelling parameters SSR and MSR

Sample	ρ, g·cm^{-3}	s, %	w_{sol}, %	υ	ρ_{cross}, mmol·cm^{-3}	M_c
Sylgard 184	1.00	190±21	4.1±0.4	0.48±0.01	11.6	865
PDMS-*graft*-PSt (40% styrene)	1.16	212±22	5.5±0.4	0.37±0.02	5.00	2316
SSR25	1.21	166±20	3.0±0.7	0.50±0.01	13.3	910
MSR25	1.05	281±13	10.0±0.6	0.30±0.01	3.2	3716
SSR50	1.11	340±12	16.5±1.5	0.16±0.02	0.50	22298

Thus, among the synthesized silicone rubbers, SSR25 has the closest values of ρ_{cross} and M_c to the Sylgard 184 and can be used as its analogue. The relatively high degree of crosslinking is explained by the high content of Si–H groups in the initial S–PMHS50 compared to S–PMHS75, which were used to synthesize SSR25 and SSR50, respectively. However, MSR25 is inferior to SSR25 in its ρ_{cross} value, which may be due to the steric factor (the effect of different volume/size of substituents).

2.1.5 Tensile properties of SSR and MSR

Since the main method for separating NW/PDMS membranes is peeling-off with a blade, the silicone matrix must have not only low adhesion to the growth silicon substrate, but also a relatively high mechanical strength. In this regard, a study of the mechanical characteristics of the obtained SSR and MSR was carried out. The investigated silicone rubbers are characterized by a range of elongation at break (ε) from 45 to 130%. Other important characteristics are tensile strength (σ) and Young's modulus (E). According to **Table 3** and **Figure 25** the values of ε increase in the series SSR25–MSR25–SSR50, while the values of σ and E decrease in this series. These results are in full agreement with the above described swelling properties of the samples and the calculated degrees of cross-linking. SSR50 have a lower degree of cross-linking compared to SSR25 (ρ_{cross} = 3.2 mmol·cm^{-3} and ρ_{cross} = 13.3 mmol·cm^{-3}, respectively), which contributes to a decrease in the values of σ and E and an increase in the parameter ε.

According to the tensile diagram shown in **Figure 25** and **Table 3**, SSR50 has a relatively high elongation at break (ε = 130%) and lower tensile strength (σ = 0.2 MPa) compared to the commercially

available Sylgard 184 (ε = 92%, σ = 2.4 MPa) and previously described [35] PDMS-*graft*-PSt (ε = 90%, σ = 1.9 MPa)[3].

Table 3 – Mechanical properties of SSR and MSR

Sample	Tensile properties		
	E,[a)] MPa	σ, MPa	ε, %
Sylgard 184	1.1±0.3	2.4±0.6	92±8
PDMS-*graft*-PSt (40% of styrene)	1.9±0.3	1.9±0.6	90±29
SSR25	3.4±0.7	1.5±0.4	45±5
MSR25	0.6±0.1	0.6±0.1	90±19
SSR50	0.2±0.7	0.2±0.1	130±20

[a)] Young's modulus was determined in the range of 1–5% strain (40 mm/min).

SSR25 is slightly inferior in its strength characteristics (σ = 1.5 MPa) Sylgard 184 and PDMS-*graft*-PSt (σ = 2.4 MPa and σ = 1.9 MPa, respectively), however, it has a large Young's modulus (E = 3.4 MPa instead of 1.1 MPa and 1.9 MPa, respectively). High values of the Young's modulus are an important factor in the separation of thin films from the growth silicon substrate, as they ensure the resistance of the SSR25/NWs membrane to deformations and ruptures. [35]. Together with reduced adhesion and optical transparency, the mechanical properties of SSR25 make it possible to distinguish it among the silicone rubbers studied in this work as the most promising material for a flexible supporting matrix for NWs arrays.

[3] Measurements of the mechanical characteristics of PDMS-*graft*-PSt were carried out within the framework of the presented dissertation work.

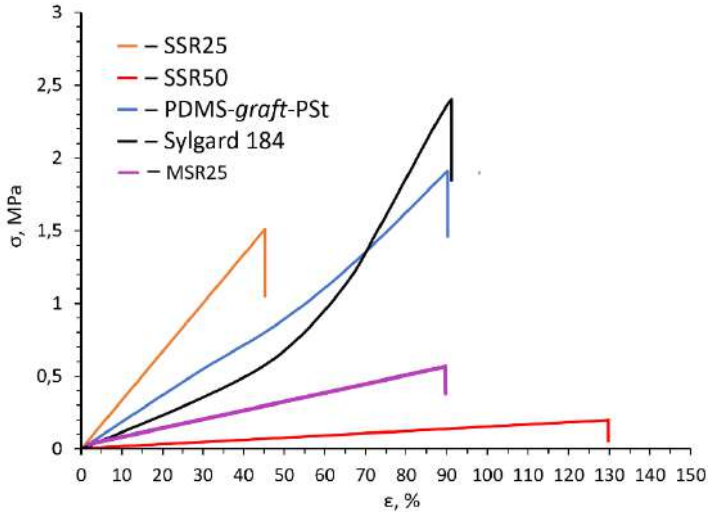

Figure 25 – Tensile mechanical properties of silicone rubber: curves stress–strain at a strain rate of 40 mm·min^{-1}. Sample form according to ISO 37 type 3

Thus, the use of SSR25 to encapsulate NW arrays makes it possible to create relatively strong and flexible membranes, which, due to their adhesive properties, can be easily separated from the Si substrate, while ensuring complete transfer of NWs into the membrane.

2.1.6 Thermal characteristics of SSR and MSR

TG analysis has shown temperature of decomposition ($T_{1\%}$ is the temperature at which the sample loses 1% of its mass) for SSR and MSR in air and argon is equal to 210 °C and 220 °C, respectively, which are characteristic values for cross-linked silicone materials based on PDMS [2,6]. A 10% loss of mass ($T_{10\%}$) for MSR25, SSR50 and SSR25 in experiments in air occurs at 377 °C, 394 °C and 400 °C, respectively, and in an argon atmosphere at 330 °C, 390 °C and 395 °C, respectively. According to TG curves, SSR25 and SSR50 have a higher $T_{10\%}$ compared to MSR25 presumably due to the impact of phenylethyl substituents, which could help increase the thermal stability of PDMS [18].

Thus, in the case of thermal treatment in air at 750 °C, approximately 8–30% more mass remains than during heat treatment in an interstate atmosphere. The residual masses at 750 °C for MSR25, SSR50 and SSR25 after TG in air were 46, 50 and 61%, and in an inert atmosphere of argon 13, 35 and 53%, respectively (**Figure 26**).

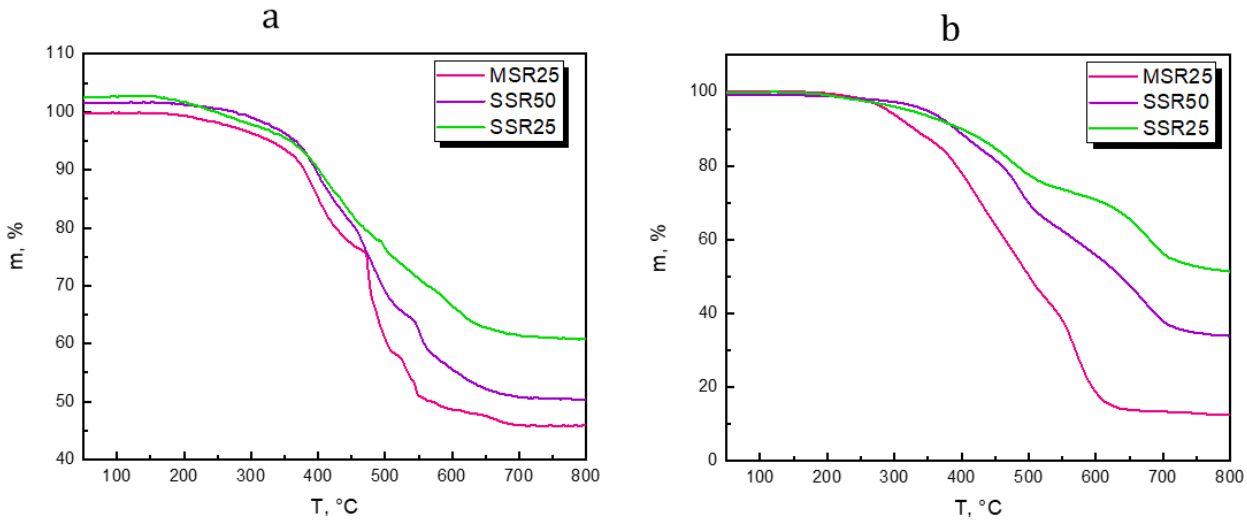

Figure 26 – TG curves of SSR 25, SSR 50, MSR 25 in air and in an inert atmosphere of argon

The mechanism of thermal decomposition is described in detail in the literature and includes radical depolymerization of polysiloxane chains and radical dehydrocoupling reaction [6,113–115]. The different results in an inert atmosphere and in air are explained by the mechanism of thermal decomposition. In experiments in air, the residual mass is higher than in an argon atmosphere due to two factors. Firstly, oxygen promotes the formation of new cross-links through the mechanisms of dehydrocoupling and oxidative dehydrocoupling, which leads to less weight loss. Secondly, during decomposition in air the main component of the residual mass is SiO_2, and in an argon atmosphere it is Si or SiC [6].

2.1.7 SSR25 Employement as Encapsulating Support Matrix

Flexible, transparent and strong SSR25/NWs membranes were used as a flexible base for a hybrid green LED. GaP NWs have excellent electrical properties of charge transport and can be doped to n- and p-types of conductivity. At the same time, due to its indirect-gap nature, this semiconductor material is completely transparent in the visible and near-IR ranges. [116]. GaP NWs are also capable of withstanding mechanical deformations during bending due to their high length-to-diameter ratio. Thus, membranes based on arrays of GaP NWs partially encapsulated in a silicone matrix can provide both good mechanical support for the entire structure of a light-emitting diode and efficient electrical contact with perovskite. Metal halide perovskite $CsPbBr_3$ is a widely used and effective light-emitting material in perovskite optoelectronics, with a band gap Eg=2.31 eV and pronounced photoluminescence in the green spectral region.

In contrast to perovskite LEDs with standard architecture, the use of SSR25/n-GaP NW membranes as a distributed electrode makes it possible to increase the thickness of the perovskite layer

(the standard thickness of the perovskite layer is 400−500 nm). This potentially results in an increase in the volume of light-emitting material and, therefore, in the intensity of light emission without increasing recombination losses.

Metal halide perovskite $CsPbBr_3$ in a polyethylene oxide (PEO) mixture serving as the perovskite crystallization matrix was spin-coated over the obtained SSR25/n-GaP NW membrane. To form external electrical contacts, pads of SWCNT layers with a transparency of 90% [117] were deposited on the lower part of the SSR25/n-GaP NWs membrane (contact to NWs array) nd directly on the front side of the perovskite layer. The schematic diagram of the LED structure and a cross-sectional SEM image of the LED structure are shown in **Figure 27**.

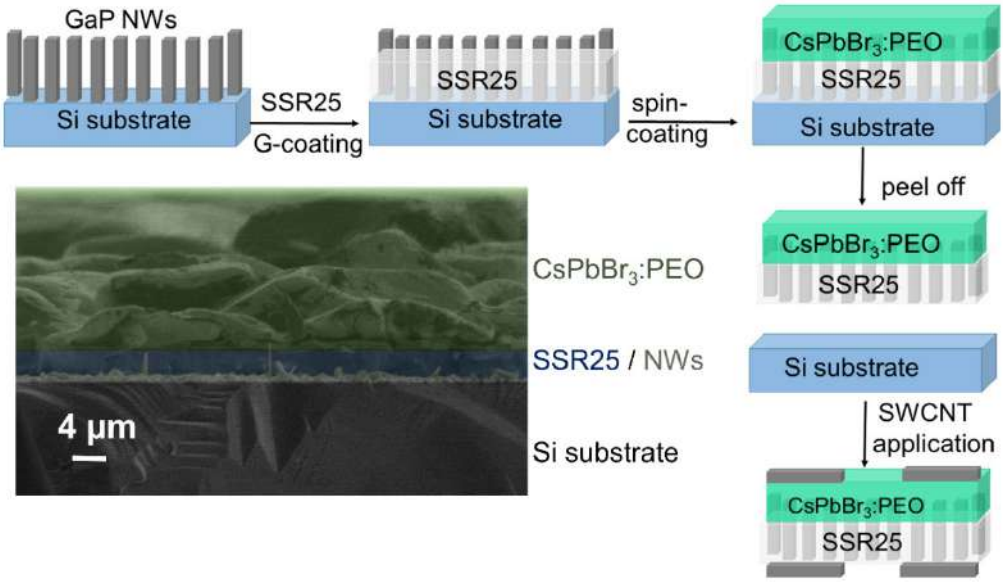

Figure 27 – Scheme a flexible SSR25/n-GaP NWs/$CsPbBr_3$/SWCNT PLED fabrication and cross-sectional SEM image of the structure on a Si substrate before separation

To study the electrical properties of the fabricated LED samples, the I-Vcurves was measured after bending and relaxation. According to the measurement results, the I-Vcurves has a typical diode character (**Figure 28 (b)**). This indicates the absence of electrical shunts and other membrane defects leading to current leakage. The operating voltage of the LED is 5 V, which is a typical value for a $CsPbBr_3$:PEO PLED [118,119] and confirms the absence of high potential barriers for the majority charge carriers at the NW/SWCNT, NW/perovskite, and perovskite/SWCNT interfaces.

An optical image of a hybrid LED operating at an applied external voltage of 5 V and the corresponding electroluminescence (EL) spectrum are shown in **Figure 28 (a)**. The observed spectral position of the EL peak at about 538 nm corresponds to an optical transition in $CsPbBr_3$ [119], which confirms the efficient injection of holes and electrons into the perovskite layer through the upper areas of SWCNTs and n-GaP NWs, respectively.

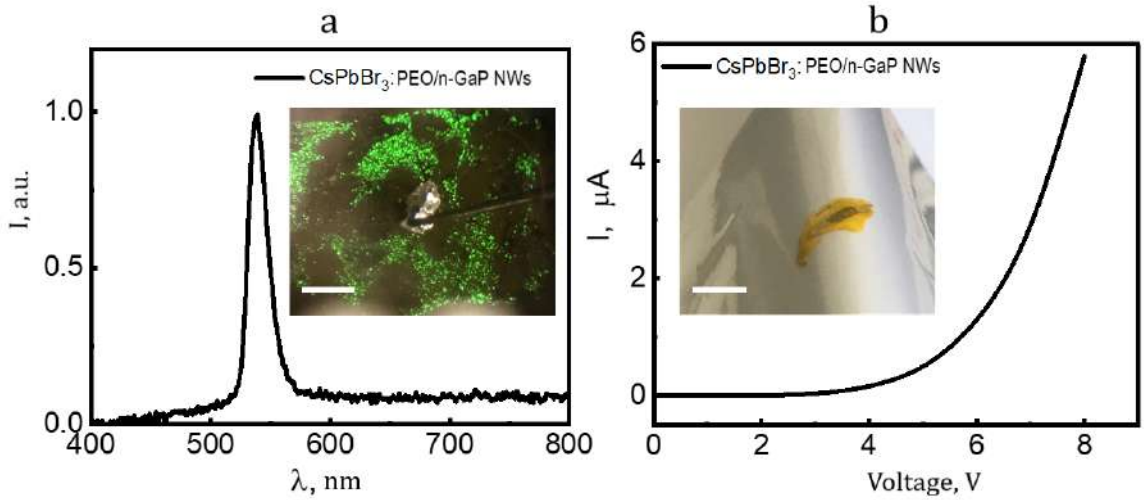

Figure 28 – EL spectrum and optical image of a hybrid LED operating with an applied **(a)** external electrical voltage of 5 V (scale bar 2 mm). I-Vcurves and optical image of a hybrid LED (scale bar 10 mm) **(b)**

It should be noted that the PLED continues to operate at reasonable applied voltages (less than 8 V) after 30 bending cycles (bending was performed manually) (**Figure 29**). In this case, the deformation of the membrane during bending, defined as the ratio of the thickness of the membrane to the radius of curvature, is approximately 2%. The instability of contacts between the SWCNT layers and the perovskite layer or NW bases during membrane bending leads to a slight increase in the opening voltage of the diode structure, a decrease in current, and, as a result, to only a slight deterioration in the PLED characteristics.

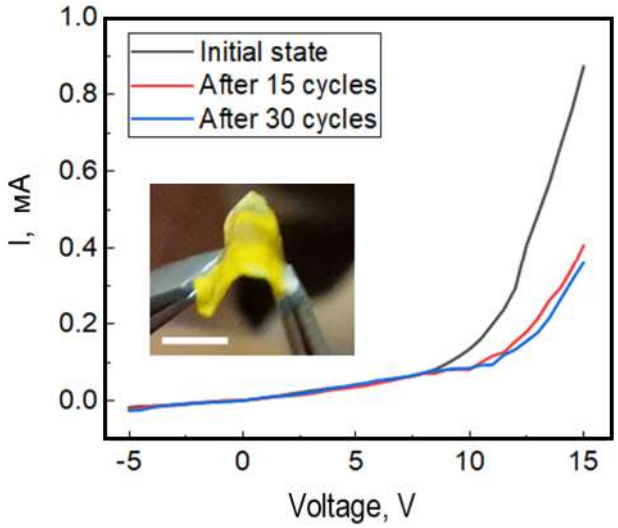

Figure 29 – I-Vcurves of the PLED in the initial state and after 15 or 30 bending cycles. The inset shows an optical image of a curved PLED membrane. Scale bar 1cm. Membrane deflection in bending, defined as the ratio of the membrane thickness to the radius of curvature, is approximately 2%

In conclusion to this chapter, it can be noted that transparent silicone rubbers MSR25, SSR25 and SSR50 were obtained. The substitution of 50% of the hydride groups of PMHS with 2-methyl-3-methoxy-3-oxopropyl and phenylethyl functional groups (MSR25 and SSR25) reduces the adhesion to the growth substrate by about 2 times relative to Sylgard 184. Cross-linking with *v*-PDMS makes it possible to give the material improved tensile strength up to $\sigma = 1.5$ MPa (SSR25) and elasticity up to $\varepsilon = 90\%$ (MSR25). SSR25 has a high Young's modulus $E = 3.4$ MPa compared to MSR25 and Sylgard 184, which makes it possible to separate thin SSR25 membranes with encapsulated NW arrays from the growth silicon substrate without damage. Thus, SSR25/NWs membranes can be used in flexible light-emitting diodes with a new architecture as a flexible distributed electrode to a layer of light-emitting perovskite and SWCNT electrical contacts. For the first time, a flexible, air-stable PLED with the SSR25/n-GaP/$CsPbBr_3$/SWCNT architecture was presented, demonstrating electroluminescence in the green region of the spectrum (538 nm) at an operating voltage of 5 V. The PLED is able to maintain its performance characteristics after 30 bending/relaxation cycles.

The results of the presented study were published:

- Miroshnichenko A.S, Deriabin K.V., Baeva M., Kochetkov F.M., Neplokh V., Fedorov V.V., Mozharov A.M., Koval' O., Krasnikov D.V., Sharov V.A., Filatov N.A., Gets D.S., Nasibulin A.G., Makarov S.V., Mukhin I.S., Kukushkin V.Y., Islamova R.M. Flexible perovskite $CsPbBr_3$ light emitting devices integrated with GaP nanowire arrays in highly transparent and durable functionalized silicones // Journal of Physical Chemistry Letters. – 2021. – V. 12. – №39 – P. 9672–9676. DOI: 10.1021/acs.jpclett.1c02611.

- Miroshnichenko A.S., Deriabin K.V., Mukhin I.S., Islamova R.M. Low-adhesive silicone rubbers for flexible light-emitting devices // St. Petersburg Polytechnical University Journal: Physics and Mathematics. – 2022. – V. 15. – № 3 – P. 320–325. DOI: 10.18721/JPM.153.363

.

2.2 Polymer metal complexes based on bipyridinedicarboxamide-*co*-polydimethylsiloxanes and Eu^{3+}, Tb^{3+}

2.2.1 Preparation of Eu-Bipy-PDMS and Tb-Bipy-PDMS

Self-healing luminescent silicone rubbers based on lanthanide(III) polymer metal complexes were obtained. The polymeric ligands of 2,2'-bipyridine-6,6'-dicarboxamide-*co*-polydimethylsiloxanes (Bipy-PDMS5000 and Bipy-PDMS25000) were synthesized by a polycondensation reaction between 2,2'-bipyridine-6,6'-dicarboxylic acid dichloride and *α,ω*-di(3-aminopropyldimethylsiloxy)polydimethylsiloxanes (APDMS) with a number average molecular weight M_n = 5000 and 25000, respectively. Cross-linked silicone materials were obtained by the reaction of complex formation of Bipy–PDMS obtained by and the chloride of the corresponding lanthanide(III) — $EuCl_3$ and $TbCl_3$ (**Figure 30**).

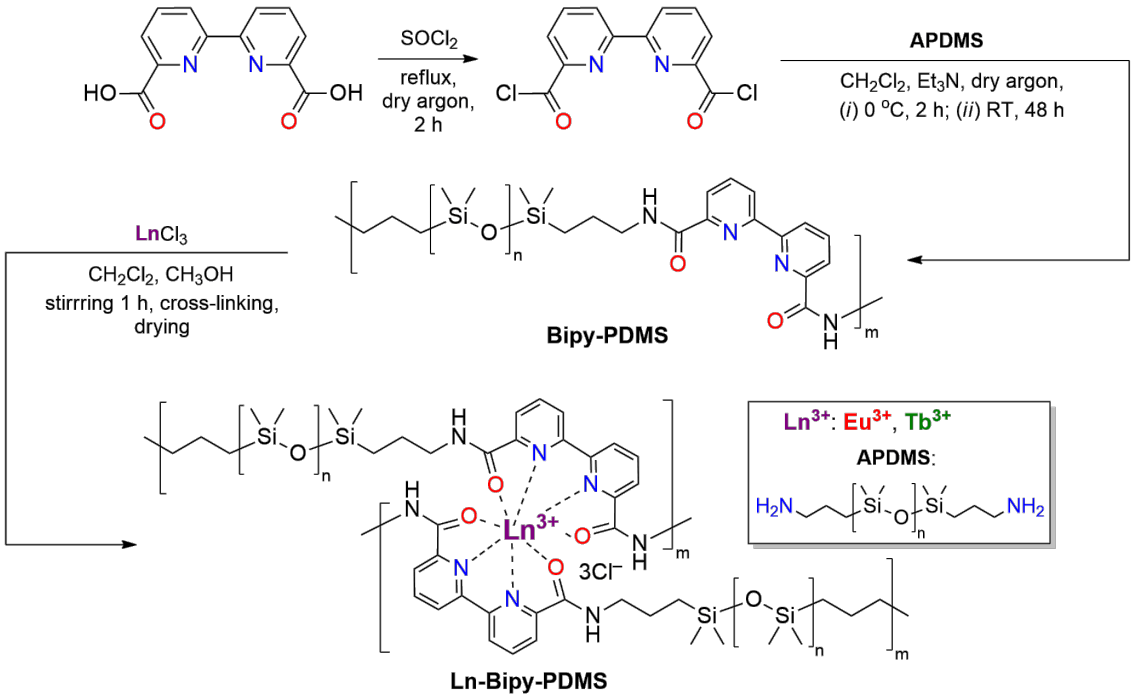

Figure 30 – Scheme of Ln-Bipy-PDMS synthesis

The structure of Bipy-PDMS was confirmed by ^1H and ^{13}C NMR spectroscopy. At ^1H NMR spectrum (**Figure 31**) there is a signal at δ = 8.17 ppm, corresponds to -$CH_2CH_2CH_2N\boldsymbol{H}C(=O)$-, and the signal of amino groups at δ = 1.26 ppm is almost completely absent. At ^{13}C NMR spectrum a signal is observed at δ = 163.9 ppm which belongs to the carbonyl carbon of the -NH***C***(=O) - group.

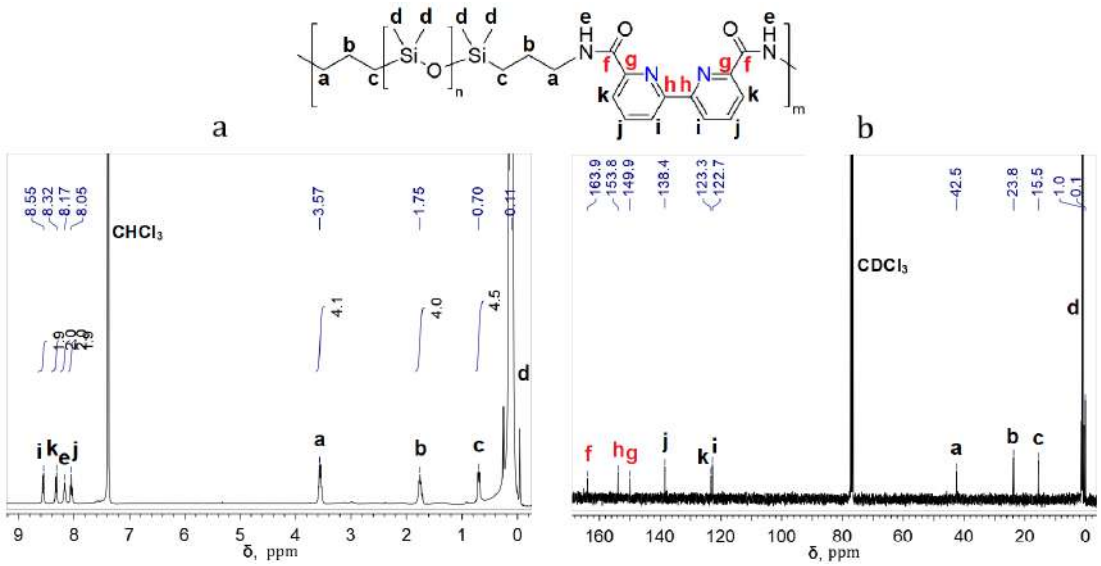

Figure 31 – ^{1}H NMR **(a)** and ^{13}C NMR **(b)** spectra of Bipy-PDMS5000

At the second stage, complex formation reactions of the obtained Bipy–PDMS were carried out with anhydrous lanthanide(III) chlorides ($EuCl_3$ and $TbCl_3$), which were added in a molar ratio of lanthanide:bipyridine fragment equal to 1:2. The reaction proceeded at room temperature (21 °C) in a solution of a mixture of anhydrous dichloromethane and methanol for 1 h. Then, the PMC was cured in a PTFE mold at room temperature (21 °C) for 24 h in air followed by drying at 100°C for 24 h.

2.2.2 Structure of Eu-Bipy-PDMS and Tb-Bipy-PDMS

The structure of the PMC was studied by IR spectroscopy using the example of Eu–Bipy–PDMS5000. At the IR spectra of Eu–Bipy–PDMS5000 the bands *C=O* (amide I) at 1646 cm^{-1} and N–H (amide II) at 1550 cm^{-1} (**Figure 32**). Practically similar bands were observed in the IR spectrum of the initial ligand Bipy–PDMS5000. According to the IR spectra of Eu–Bipy–PDMS5000, the *C=O* fragment participates in coordination with the metal center. No –OH vibration (3200–3600 cm^{-1}) signal was found on the PMCs spectra, which indirectly indicates the absence of water (**Figure 32**).

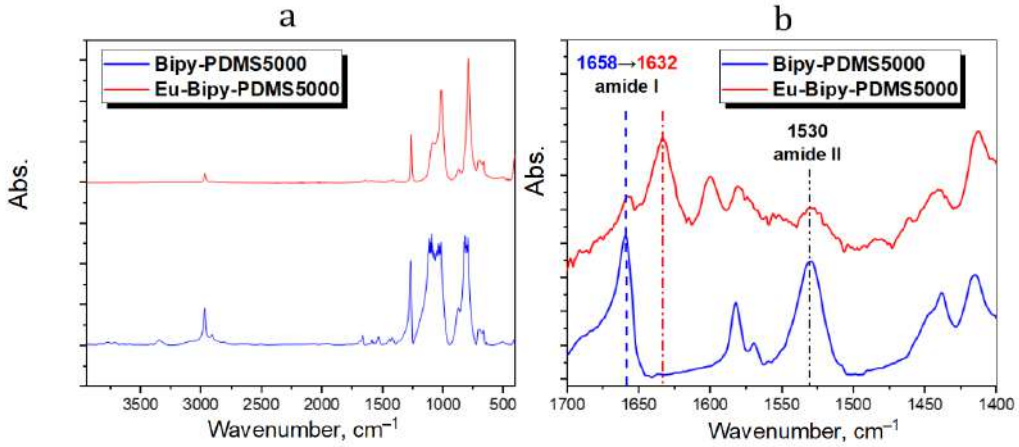

Figure 32 – FTIR spectra of Bipy–PDMS5000 and Eu–Bipy– PDMS5000 in range of 400–4000 cm^{-1} **(a)** and 1400–1700 cm^{-1} **(b)**

The FTIR spectra of Tb–Bipy–PDMS5000 presumably have a similar shape due to similar type of metal center nature. However, the above is an indirect evidence of the structure of the studied PMCs. To establish the Ln–Bipy–PDMS structure, model complexes with low molecular weight were synthesized.

2.2.2.1 Model lanthanide-containing complexes

Low molecular weight model complexes $[Eu(BDCA)_2(H_2O)]Cl_3$ and $[Tb(BDCA)_2(H_2O)]Cl_3$ were synthesized at room temperature from *N*^{6},*N*^{6}–diisopropyl–2,2'–bipyridine–6,6'-dicarboxamide (BDCA) and anhydrous europium(III) and terbium(III) chlorides using the same solvents (dichloromethane and methanol) as in the preparation of the PMC (**Figure 32).**

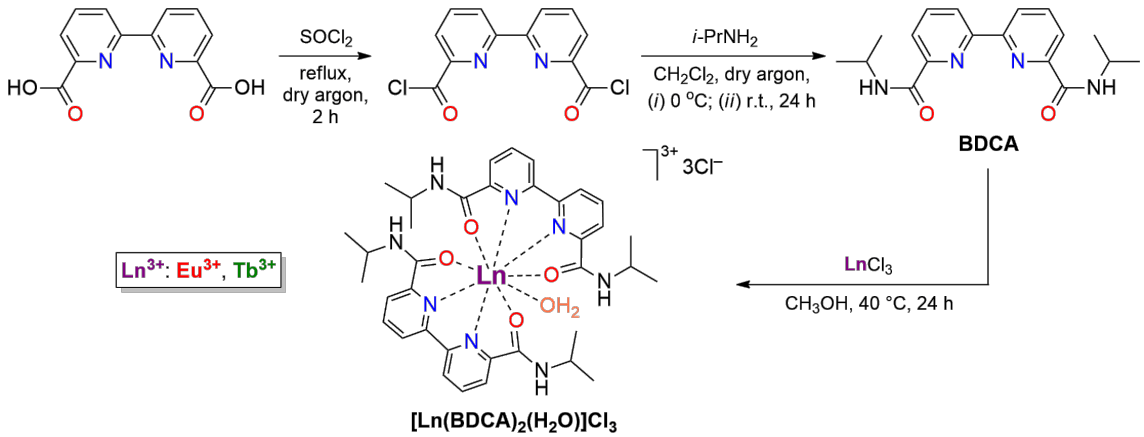

Figure 33 – Scheme of model complexes $[Eu(BDCA)_2(H_2O)]Cl_3$ and $[Tb(BDCA)_2(H_2O)]Cl_3$ synthesis

Low molecular weight model complexes were characterized by X-ray diffraction analysis (XRD) and high resolution mass spectrometry (HRESIMS). The XRD study of model complexes [120] showed that Eu^{3+} and Tb^{3+} coordination with ligand proceed *via* lanthanide-N_{Bipy} (Ln–N_{Bipy}, Ln: Eu, Tb) and lanthanide–$O_{carboxyl}$ (Ln–O) bonds. As in the case of PMC, complex formation between BDCA and Ln^{3+} occurs due to the binding of *O,N,N,O*- chelating fragments. Thus, taking into account the coordination number 9 Ln^{3+}, the metal–ligand molar ratio as 2:1 was suggested. The europium and terbium complexes have the same nine-vertex polyhedron geometry and distorted pentagonal coordination formed by oxygen atoms in the equatorial position and nitrogen atoms along the tetragonal tetrahedron in apical positions. This coordination polyhedron contains 2nd order crystallographic axes passing through the metal atom and the coordinated water molecule (**Figure 33**).

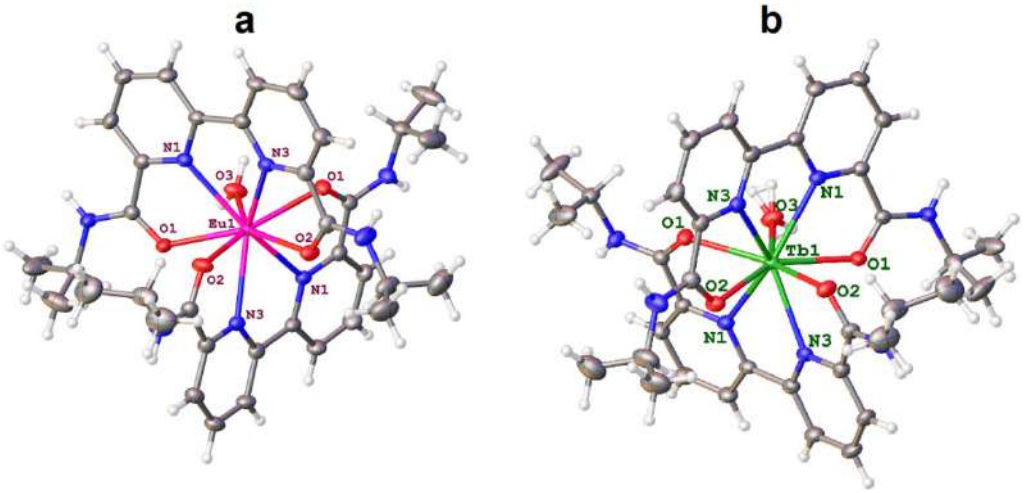

Figure 34 –Molecular structures of $[Eu(BDCA)_2(H_2O)]Cl_3$ **(a)** and $[Tb(BDCA)_2(H_2O)]Cl_3$ **(b)**. The Cl^- anions and water molecules are omitted for better representability

In the HRESIMS spectra, the $[Eu(BDCA)_2]^{3+}$ (*m/z* = 268.4233) and $[Tb(BDCA)_2]^{3+}$ ions (*m/z* = 270.4241) were indicated with their characteristic isotopic distribution (**Figure 34**).

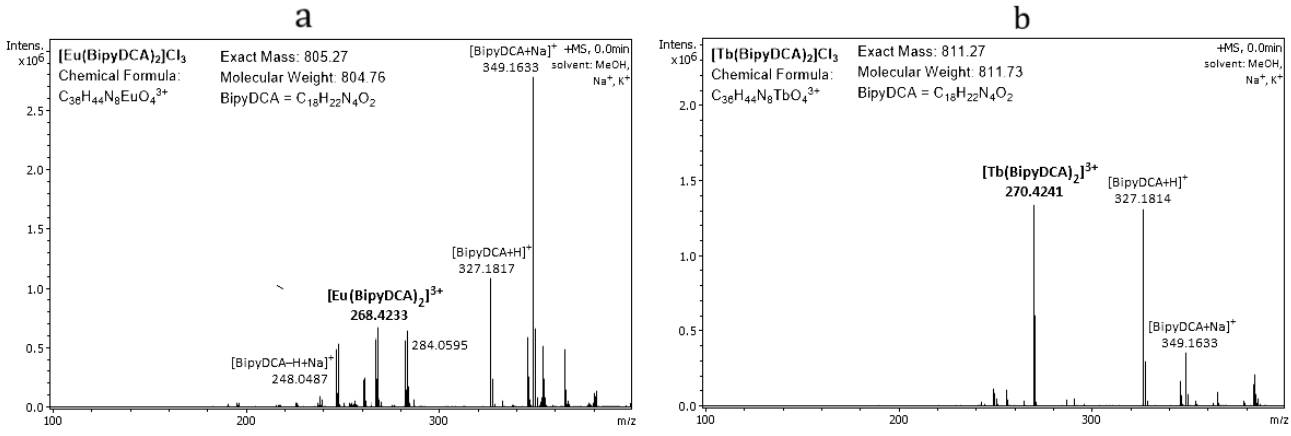

Figure 35 – HRESIMS spectra of $[Eu(BDCA)_2(H_2O)]Cl_3$ **(a)** and $[Tb(BDCA)_2(H_2O)]Cl_3$ **(b)**

Structure of $[Eu(BDCA)_2(H_2O)]Cl_3$ and $[Tb(BDCA)_2(H_2O)]Cl_3$ was also confirmed by IR-spectroscopy. In the FTIR spectra of $[Eu(BDCA)_2(H_2O)]Cl_3$ and $[Tb(BDCA)_2(H_2O)]Cl_3$ the amide I ν(C=O) band was shifted from 1653 to 1631 cm^{-1} in comparison with the BDCA (**Figure 35**). Such shifts are similar to those observed in the IR spectra of Eu–Bipy–PDMS (**Figure 32**).

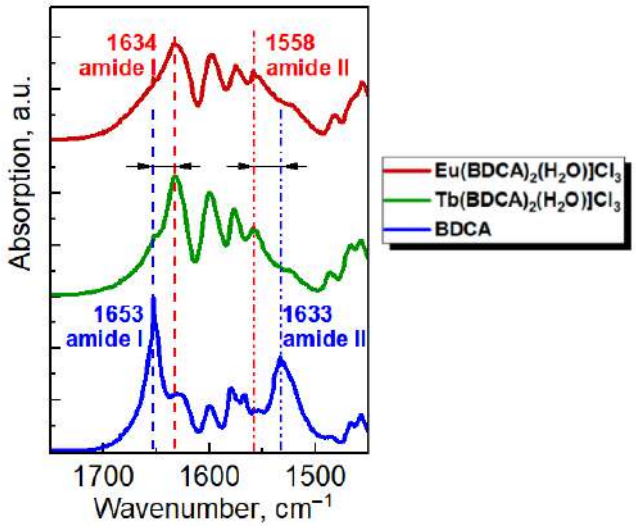

Figure 36 – FTIR spectra of $[Eu(BDCA)_2(H_2O)]Cl_3$, $[Tb(BDCA)_2(H_2O)]Cl_3$ and BDCA in range of 1450–1750 cm^{-1}

Thus, the analysis of the IR-spectra data showed that the ligand environment of the Ln^{3+} coordination centers in Ln–Bipy–PDMS is similar to that in the model complex.

UV-spectroscopy of low molecular weight model complexes. In the UV-vis spectra of $[Eu(BDCA)_2(H_2O)]Cl_3$ and $[Tb(BDCA)_2(H_2O)]Cl$ a peak at 291 nm (with two shoulders at 283 and 302 nm) are observed (**Figure 37, a**). According to quantum chemical calculations and simulations based on the time-dependent density functional theory (TD-DFT) [120], this band in the UV spectrum corresponds to ligand-to-metal charge transfer (LMCT) between BDCA and Ln^{3+} in $[Eu(BDCA)_2(H_2O)]Cl_3$ and $[Tb(BDCA)_2(H_2O)]Cl_3$ (**Figure 37 b**).

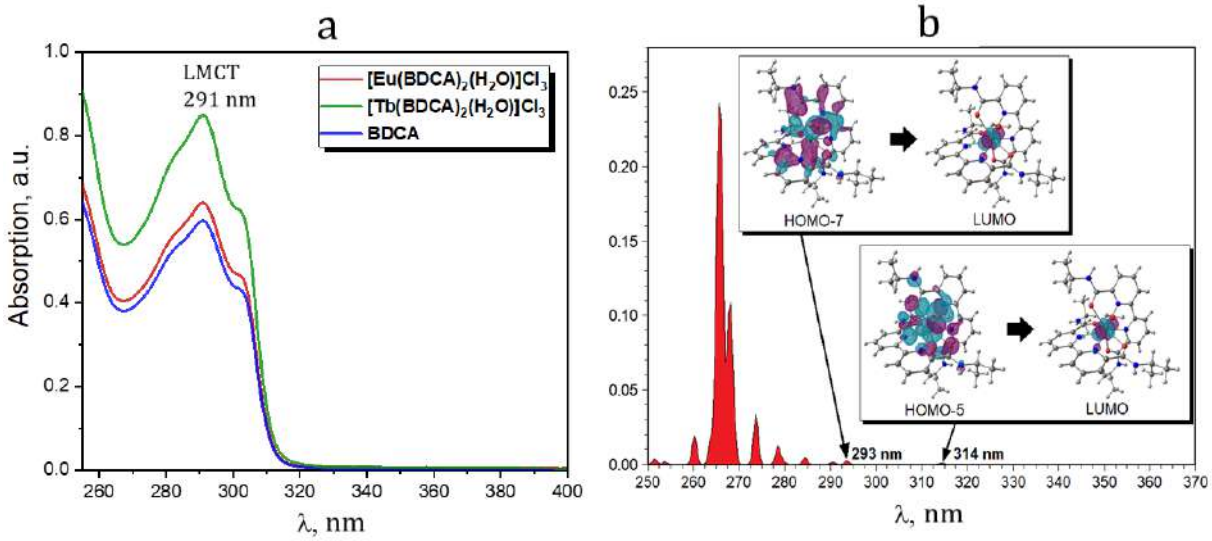

Figure 37 – UV absorption spectra of 0.001 M solutions of $[Eu(BDCA)_2(H_2O)]Cl_3$, $[Tb(BDCA)_2(H_2O)]Cl_3$ and in DMSO in the range of 255–400 nm (cell width 1 cm) **(a)** and calculated TD-DFT UV-visible absorption spectrum of $[Eu(BDCA)_2(H_2O)]Cl_3$ **(b)**

Energies of coordination bonds in Eu–Bipy–PDMS and Tb–Bipy–PDMS. To determine the energies of coordination bonds, quantum-chemical calculations were also carried out (at the level of theory ωB97XD/6-31+G, QTAIM method [121]) with the involvement of model optimized structures $[Eu(BDCA)_2(H_2O)]Cl_3$ and $[Tb(BDCA)_2(H_2O)]Cl_3$.[4] The calculated bond energies of $Eu–O_{carboxyl}$, $Eu–N_{Bipy}$, Eu–Cl, $Tb–O_{carboxyl}$ and $Tb–N_{Bipy}$ are given in **Table 4**.

Table 4 – Calculated parameters of $Eu–O_{carboxyl}$, $Eu–N_{Bipy}$, Eu–Cl, $Tb–O_{carboxyl}$ and $Tb–N_{Bipy}$ coordination bonds in optimized equilibrium model structures

Model structure	Bond	Binding energy, E_{int}, kcal·mol^{-1}	Bond length, l, Å
$[Eu(BDCA)_2(H_2O)]Cl_3$	Eu–O	12.6	2.214
	Eu–O	15.7	2.214
	Eu–O	15.7	2.136
	Eu–O	15.1	2.136
	Eu–O	15.1	1.992
	$Eu–N_{Bipy}$	11.3	2.121
	$Eu–N_{Bipy}$	11.3	2.121
	$Eu–N_{Bipy}$	11.6	2.060
	$Eu–N_{Bipy}$	11.6	2.060
$[Tb(BDCA)_2(H_2O)]Cl_3$	Tb–O	12.9	2.444

[4] Quantum-chemical calculations were carried out by Ph.D., senior researcher. A.S. Novikov at the Department of Physical Organic Chemistry, Institute of Chemistry, St. Petersburg State University.

	Tb–O	16.0	2.381
	Tb–O	16.0	2.381
	Tb–O	15.1	2.389
	Tb–O	15.1	2.389
	Tb–N_{Bipy}	11.6	2.517
	Tb–N_{Bipy}	11.6	2.517
	Tb–$N_{Bipy'}$	11.9	2.512
	Tb–$N_{Bipy'}$	11.9	2.512

In $[Eu(BDCA)_2(H_2O)]Cl_3$ the Eu–N_{Py} coordination bonds have a shorter length and higher energies (about 1.5 times) compared to the (**Table 4**). Both ligands are equally bound to the Eu^{3+} metal center (Eu–N_{Bipy} bond energies are 11.3 and 11.6 kcal mol^{-1}), which may be the reason for the high strength of Eu–Bipy–PDMS under mechanical deformation and lead to a non-autonomous self-healing mechanism. Analogously, in $[Tb(BDCA)_2(H_2O)]Cl_3$, Tb–N_{Bipy} bond have a shorter length and 1.5 times higher energies than bonds Tb–$O_{carboxyl}$ (**Table 4**). Both ligands are also equally bound to the Tb^{3+} metal center the Tb–N_{Bipy} bond energies are 11.6 and 11.9 kcal/mol).

According to the data of IR, UV, HRESIMS spectra, as well as XRD, it can be concluded that the formation of PMC based on Eu^{3+} and Tb^{3+} occurs through the coordination bonds of lanthanide–N_{Bipy} and lanthanide–$O_{carboxyl}$ and, probably, one H_2O molecule is also present in the structure of PMC. Presumably, the structure of the PMC is a combination of homo- (Eu^{3+} or Tb^{3+} coordinated only with Bipy–PDMS polymer ligands) and heteroleptic complexes (Eu^{3+} or Tb^{3+} coordinated with Bipy-PDMS polymer ligands, as well as Cl^- and H_2O)[120]. An equilibrium is observed between homoleptic and heteroleptic complexes in three-dimensional Eu–Bipy–PDMS and Tb–Bipy–PDMS polymer networks. Apparently, heteroleptic complexes transform into homoleptic complexes when heated to 100 °C, which corresponds to the self-healing temperature of the PMC. In turn, homoleptic complexes transform into heteroleptic ones at room temperature, absorbing moisture from the air.

Thus, it has been proven that the Bipy–PDMS polymeric ligands are coordinated with the metal center via the Ln–N_{Bipy} and Ln–$O_{Carboxyl}$ bonds due to the presence of *O,N,N,O*-chelating fragments and *C=O* groups in *ortho*-position. This coordination makes it possible to introduce a larger amount of Ln^{3+} into the PMC (the ligand–metal molar ratio is 2:1) compared to the previously known Ln–Py–PDMS. [2]. This leads to the formation of approximately 1.5 times more coordination cross-links between Bipy–PDMS chains compared to Ln–Py–PDMS.

2.2.3 Mechanical and thermal properties of Ln–Bipy–PDMS

Tensile tests showed that the investigated PMCs have relatively high strength characteristics σ and E and reach values of 1.6 and 3.6 MPa, respectivelyAt the same time, ε, whose values are quite high and reach (185–255)%, is less than those described in the literature Ln–Py–PDMS [2] (**Table 5**). The use of BDCA as a ligand makes it possible to introduce a larger amount of Ln^{3+} and, as a result, leads to the formation of a larger number of coordination crosslinks between the Bipy–PDMS chains, which contributes to an increase in the relative tensile strength.

Table 5 – Tensile properties [a)] of Eu-Bipy-PDMS and Tb-Bipy-PDMS

Samle	Lanthade content,[b)] wt.%	E,[c)] MPa	σ, MPa	ε, %
Eu – Bipy–PDMS5000	3.9±0.5	3.6±0.13	1.55±0.09	185±12
Eu – Bipy–PDMS25000	0.4±0.2	0.5±0.04	0.10±0.09	220±27
Tb – Bipy–PDMS5000	2.7±0.3	3.6±0.13	1.48±0.08	190±30
Tb – Bipy–PDMS25000	0.5±0.2	0.5±0.04	0.13±0.05	255±33

[a)] Tensile tests were carried out at room temperature at a constant tensile rate of 40 mm·min^{-1};

[b)] The metal content was determined using the method of energy dispersive X-ray spectroscopy (EDX);

[c)] Young's modulus was determined in the low strain region (1–5% stretch).

An increase in the number average molecular weight of the polydimethylsiloxane moiety from 5000 to 25000 in the Bipy–PDMS polymeric ligand results in a fivefold decrease in the amount of *O,N,N,O*–chelating moieties in Bipy–PDMS. This favors the formation of approximately 5 times fewer coordination crosslinks between the Bipy–PDMS chains during the transition from Eu–Bipy–PDMS5000 to Eu–Bipy–PDMS25000. This fact is confirmed by an increase in the value of ε (from 185 to 220%) and a decrease in σ (from 1.55 to 0.1 MPa) in the studied PMCs. (**Figure 38 a**). In this case, the parameters ε and σ do not depend on the nature of the lanthanide-metal center.

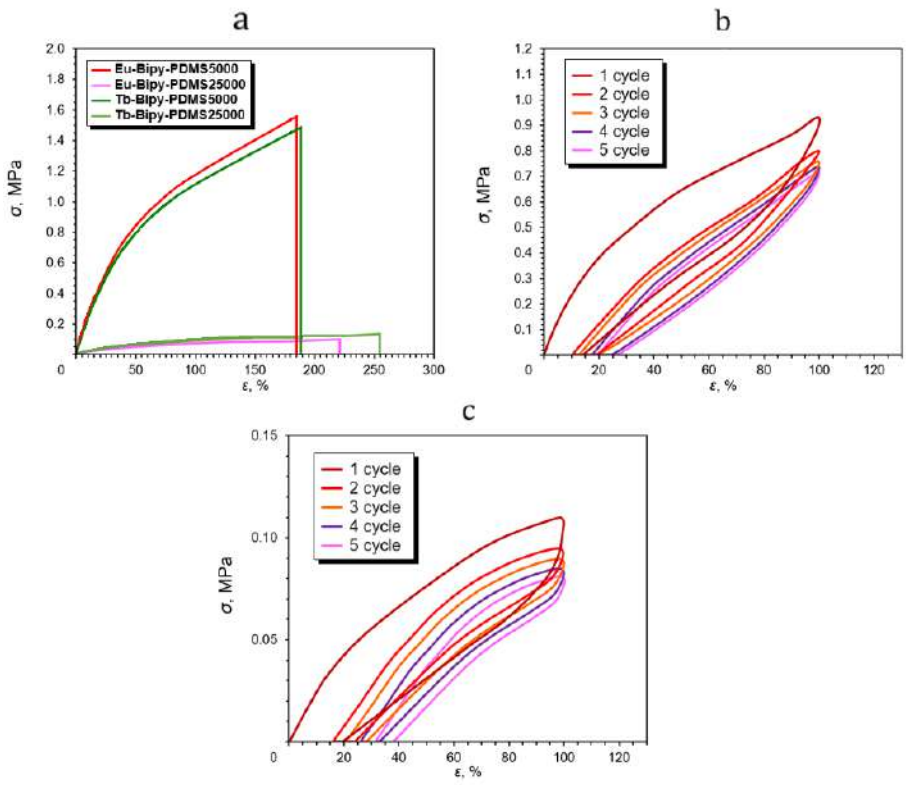

Figure 38 –Tensile properties of PMC: stress–strain curves at a strain rate of 40 mm·min^{-1} **(a)**, strain curves of cyclic tension–compression tests for Eu–Bipy–PDMS5000 **(b)** and Eu–Bipy–PDMS25000 **(c)** at a strain rate of 10 mm·min^{-1}. Sample form according to ISO 37 type 3

Eu–Bipy–PDMS5000 and Eu–Bipy–PDMS25000 show permanent permanent deformation of 27% and 38%, respectively (after 5 cycles, 100% deformation) (**Figure 38 b, c**).

Thus, an increase in the metal content in the PMC upon going from Eu–Bipy–PDMS25000 to Eu–Bipy–PDMS5000 leads to an increase in the tensile strength. Apparently, this is due to an increase in the number of coordination crosslinks in the series Eu–Bipy–PDMS25000–Eu–Bipy–PDMS5000. Similar dependences are observed in the case of Tb–Bipy–PDMS.

With a relatively high mechanical strength (compared to the known monopyridyl complexes Ln–Py–PDMS [2]), the synthesized lanthanide-containing Eu–Bipy–PDMS and Tb–Bipy–PDMS exhibit the properties of non-autonomous self-healing, i.e., the ability to restore their original characteristics after mechanical damage at elevated temperature (100 °C). At 25°C, the self-healing efficiency (η) is only 9% after 72 hours (3 days) after mechanical damage, while at 100°C, η increases from 33% to 85% within 48 hours (2 days) (**Figure 39**) [49,52].

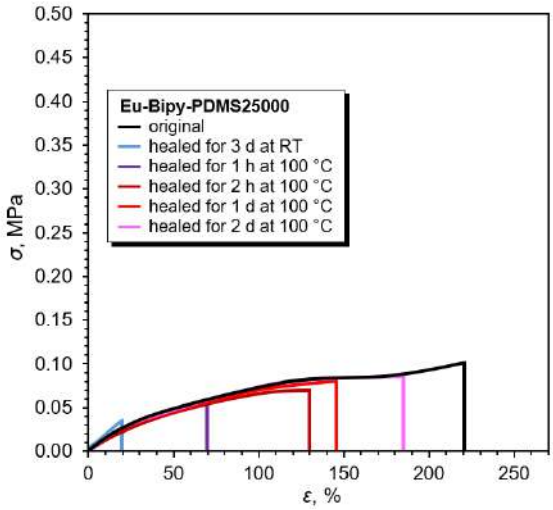

Figure 39 – Stress-strain curves of self-healed Eu–Bipy–PDMS25000 at 100°C. Stretching speed 40 mm·min^{-1}. Sample form according to ISO 37 type 3

TG in air (**Figure 40**) indicates that, thermal decomposition for all studied PMCs begins at a temperature of 400°C, which compares them favorably with cross-linked silicone materials based on PDMS and Ln–Py–PDMS described in the literature, which are characterized by decomposition temperatures 250 °C and 300 °C, respectively [2,6]. Ln–Bipy–PDMS25000 achieve degradation to 18% residual mass at 570°C, while shorter chain length PMCs Ln–Bipy–PDMS5000 achieve these values (22% residual mass) at 530°C. The mechanism of thermal decomposition of polysiloxanes is described in detail in the literature [6,113–115]. Since the nature of the lanthanide does not affect the thermal properties of the PMC, the TG analysis in argon was carried on Eu–Bipy–PDMS samples. Eu–Bipy–PDMS25000 achieve decomposition to a residual mass of 10% at temperatures of 680 °C, while the PMC with shorter chain length (Eu–Bipy–PDMS5000) achieve these values at 520 °C (**Figure 40 b**). Thus, an increase in the molecular weight of the polysiloxane fragment contributes to an increase in the thermal stability of PMC.

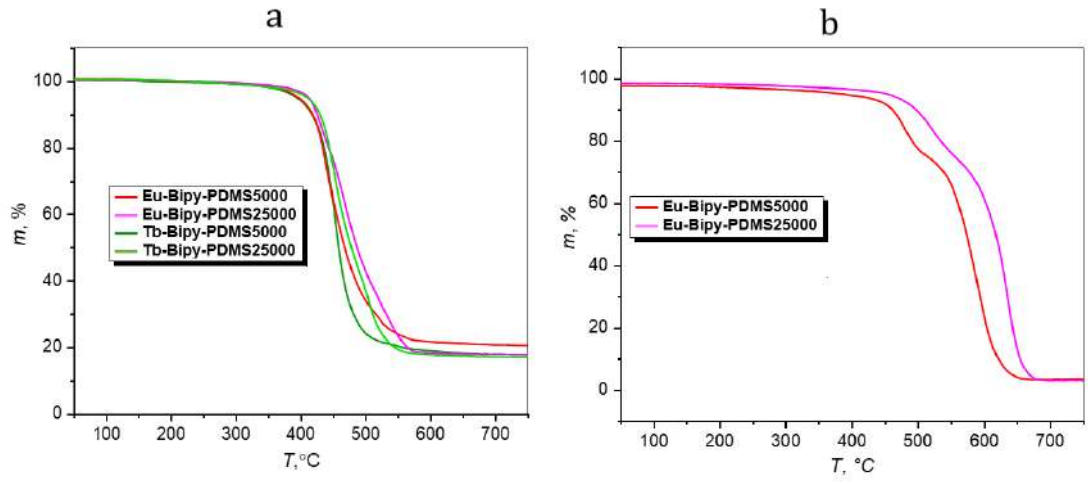

Figure 40 – Thermal properties of PMC: TG curves of Eu–Bipy–PDMS, Tb–Bipy–PDMS in air **(a)** and in argon **(b)** from 20 to 750 °C

The TG curves of $[Eu(BDCA)_2(H_2O)]Cl_3$ and $[Tb(BDCA)_2(H_2O)]Cl_3$ indicate several stages of weight loss (**Figure 41**): 5–7% weight loss at 100°C (apparently, dehydration), 15–20% at 280°C, 35% at 380°C, and 75% at 485°C. $Eu(BDCA)_2(H_2O)]Cl_3$ each a residual mass of 23% at 530°C, $[Tb(BDCA)_2(H_2O)]Cl_3$ – 27% at 580°C. The data obtained in air and in argon are comparable. However, low molecular weight complexes are noticeably less thermaly stable compared to the PMC.

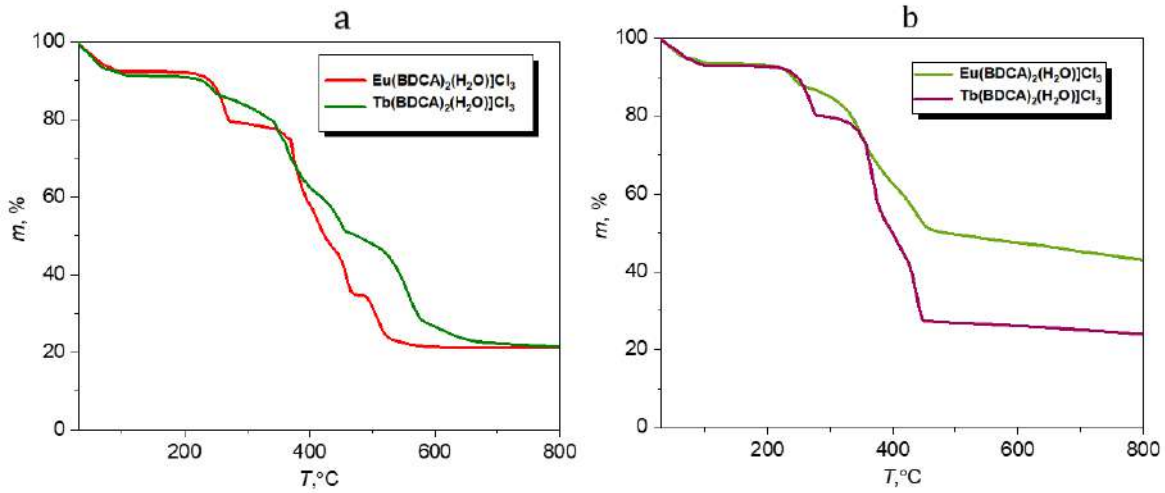

Figure 41 – Thermal properties of PMC: TG curves of $[Eu(BDCA)_2(H_2O)]Cl_3$ and $[Tb(BDCA)_2(H_2O)]Cl_3$ in air **(a)** and in argon **(b)** from 20 to 800 °C

Thus, the use of BDCA as a ligand promotes the formation of coordinatively saturated PMCs and stronger coordination of the lanthanide(III) and the bipyridine fragment. This is confirmed by the relatively high mechanical strength and the manifestation of non-autonomus self-healing under the influence of high temperatures (100°C), as well as the high thermal stability of Ln–Bipy–PDMS compared to Ln–Py–PDMS and PDMS [2,6].

2.2.4 Luminescent characteristics of Ln-Bipy-PDMS

Due to the structural features 2,2-bipyridine-6,6'-dicarboxylate is a highly effective sensitizer of the "antenna effect" [6], which ensures efficient energy transfer to the excited states of Ln^{3+} and subsequent radiative energy transitions $^5D_0 \rightarrow {}^7F_J$ (J = 0 – 4) for Eu^{3+} and $^5D_4 \rightarrow {}^7F_J$ (J = 6 – 3) for Tb^{3+}.

Lanthanide-containing model complexes $[Eu(BDCA)_2(H_2O)]Cl_3$ and $[Tb(BDCA)_2(H_2O)]Cl_3$ and PMC in air exhibit UV-excited photoluminescence (PL) in the visible spectral region. For each of the lanthanides, the excitation spectra have almost the same form for the corresponding PMC and the analogous low molecular weight complex (**Figure 42**).

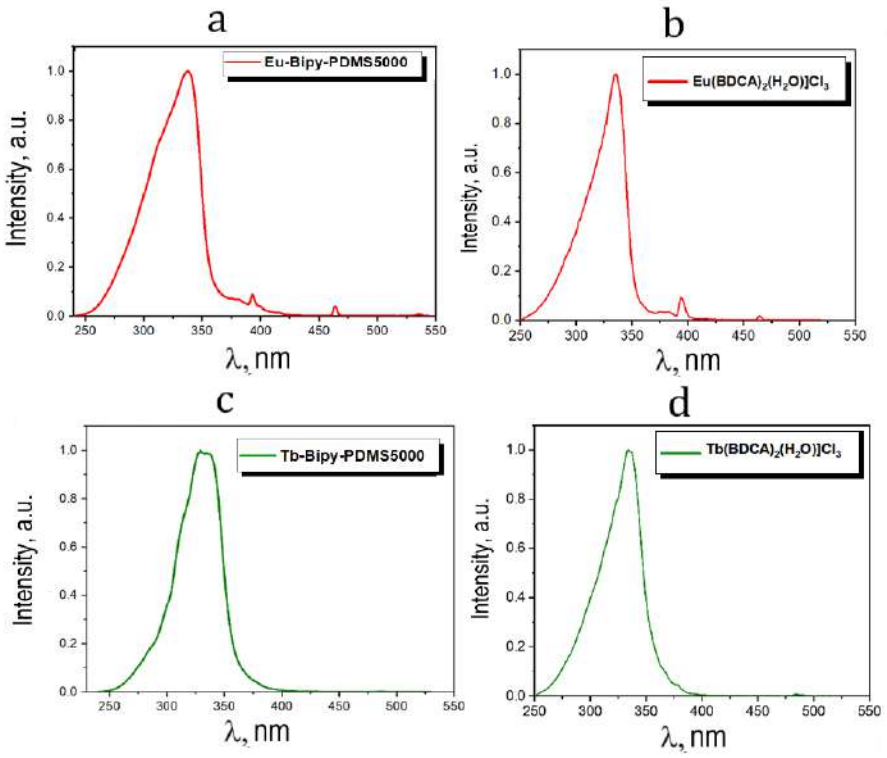

Figure 42 – Normalized on maximum excitation spectra of Eu–Bipy–PDMS **(a)**, **[**$Eu(BDCA)_2(H_2O)]Cl_3$ **(b)**, Tb–Bipy–PDMS **(c)** and $[Tb(BDCA)_2(H_2O)]Cl_3$ **(d)**

Excitation wavelengths (λ_{ex}) for lanthanide-containing complexes range from 250 to 400 nm. Maximum excitation is achieved at an excitation wavelength of 320–340 nm (**Figure 40**).

At an excitation wavelength of 340 nm, Tb–Bipy–PDMS and $[Tb(BDCA)_2(H_2O)]Cl_3$ exhibit the of terbium ions Tb^{3+} characteristic spectral lines $^5D_4 \rightarrow {}^7F_J$ (J = 6–3) in the green region of the spectrum (**Figure 43, Table 6**). Analogously, Eu–Bipy–PDMS and $[Eu(BDCA)_2(H_2O)]Cl_3$ demostrate Eu^{3+} ions characteristic spectral lines $^5D_0 \rightarrow {}^7F_J$ (J = 0–4) in the red region of the spectrum (**Figure 43, Table 6**).

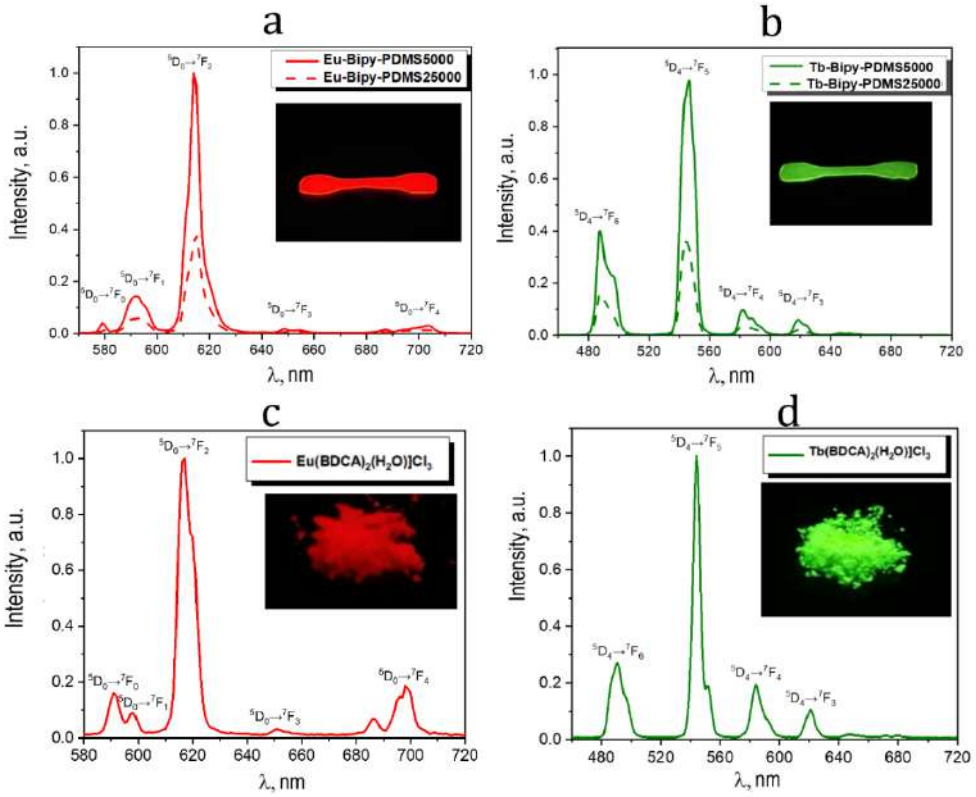

Figure 43 – Normalized on maximum PL spectra at an excitation wavelength of 340 nm of Eu–Bipy–PDMS **(a)**, Tb–Bipy–PDMS **(b)**, $[Eu(BDCA)_2(H_2O)]Cl_3$ **(c)** and $[Tb(BDCA)_2(H_2O)]Cl_3$ **(d)**. The insets show various possible optical transitions and optical images of Ln–Bipy–PDMS films and low molecular weight model complexes.

Table 6 – Luminescent characteristics of lanthanide-containing complexes.

Lanthanide-containing complex	$\lambda^{a)}$, nm (λ_{ex}=320-340 nm)	$\tau^{b)}$, ms	$\Phi^{c)}$, %
$[Eu(BDCA)_2(H_2O)]Cl_3$	580 ($^5D_0 \rightarrow {}^7F_0$), 592 ($^5D_0 \rightarrow {}^7F_1$), 614 ($^5D_0 \rightarrow {}^7F_2$), 649 ($^5D_0 \rightarrow {}^7F_3$), 700 ($^5D_0 \rightarrow {}^7F_4$)	1.26	12.6
Eu–Bipy–PDMS5000		1.50	10.5
Eu–Bipy–PDMS25000			7.0
$[Tb(BDCA)_2(H_2O)]Cl_3$	487 ($^5D_4 \rightarrow {}^7F_6$), 547 ($^5D_4 \rightarrow {}^7F_5$), 581 ($^5D_4 \rightarrow {}^7F_4$), 614 ($^5D_4 \rightarrow {}^7F_3$)	1.26	36.5
Tb–Bipy–PDMS5000		2.00	18.5
Tb–Bipy–PDMS25000		2.00	11.0

[a] λ – photoluminescence wavelength;

[b] τ – luminescence lifetime;

[c] Φ – photoluminescence quantum yield.

As the molecular weight of the ligand increases, quantum yields (Φ) of the PMCs and $[Eu(BDCA)_2(H_2O)]Cl_3$ and $[Tb(BDCA)_2(H_2O)]Cl_3$ naturally decrease, which is associated with quenching of luminescence in the polymer matrix Bipy-PDMS [122]. The highest quantum yields of 36.5% and 12.6% are exibitrd by $[Tb(BDCA)_2(H_2O)]Cl_3$ and $[Eu(BDCA)_2(H_2O)]Cl_3$, respectively. Tb-Bipy–PDMS5000 and Tb–Bipy–PDMS25000 exhibit quantum yields of 18.5% and 11.0%, which are higher than the values of similar europium-containing PMCs, 10.5% and 7.0% for Eu–Bipy–PDMS5000 and Eu–Bipy–PDMS25000, respectively.

Thus, the influence of the molecular weight (length of the polysiloxane chain) of the ligand on the quantum yield of Eu–Bipy–PDMS and Tb–Bipy–PDMS has been shown. For further study of the possibility of controlling the color of photoluminescence, PMCs with a lower molecular weight of the ligand and high quantum yields, Eu–Bipy–PDMS5000 (10.5%) and Tb–Bipy–PDMS5000 (18.5%), were chosen.

2.2.5 Ln-Bipy-PDMS photoluminescence color tuning

Thin films with a thickness of 100 μm Eu–Bipy–PDMS and Tb–Bipy–PDMS demonstrate red and green photoluminescence when excited by long wavelength UV radiation λ_{ex} = 340 nm. When color films were superimposed on top of each other in the X:Y(X=1–4, Y=1–3) ratios, the photoluminescence color was adjusted from green to red through intermediate yellow and orange colors (**Figure 44**).

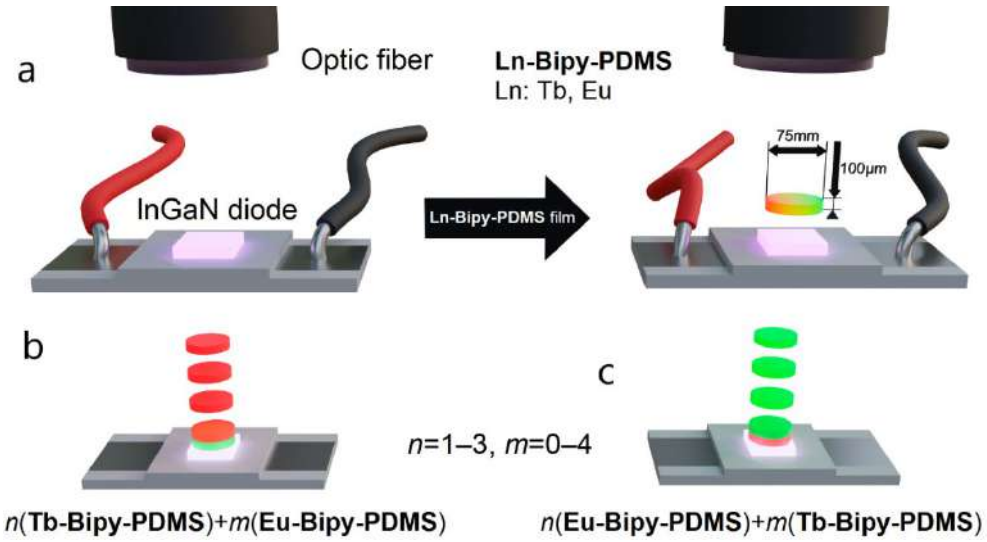

Figure 44 – Set-up scheme **(a)**, first **(b)** and second **(c)** routes of photoluminescence color tuning study

In the course of the study, Tb–Bipy–PDMS5000 films were used as bottom layers, on top of which Eu–Bipy–PDMS5000 films were superimposed and in the reverse order (**Figure 44**, **b**). As a result, a slight increase in the intensity of the $^5D_0 \rightarrow {}^7F_2$ peaks was observed with the number of top Eu-Bipy–PDMS5000 layers, which led to a transition from green to yellow luminescence (**Figure 45**). Two or more bottom layers of Tb–Bipy–PDMS5000 prevent effective UV excitation of the upper Eu Bipy PDMS5000 films. Thus, mainly Tb^{3+} optical response is observed, corresponding to the green and yellow colors of the emission (**Figure 45**).

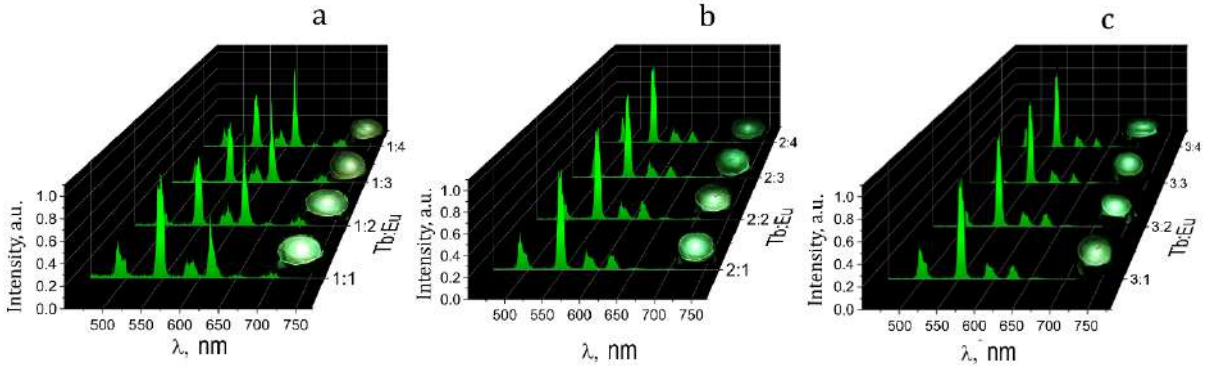

Figure 45 – Photoluminescence spectra n (Tb–Bipy–PDMS5000) + m (Eu–Bipy–PDMS5000), m = 1–4, n = 1 **(a)**, n = 2 **(b)** and n = 3 **(c)**. The insets show optical images of the films under UV excitation.

Then, a study of PL spectra tuning was conducted with Eu–Bipy–PDMS5000 as the bottom films. (**Figure 45**). The adding of Tb–Bipy–PDMS5000 films over them leads to the appearance of Tb^{3+} signals (corresponding to the $^5D_4 \rightarrow {}^7F_5$ energy transitions at 546 nm). Therefore, a transition of the photoluminescence color from red to yellow is observed. However, as in the previous case, two or more bottom layers of Eu–Bipy–PDMS5000 prevent effective UV excitation of the top films. The PL spectra mainly exhibit the characteristic peaks $^5D_0 \rightarrow {}^7F_2$ Eu^{3+} at 620 nm, which correspond to the red color of the PL.

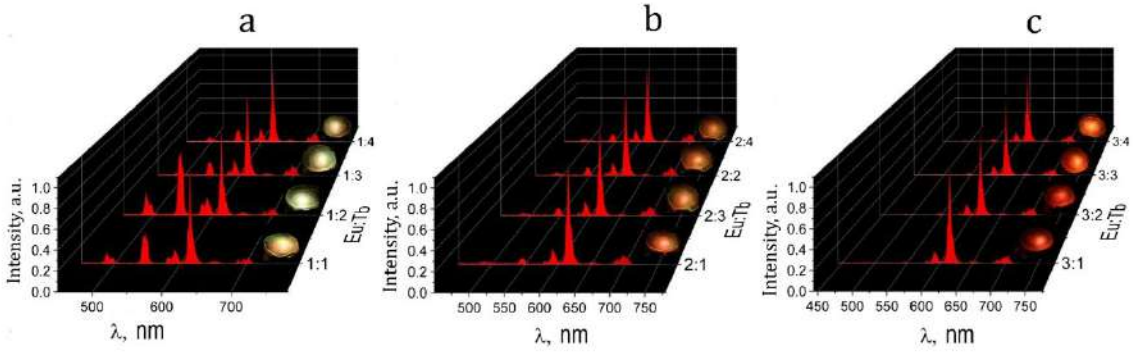

Figure 46 – Photoluminescence spectra n (Eu–Bipy–PDMS5000) + m (Tb–Bipy–PDMS5000), m = 1–4, n = 1 **(a)**, n = 2 **(b)** and n = 3 **(c)**. The insets show optical images of the films under UV excitation

Figure 46 shows optical images of combinations of superimposed films from different amounts of "red" and "green" films. The first and last rows represent X (Tb–Bipy–PDMS5000) and X (Eu–Bipy–PDMS5000), respectively, where X=1–4. The remaining rows show images of superimposed films in X:Y ratios (X=1–4, Y=1–3), where the maximum number of films in one stack is 7 (the thickness of such a stack is 700 μm). The optical images in **Figure 46** are sorted by the ratio of "green" to "red" peaks in the spectra. The first rows reflect the predominance of Tb^{3+} spectral lines, while the last rows show the predominance of Eu^{3+} lines (**Figure 46**). The ratio of signal intensities in the cases of X≥2 and Y≥2 does not correspond to a linear relation. This is apparently due to the reflection of radiation at the boundary of two films stacked together, as well as the absorption of re-emitted light.

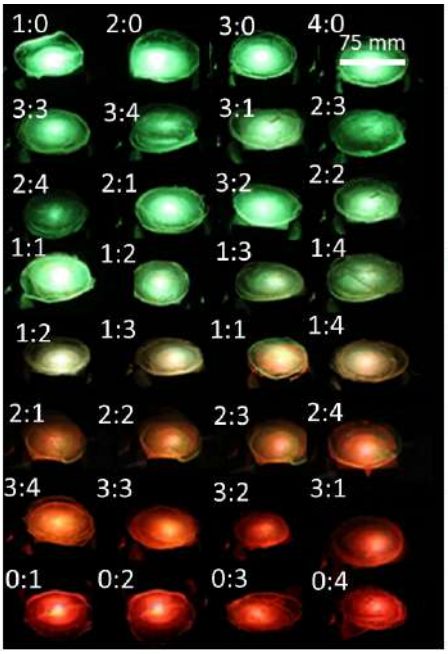

∞:0	∞:0	∞:0	∞:0
6,87:1	6,8:1	6,2:1	6,08:1
5,94:1	5,78:1	5,76:1	4,77:1
1,62:1	0,70:1	0,70:1	0,65:1
1:1,37	1:2,27	1:3	1:6
1:8,98	1:9,2	1:12,27	1:15
1:32	1:49	1:54	1:86
0:∞	0:∞	0:∞	0:∞

Figure 47 – Optical images of green and red films superimposed in different ratios on each other. The table shows the corresponding ratio of green and red emission lines

Thus, the color of photoluminescence emission can be controlled by varying the ratio and number of films of different colors (Tb–Bipy–PDMS5000 and Eu–Bipy–PDMS5000). The color of the photoluminescence is determined by the ratio of the intensities of the lines corresponding to the $^5D_4 \rightarrow {}^7F_5$ (green) and $^5D_0 \rightarrow {}^7F_2$ (red), transitions, which leads to the achievement of intermediate photoluminescence colors – yellow or orange (**Figure 48**) is shown in the CIE 1931 diagram.

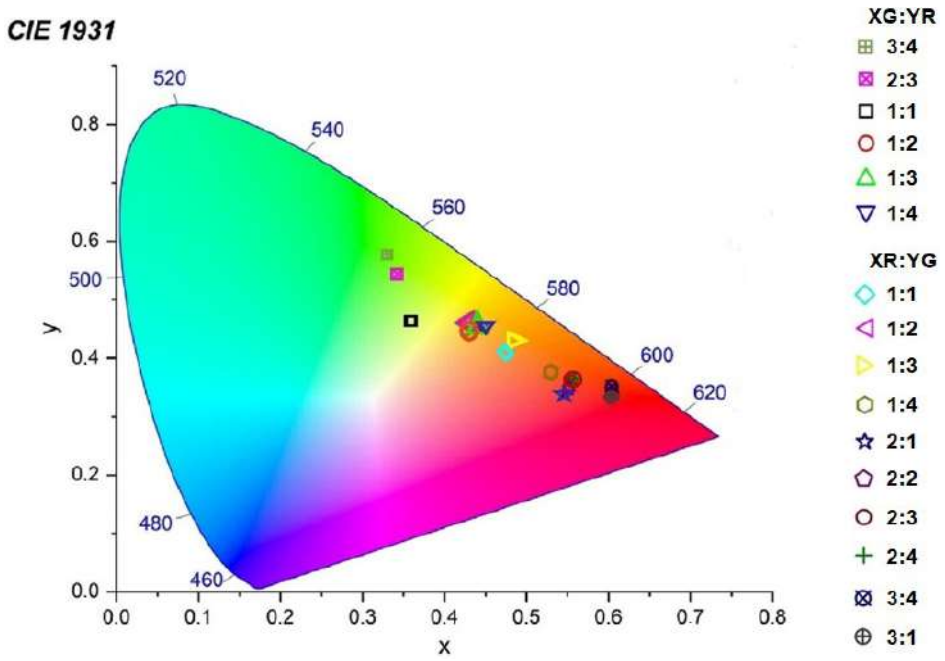

Figure 48 – CIE 1931 chart of intermediate color combinations of Tb–Bipy–PDMS5000 (G) and Eu–Bipy–PDMS5000 (R), X and Y indicate the number of PMC layers

The Tb–Bipy–PDMS5000 and Eu–Bipy–PDMS5000 obtained have the property of non-autonomus self-healing. This property ensured the production of monolithic membranes by laying luminescent films on top of each other and cross-linking them As an example, a flexible membrane was

obtained, consisting of 1 red and 2 green (100 μm thick) films, which are “sintered” into a single monolithic film (due to self-healing properties) at 100 °C for 4 h (**Figure 49**).

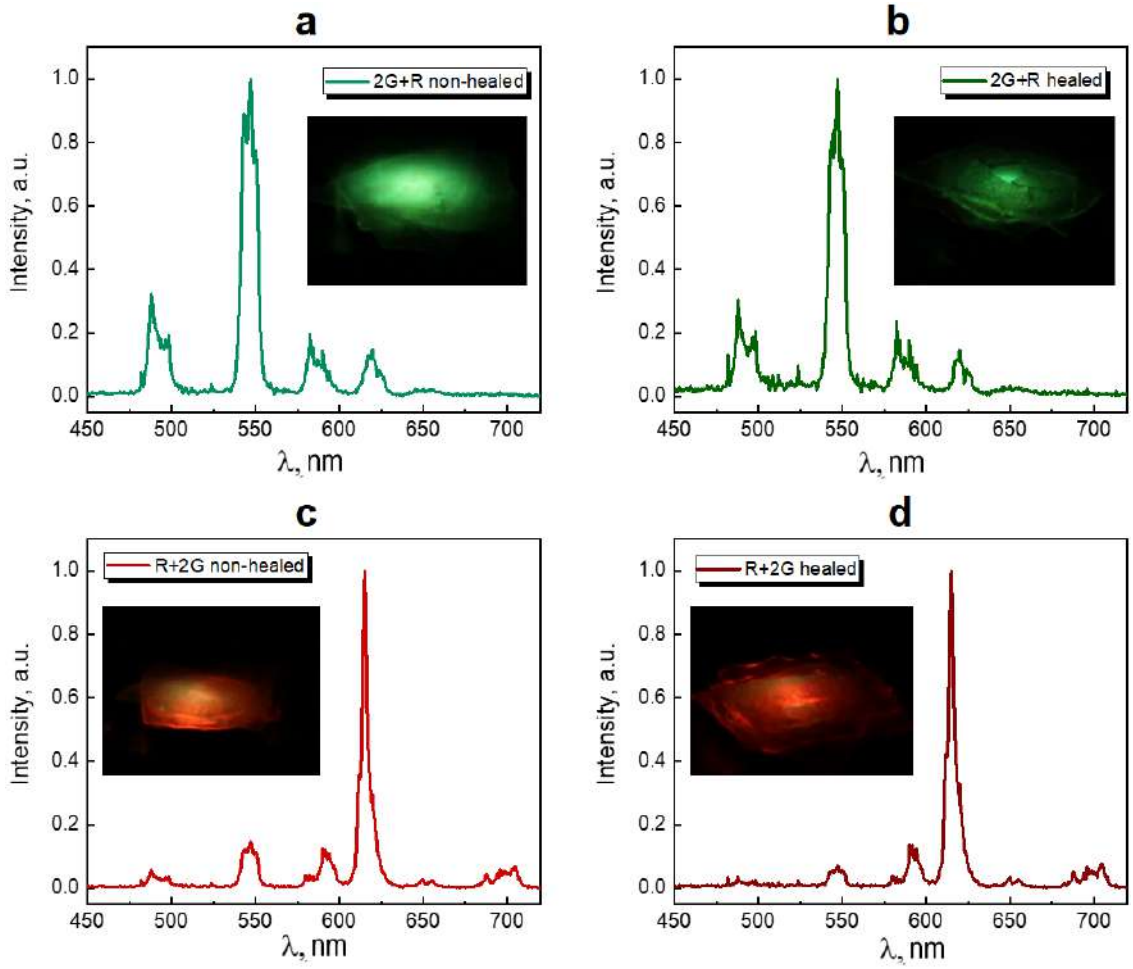

Figure 49 – Maximum-normalized photoluminescence spectra of superimposed thin films consisting of two green Tb–Bipy–PDMS5000 films and one red Eu–Bipy–PDMS5000 film before **(a, c)** and after **(b, d)** membrane healing at temperature; **(a)** and **(b)** correspond to the green films located on the LED, **(c)** and **(d)** correspond to the opposite geometry

The PL spectra of the “healed” membrane somewhat differ from the spectra of the initial superimposed membranes, which can be explained, apparently, by the high temperature-induced ligand exchange between BDCA, Cl^- and H_2O molecules (**Figure 50**) with a shift in equilibrium towards the formation of a heteroleptic complex [49,123].

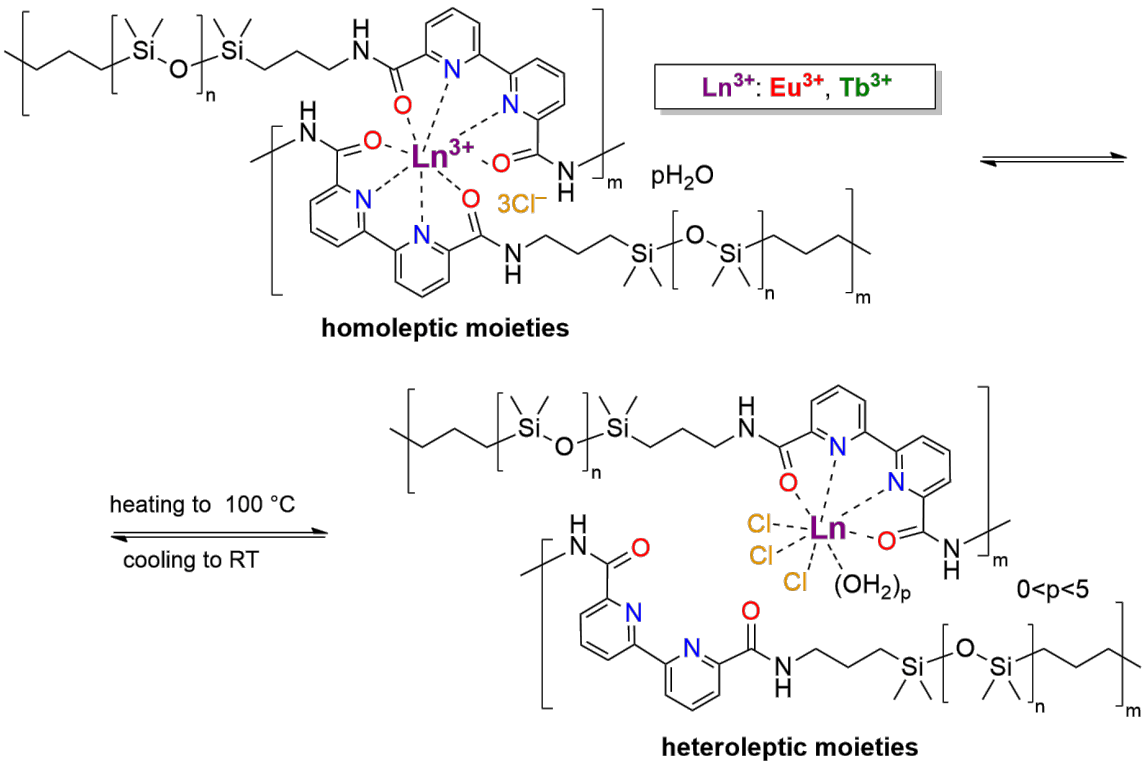

Figure 50 – Suggested self-healing mechanism of Ln–Bipy–PDMS

Thus, the nature of the coordination center (lanthanide) makes it possible to control the color of photoluminescence by applying thin films containing different types of lanthanides. Due to non-autonomous self-healing properties, superimposed thin films can be transformed into monolithic systems by heating at 100℃. Such "monoliths" have two colors of photoluminescence, which are determined by the ratio of films of each type.

2.2.6 Tb-Bipy-PDMS5000 and Eu-Bipy-PDMS5000 application in NWs-based flexible UV-LEDs

Tb–Bipy–PDMS5000 and Eu–Bipy–PDMS5000 were tested as a photoluminescent layer in a flexible UV LED based on GaN/AlGaN NWs with radial geometry (core-shell) [124]. The flexible LED was produced according to the method described earlier (see chapter 2.1.3 2.1.7). By G-coating, arrays of GaN/AlGaN NWs grown on a sapphire (Al_2O_3) substrate were encapsulated in a Sylgard 184 layer so that the upper parts protruded from the polymer layer. Sylgard 184 was used as a flexible support matrix, since sapphire substrates are used for GaN NW growth, which do not have adhesion problems (SSR25 also could be employed). The thickness of the (GaN/AlGaN NW)/Sylgard 184 membrane estimated by SEM was ~10 μm (**Figure 51**). To create an electrical contact with NWs, SWCNT pads were deposited on a blade-separated (GaN/AlGaN NW)/Sylgard 184 membrane from both sides, forming a mechanically flexible UV-LED.

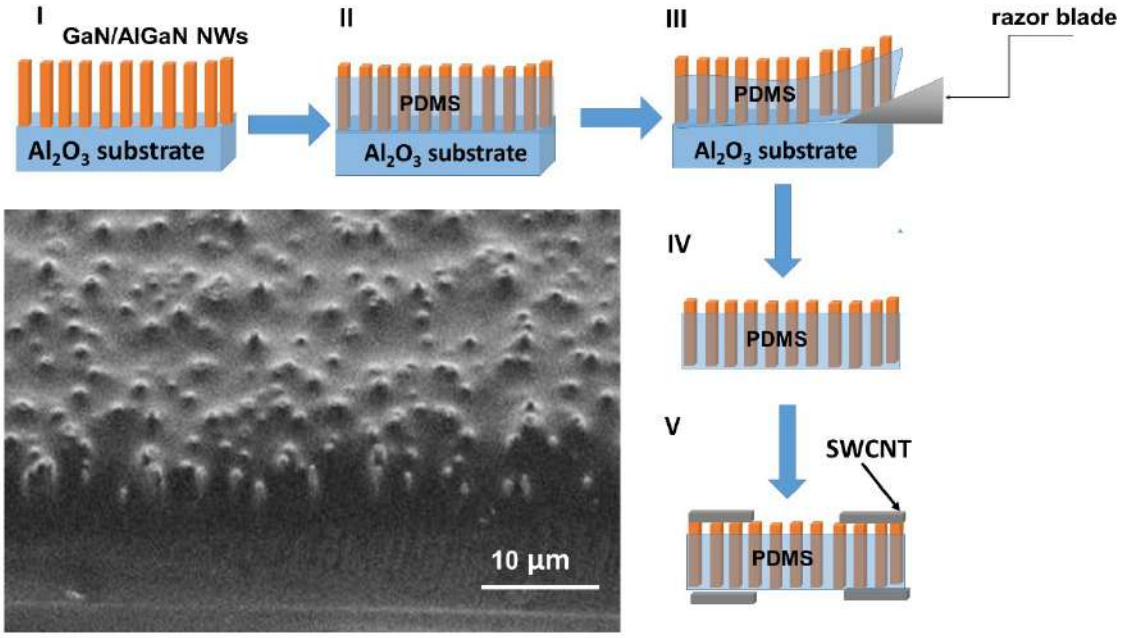

Figure 51 – Scheme for creating a flexible UV LED. The inset represents the SEM image of the LED cross-section

The fabricated LED had two electroluminescence bands in the UV region, corresponding to 350 and 370 nm (**Figure 53 (a)**). To cut off spurious radiation from GaN defects in the yellow spectral region, we used a black glass optical filter located directly above the membrane (**Figure 52**). The PL of PMC films located immediately after the optical filter was excited by UV radiation from a flexible LED operating with a current of 30 A/cm^2

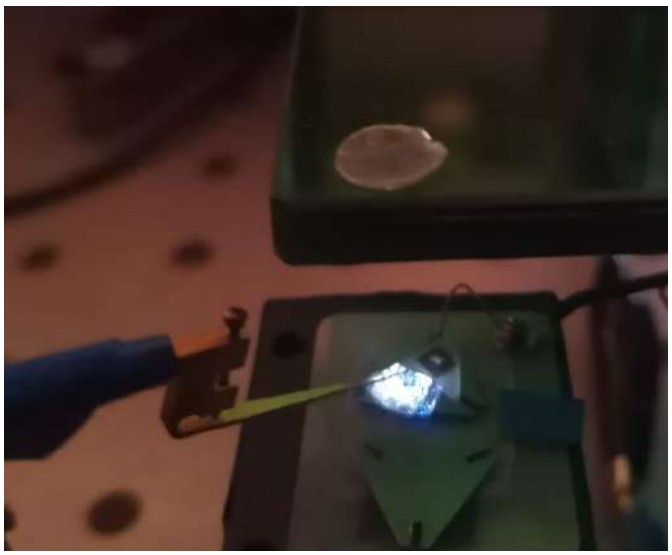

Figure 52 – Image of excitation of the Eu–Bipy–PDMS5000 film from the radiation of an operating UV LED through an optical filter

The emission spectrum of a film superimposed over a flexible Tb-Bipy-PDMS5000 UV LED exhibits all signals characteristic of energy transition $^5D_4 \rightarrow {}^7F_J$ (J = 6–3). The spectrum (**Figure 53**) shows a 2 times drop in the diode emission signals at 340 nm after applying the Tb-Bipy-PDMS5000 film, while for the signal at 380 nm a slight drop by 0.7 times is observed. It follows from this that the main contribution to the excitation of the PMC comes from the absorption of diode radiation at a length of 340 nm

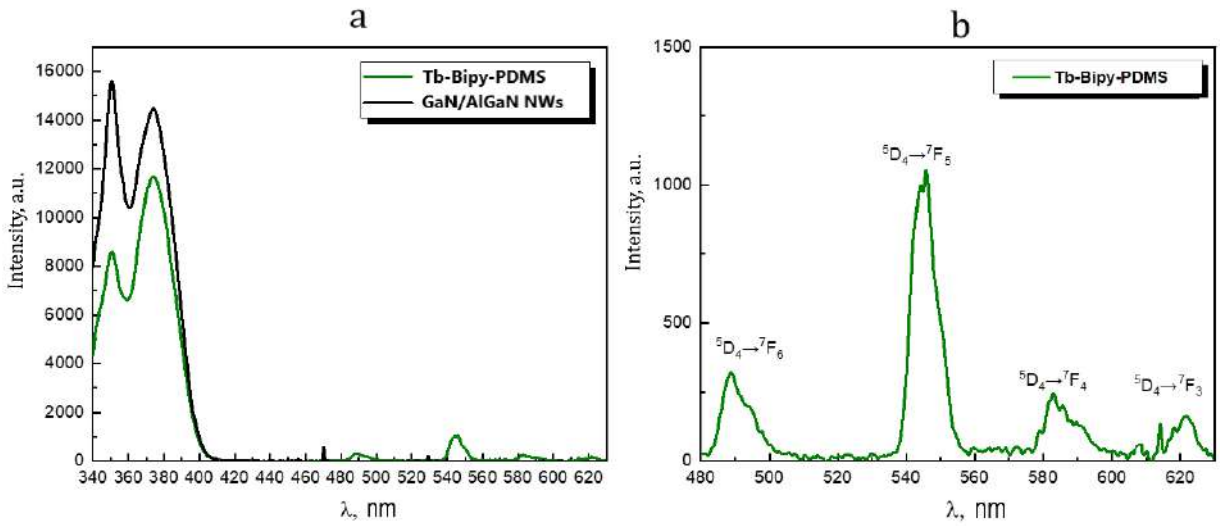

Figure 53 – Electroluminescence spectrum of a UV LED with a superimposed Tb–Bipy–PDMS5000 film in the wavelength range of 340–630 nm **(a)** and in the emission region of Tb–Bipy–PDMS5000 (480–630 nm) **(b)**

In the case of Eu–Bipy–PDMS5000, the emission spectrum exhibits bands corresponding to the Eu^{3+} energy transitions $^5D_0 \rightarrow {}^7F_J$ (J = 0–2). Signals of $^5D_0 \rightarrow {}^7F_J$ (J = 3–4) energy transitions was not observed due to the low light power of the flexible UV LED. Eu–Bipy–PDMS5000 absorb radiation at a wavelength of 340 nm more strongly than Tb–Bipy–PDMS5000, which is consistent with the excitation spectra studied for the PMC (**Figure 54**, **Figure 42**). Apparently, this is due to the nature of the lanthanide coordination center [82].

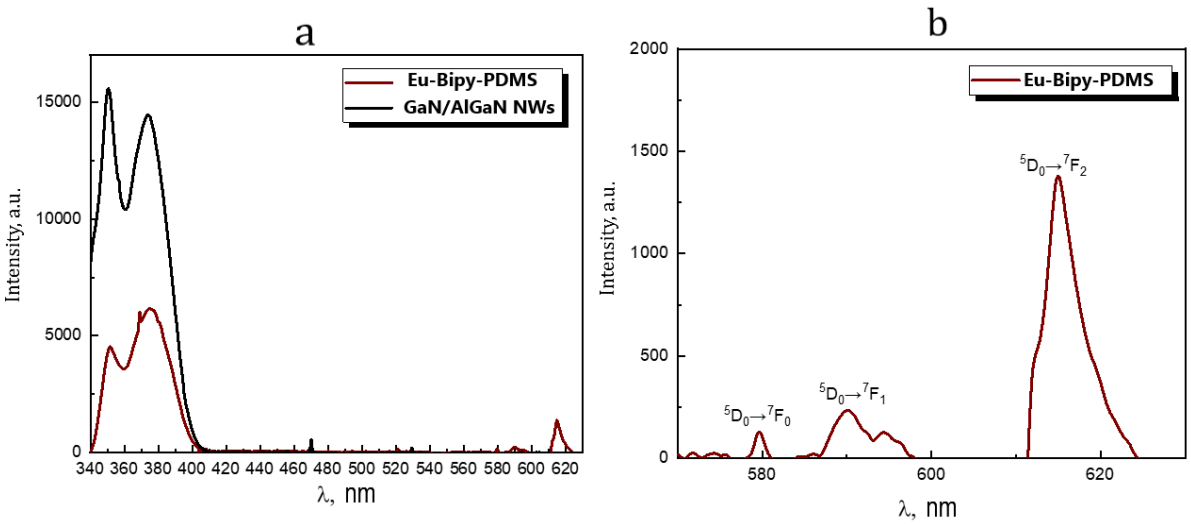

Figure 54 – Electroluminescence spectrum of a UV LED with a superimposed Eu–Bipy–PDMS5000 film in the wavelength range of 340–630 nm **(a)** and in the Tb emission region of Eu–Bipy–PDMS5000 (580–630 nm) **(b)**

Thus, the obtained luminescent lanthanide-containing polysiloxanes were tested as photoluminescent layers for a flexible UV LED (GaN/AlGaN NW)/Sylgard 184. This opens up the possibility of using the resulting PMCs in flexible optoelectronic devices based on NW arrays characterized by UV luminescence

The results of the presented study were published:

- Miroshnichenko A.S., Deriabin K.V., Baranov A.I., Neplokh V., Mitin D.M., Kolesnikov I.E., Dobrynin M.V., Parshina E.K., Mukhin I.S., Islamova R.M. Lanthanide(III)-incorporating polysiloxanes as materials for light-emitting devices // ACS Applied Polymer Materials — 2022. – V. 4. – № 4. – P. 2683–2690. DOI: 10.1021/acsapm.2c00017.
- Miroshnichenko A., Deriabin K.V., Rashevskii A.A., Suslonov V.V., Novikov A.S., Mukhin I.S., Islamova R.M. Structural features of Eu^{3+} and Tb^{3+}-bipyridinedicarboxamide complexes // MDPI Polymers — 2022. –V. 14. – № 24. – P. 5540. DOI: 10.3390/polym14245540.

CHAPTER 3. EXPERIMENTAL PART

Chemical reagents and materials

PMHS (number average molecular weight M_n = 3200, viscosity 45 cSt, Abcr GmbH, Karlsruhe, Germany), APDMS (two polymers with M_n = 5000, 25000 and viscosity 100–120 and 900–1100 cSt, respectively; Abcr GmbH, Karlsruhe, Germany), Karstedt's catalyst (0.1 M solution of platinum(0) complex with 1,3 divinyl-1,1,3,3 tetramethyldisiloxane in xylene, Abcr GmbH, Karlsruhe, Germany) and *v*-PDMS (weight average molecular weigh M_w = 25000, viscosity 850–1150 cSt, Sigma Aldrich, St. Louis, USA) were purchased from commercial suppliers and fully characterized by NMR spectroscopy prior to use. Anhydrous $EuCl_3$ (99.99%) and anhydrous $TbCl_3$ (99.99%) were purchased from ChemCraft Ltd. (Russia). Triethylamine (99%) was also purchased from Abcr GmbH (Karlsruhe, Germany) and their purity was confirmed by NMR spectroscopy before use. 2,2' bipyridine-6,6' dicarboxylic acid (98%) was purchased from Abcr GmbH (Karlsruhe, Germany), the purity was checked by NMR spectroscopy before use. Thionyl chloride (97%, Vecton, St. Petersburg, Russia) was distilled under argon just prior to use. Anhydrous sodium sulfate (99%) and phosphorus(V) oxide (98%, ACS) were purchased from Vekton (St. Petersburg, Russia). Chloroform (99%) and acetone (99%) were purchased from Vecton (St. Petersburg, Russia) and used without additional purification. Anhydrous dichloromethane (99%, Vecton, St. Petersburg, Russia) was distilled over phosphorus(V) oxide under argon before use. Anhydrous methanol (99%, Vecton, St. Petersburg, Russia) was distilled over magnesium methoxide. Toluene (99%) was purchased from Vecton (St. Petersburg, Russia) and distilled over the sodium/benzophenone system under argon.

3.1 Synthesis

3.1.1 S–PMHS50 and S–PMHS75

Styrene (3.94 g) (S–PMHS50) and 4.80 g (S–PMHS75) were placed into a single-necked flask, and a 0.1 M solution of Karstedt's catalyst in xylene (440 μL) in 40 mL of anhydrous toluene was added. The mixture was stirred for 1 hour in an argon atmosphere at room temperature (21°C). Then, after purging with argon, a solution of PMHS (4.55 g for S–PMHS50 and 3.70 g for S–PMHS75) in 40 mL of anhydrous toluene was added dropwise to the reaction mixture. The reaction was carried out with stirring for 72 hours in an argon atmosphere at room temperature.

The molar fraction of phenylethyl units ($PhCH_2CH_2(CH_3)SiO$) in S–PMHS was calculated from the ratios of the integral signal intensities δ = 4.75–4.81 ppm (of the remaining Si–***H*** groups) and 7.50–

7.00 ppm (C_6H_5 linker), which was approximately 50 mol.% for S–PMHS50 and 71 mol.% for S–PMHS75.

$$\omega\% = \frac{I[C_6H_6]/5}{I[Si-H]/1 + I[C_6H_6]/5} = \frac{I[7.5-7]/5}{I[5-4.5]/1 + I[7.5-7]/5} \times 100 = 52\%, \qquad (1)$$

where $\omega\%$ – is the molar content of C_6H_6, I – I is the integral intensity of the signal in the spectrum ^1H.

S–PMHS50. Yield: 8.32 g (98%); transparent flexible film. ^1H SSNMR (δ): 0.07 (w s, $SiCH_3$), 0.75 (w m, $SiCH(CH_3)Ph$), 1.19 (w m, $SiCH_2CH_2Ph$), 2.01 (w m, $SiCH_2CH_2Ph$), 2.51 w m, $SiCH(CH_3)Ph$), 4.73 (w s, SiH), 6.89 (w m, Ph). ^{13}C SSNMR (δ): –2.5 ($SiCH_3$), 0 ($SiCH_3$), 1.7 ($SiCH_3$), 15.2 ($PhCH(CH_3)$), 19.8 ($PhCH_2CH_2$), 29.5 ($PhCH_2CH_2$), 31.1 ($PhCH(CH_3)$), 126.0 (4-C_6H_5), 128.3 (2,6-C_6H_5), 128.7 (3,5-C_6H_5), 130.0 (*ipso*-C_6H_5). ^{29}Si SSNMR (δ): –66, –57 (w, Si–O–Si cross-links), –35 (w, SiH), –26 (w, Si–Si cross-links), –22 (–$OSi(CH_3)(CH_2CH_2Ph)$– and –$OSi(CH_3)(CH(CH_3)Ph)$– units), 8 (terminal $(CH_3)_3Si$).

S–PMHS75. Yield: 8.25 g (97%); transparent flexible film. ^1H SSNMR (δ): 0.07 (w s, $SiCH_3$), 0.74 (w m, $SiCH(CH_3)Ph$), 1.19 (w m, $SiCH_2CH_2Ph$), 2.01 (w m, $SiCH_2CH_2Ph$), 2.51 (w m, $SiCH(CH_3)Ph$), 4.73 (w s, SiH), 6.90 (w m, Ph). ^{13}C SSNMR (δ): –2.5 ($SiCH_3$), 0.1 ($SiCH_3$), 1.7 ($SiCH_3$), 15.2 ($PhCH(CH_3)$), 19.8 ($PhCH_2CH_2$), 29.5 ($PhCH_2CH_2$), 31.2 ($PhCH(CH_3)$), 126.1 (4-C_6H_5), 128.3 (2,6-C_6H_5), 128.8 (3,5-C_6H_5), 130.0 (*ipso*-C_6H_5). ^{29}Si SSNMR (δ): –66, –57 (w, Si–O–Si cross-links), –35 (w, SiH), –26 (w, Si–Si cross-links), –22 (–$OSi(CH_3)(CH_2CH_2Ph)$– and –$OSi(CH_3)(CH(CH_3)Ph)$– units), 9 (terminal $(CH_3)_3Si$).

3.1.2 SSR25 and SSR50

Styrene (2.0 g for SSR25, 3.0 g for SSR50) and 0.1M Karsted's catalyst in xylene (220 µl) in anhydrous toluene (20 ml) were placed in a single-necked flask and stirred for one hour under argon. Next, a solution of PMHS (2.31 g) 15 ml of toluene was added dropwise to the reaction mixture. The reaction was carried out with stirring for 72 hours in an argon atmosphere at room temperature. To achieve the molar content of phenylethyl units of 50% and 25% in the obtained phenylethyl-functionalized silicone rubber (SSR50 and SSR25, respectively), a solution of *v*-PDMS (1.42 g and 2.84 g) in 15 ml with stirring for an hour in an argon atmosphere at room temperature. Next, the solvent was removed on a rotary evaporator until 1/3 of the initial volume of the SSR solution was reached under reduced pressure and a temperature of 60°C. Then the resulting gel was poured on a Teflon substrate into a rectangular polymer clay mold with an area of 64 cm^2 and a side height of 1 cm.

SSR25. Yield: 7.10 g (99%); flexible transparent silicone rubber.^{1}H SSNMR (δ): –0.87, 0.48 (w s, SiC*H*$_2$CH$_2$Ph), 6.04 (w m, Ph). ^{13}C SSNMR (δ): –3.2, 0.1 (SiCH$_3$); 15.3 (SiCH(*C*H$_3$)Ph), 19.6 (Si*C*H$_2$CH$_2$Ph), 29.5 (SiCH$_2$*C*H$_2$Ph), 31.1 (Si*C*H(CH$_3$)Ph), 123.9 (4-*C*$_6$H$_5$), 126.6 (2,6-*C*$_6$H$_5$), 127.8 (3,5-*C*$_6$H$_5$), 129.9 (*ipso*-*C*$_6$H$_5$). ^{29}Si SSNMR (δ): –67, –57 (Si–O–Si cross-links), – 35 (SiH), –26 (w, Si–Si cross-links), –22 (–O*Si*(CH$_3$)(CH$_2$CH$_2$Ph)–,– O*Si*(CH$_3$)(CH(CH$_3$)Ph)–, and –O*Si*(CH$_3$)$_2$– units), 8 (terminal (CH$_3$)$_3$Si).

SSR50. Yield: 6.69 g (99%); flexible transparent silicone rubber. ^{1}H SSNMR (δ): –1.22, –0.86, 0.49 (w s SiCH**3**); 0.24 (w m, SiCH(C*H*$_3$)Ph), 0.61 (w m, SiC*H*$_2$CH$_2$Ph), 1.52 (w m, SiCH$_2$C*H*$_2$Ph), 1.92 (w m, SiC*H*(CH$_3$)Ph), 5.57, 5.95, 6.30 (w m, Ph). ^{13}C SSNMR (δ): 0.1, 1.4 (SiCH$_3$); 15.3 (SiCH(*C*H$_3$)Ph), 19.3 (Si*C*H$_2$CH$_2$Ph), 29.4 (SiCH$_2$*C*H$_2$Ph), 33.0 ((Si*C*H(CH$_3$)Ph), 125.9 (4-*C*$_6$H$_5$), 128.2 (2,6-*C*$_6$H$_5$), 128.7 (3,5-*C*$_6$H$_5$), 130.7 (*ipso*-C$_6$H$_5$). ^{29}Si SSNMR (δ):–66,–57 (Si–O–Si cross-links),–35 (SiH), –25 (Si–Si cross-links), –21 (–O*Si*(CH$_3$)(CH$_2$CH$_2$Ph)–,– O*Si*(CH$_3$)(CH(CH$_3$)Ph)–, and–O*Si*(CH$_3$)$_2$– units), 9 (terminal (CH$_3$)$_3$Si).

3.1.3 MSR25

Methyl methacrylate (2 g) was placed in a single-necked flask, and a 0.1 M solution of Karstedt's catalyst in xylene (100 µl) in 15 ml of toluene was added. The mixture was stirred for 1 hour under argon at room temperature. Then, after purging with argon, a solution of PMHS (2.3 g for M-PMHS50) (15 ml of toluene) was added dropwise to the reaction mixture. The reaction was carried out with stirring for 72 hours in an argon atmosphere at room temperature. Next, the calculated amount of s-PDMS was added to the obtained M-PMHS. To achieve a molar ratio of methyl methacrylate of 25% in the obtained methyl methacrylate-silicone rubber (MSR), a solution of *v*-PDMS (2.82 g) in 15 ml was added dropwise to the flask with M-PMHS and stirred for an hour in an argon atmosphere at room temperature. Next, the solvent was removed on a rotary evaporator until 1/3 of the initial volume of the MSR25 solution was reached under reduced pressure and a temperature of 60°C. Then, the obtained gel was poured on a Teflon substrate into a rectangular polymer clay mold with an area of 64 cm^2 and a side height of 1 cm.

MSR25. Yield: 7.00 g (99%); flexible transparent silicone rubber.^{1}H NMR ($CDCl_3$, δ): –0.78 ((COOCH$_3$)(CH$_3$)CHC*H*H'Si≡), 1.09 ((COOCH$_3$)(CH$_3$)CHCH*H'*Si≡), 2.65 ppm. ((COOCH$_3$)(CH$_3$)C*H*CHH'Si≡), 4.75 (Si*H*). ^{13}C ЯМР ($CDCl_3$, δ): –0.4 (SiCH$_3$), 0.5 (SiCH$_3$), 1.8 (SiCH$_3$), 34.4 ((*C*OOCH$_3$)(CH$_3$)*C*HCHH'Si≡), 51.5((COO*C*H$_3$)(CH$_3$)*C*HCHH'Si≡), 77.3 ($CDCl_3$) 125.3 (4-*C*$_6$H$_5$ *(toluene)*), 128.2 (2,6-*C*$_6$H$_5$ *(toluene)*), 129.0 (3,5-*C*$_6$H$_5$ *(toluene)*), 137.8 (*ipso*-*C*$_6$H$_5$ *(toluene)*), 177.6 ((*C*OOCH$_3$)(CH$_3$)CHCHH'Si≡).

3.1.4 2,2'-Bipyridine-6,6'-dicarboxylic acid dichloride

In a round-bottom flask, previously purged with argon and equipped with a reflux condenser, 2,2'-bipyridine-6,6'-dicarboxylic acid (2.5 g, 10.24 mmol), 2 drops of triethylamine, and freshly distilled thionyl chloride (25 ml) were placed. The mixture was refluxed for 2 h at a constant flow of argon until the complete dissolution of the dicarboxylic acid, and then cooled to room temperature. Excess thionyl chloride was removed at room temperature under reduced pressure for 3 hours to give a solid powdered dichloride.

Yield: 2.87 g (99%); beige powder; melting point 288 °C.^{1}H NMR ($CDCl_3$, δ): 8.10 (t, 2H, J = 8.0 Hz, 4-*H*-Py), 8.18 (dd, 2H, J_1 = 1.1 Hz, J_2 = 7.8 Hz, 5-*H*-Py), 8.98 (dd, 2H, J_1 = 1.1 Hz, J_2 = 7.8 Hz, 3-*H*-Py). ^{13}C NMR ($CDCl_3$, δ): 124.2 (5-C_{Py}), 125.3 (3-C_{Py}), 139.4 (4-C_{Py}), 149.3 (6-C_{Py}), 154.4 (2-C_{Py}), 169.7 (*C*=O).

3.1.5 Pyridine containing PDMS

A certain amount of triethylamine was added to a solution of APDMS (50 g) in freshly distilled anhydrous dichloromethane (80 ml) at 0°C under argon. After stirring for 1.5 h, a solution of the dichloride in anhydrous dichloromethane (20 ml) was added dropwise. The resulting mixture was stirred at 0°C for 2 h and then at room temperature for 2 days. The reaction mixture was filtered from insoluble triethylammonium chloride, concentrated to 1/3 of its initial volume under reduced pressure at 45°C, and methanol (60 ml) was added to quench the reaction. After the appearance of a white precipitate, the mixture was allowed to stand for 2 h, after which the upper transparent solution was decanted. Dichloromethane (20 ml) was added to dissolve the synthesized copolymer. The dissolution–reprecipitation–decantation process was carried out 3–4 times with dichloromethane as a solvent (20 ml) and methanol as a precipitant (80 ml). Solvent residues were removed at 45°C under reduced pressure (0.506 bar) to obtain a pure polycondensate.

Bipy-PDMS5000. Yield: 41.9 g (70%); light yellow waxy material. ^{1}H NMR ($CDCl_3$, δ): 0.11 (w s, C*H*$_3$Si), 0.70 (t, 4H, SiC*H*$_2$CH$_2$CH$_2$NH), 1.75 (quint, 4H, SiCH$_2$C*H*$_2$CH$_2$NH), 3.57 (q, 4H, SiCH$_2$CH$_2$C*H*$_2$NH), 8.05 (t, J = 7.8 Hz, 2H, 4,4'-*H*- Bipy), 8.17 (t, J = 5.6 Гц, 2H, N*H*C(= O)), 8.32 (d, J = 7.6 Hz, 2H, 5,5'-*H*-Bipy), 8.55 (d, J = 7.7 Hz, 2H, 3,3'-*H*-Bipy). ^{13}C NMR ($CDCl_3$, δ): 0.1, 1.0 (*C*H$_3$Si), 15.5 (Si*C*H$_2$CH$_2$CH$_2$NH), 23.8 (SiCH$_2$*C*H$_2$CH$_2$NH), 42.5 (SiCH$_2$CH$_2$*C*H$_2$NH), 122.7 (3,3'-C_{Bipy}), 123.3 (5,5'-C_{Bipy}), 138.4 (4,4'-C_{Bipy}), 149.9 (6,6'-C_{Bipy}), 153.8 (2,2'-C_{Bipy}), 163.9 (*C*=O).

Bipy-PDMS25000. Yield: 38.1 g (75%); colorless viscous liquid.^{1}H NMR ($CDCl_3$, δ): 0.10 (w s, C*H*$_3$Si), 0.70 (t, 4H, SiC*H*$_2$CH$_2$CH$_2$NH), 1.75 (w quint, 4H, SiCH$_2$C*H*$_2$CH$_2$NH), 3.56 (w q, 4H,

SiCH$_2$CH$_2$C*H$_2$*NH), 8.05 (t, *J* = 7.6 Hz, 2H, 4,4'-*H*-Bipy), 8.16 (w t, 2H, N*H*C(=O)), 8.32 (d, *J* = 7.6 Hz, 2H, 5,5'-*H*-Bipy), 8.56 (d, *J* = 7.7 Hz, 2H, 3,3'-*H*-Bipy).

3.1.6 Preparation of Eu-Bipy-PDMS and Tb-Bipy-PDMS

A calculated amount of a metal chloride solution in freshly distilled methanol (0.1 g ml^{-1}) was diluted with anhydrous dichloromethane (10 ml) and added dropwise to a solution of the polymeric ligand (8.5 g Bipy PDMS) in anhydrous dichloromethane (40 ml). The resulting solution was vigorously stirred at room temperature for 1 h and then concentrated under reduced pressure at 45°C (to 1/3 of its initial volume). The resulting gel was poured into a PTFE mold with dimensions of 120 mm × 50 mm and dried at room temperature for 24 h, then at elevated temperatures (65–100°C) for several hours. Then, the ≈1 mm thick polymer film was separated from the PTFE mold and cut in accordance with the requirements of further experiments.

3.1.7 *N*^{6},*N*$^{6\prime}$-diisopropyl-[2,2'-bipyridine]-6,6'-dicarboxamide (BDCA)

A freshly prepared 2,2'-bipyridine-6,6'-dicarbonyl dichloride (1.14 g, 4.06 mmol) solution in dry CH_2Cl_2 (10 mL) was added to isopropylamine (2.39 g, 40.6 mmol) solution in dry CH_2Cl_2 (20 mL) by drops at 0 °C under an argon atmosphere. The reaction mixture was stirred at r.t. for 24 h and then filtered. Afterwards, it was filtered and washed with distilled water (3×100 mL). The residue was dried under vacuum at 65 °C and washed with Et_2O to afford pure BDCA. Yield: 0.93 g (70%); beige powder. ^{1}H NMR (DMSO-*d*$_6$, δ): 1.28 (d, *J* = 6.6 Hz, 12H, CH(C***H*****$_3$**)$_2$), 4.23 (m, *J*$_1$ = 6.6 Hz, *J*$_2$ = 8.5 Hz, 2H, C***H***(CH$_3$)$_2$), 8.13 (dd, *J*$_1$ = 7.7 Hz, *J*$_2$ = 1.3 Hz, 2H, 5,5′-***H***-Bipy), 8.19 (t, *J*$_1$ = 7.7 Hz, *J*$_2$ = 7.7 Hz, 2H, 4,4′-***H***-Bipy), 8.62 (d, *J* = 8.5 Hz, 2H, C(=O)N***H***), 8.98 (dd, *J*$_1$ = 7.7 Hz, *J*$_2$ = 1.3 Hz, 2H, 3,3′-***H***-Bipy). ^{13}C NMR (DMSO-*d*$_6$, δ): 22.7 (CH(***C***H$_3$)$_2$), 41.4 (***C***H(CH$_3$)$_2$), 123.0 (3,3′-***C***$_{Bipy}$), 124.3 (5,5′-***C***$_{Bipy}$), 139.3 (4,4′-***C***$_{Bipy}$), 150.4 (6,6′-***C***$_{Bipy}$), 153.8 (2,2′-***C***$_{Bipy}$), 163.2 (***C***=O). FTIR (KBr, selected bands, *ν*, cm^{-1}): 3303 (s; *ν*(N–H)), 1653 (s; $\nu_{\text{amide I}}$ (C=O)), 1533 (s; $\nu_{\text{amide II}}$ (N–H)). UV-vis (DMSO, λ_{max}, nm): 302 (C=O, n→π*), 291 (Bipy, π→π*), 282 nm (Bipy, π→π*). HRESIMS$^+$: calculated for $C_{18}H_{22}N_4O_2$ 349.1640, found *m/z* 349.1630 [M+Na]$^+$. Single crystals of BDCA were grown from CH_3OH solution over a one-week period for XRD. Crystal lattice parameters: *a* = 9.2043(6), *b* = 11.4313(5), *c* = 9.6843(6); *α* = 90°, *β* = 116.612(8)°, *γ* = 90°; monoclinic, space group *P2*$_1$*/c* (14), temperature 100 K. CCDC number: 2215221.

3.1.8 Model complexes synthesis

BDCA (465 mg, 1.42 mmol) was placed in a round-bottom flask and dissolved in anhydrous CH_3OH (20 mL). A solution of dry $TbCl_3$ or $EuCl_3$ (175 mg, 0.68 mmol) in 2 mL of anhydrous CH_3OH was slowly added dropwise to the resulting mixture. The solution was stirred at 40 °C for 24 h, and the solvent was removed by rotary evaporation at 60 °C.

[Eu(BDCA)$_2$(H$_2$O)]Cl$_3$

The obtained residue was then washed with Et_2O (3×50 mL). Yield: 608 mg (95%); beige crystals. FTIR (KBr, selected bands, ν, cm^{-1}): 3410 (s; ν(O–H)), 3220 (s; ν(N–H)), 1634 (s; ν(C=O--Eu)), 1558 (s; $\nu_{\text{amide II}}$ (N–H)), 1456 (m; ν(Py)). UV-vis (DMSO, λ_{max}, nm): 302 (C=O, n→π*), 291 (LMCT), 283 nm (LMCT). HRESIMS$^+$: calculated for $C_{36}H_{44}N_8EuO_4^{3+}$ 268.4233, found *m/z* 268.4232 $[M–3Cl]^{3+}$. Single crystals of $[Eu(BDCA)_2(H_2O)]Cl_3$ were grown from EtOH solution over a two-week period for XRD. Crystal lattice parameters: a = 11.2713(2), b = 15.3222(2), c = 14.2917(2); α = 90°, β = 106.511(2)°, γ = 90°; monoclinic, space group *P2/c* (13), temperature 100 K. Selected bond lengths (Å): Eu1–O1 2.4137(19), Eu1–O2 2.4019(19), Eu1–O3(H_2O) 2.463(3), Eu1–N1 2.536(2), Eu1–N3 2.541(2). Selected bond angles (°): O1–Eu1–N1 64.25(7), N1–Eu1–N3 62.37(7), O2–Eu1–N3 64.30(7), O1–Eu1–O3(H_2O) 70.26(5). CCDC number: 2215232.

[Tb(BDCA)$_2$(H$_2$O)]Cl$_3$

BDCA (465 mg, 1.42 mmol) was placed in a round-bottom flask and dissolved in anhydrous CH_3OH (20 mL). A solution of dry $TbCl_3$ (180 mg, 0.68 mmol) in 2 mL of anhydrous CH_3OH was slowly added dropwise to the resulting mixture. The solution was stirred at 40 °C for 24 h, and the solvent was removed by rotary evaporation at 60 °C. The obtained residue was then washed with Et_2O (3×50 mL). Yield: 606 mg (94%); beige crystals. FTIR (KBr, selected bands, ν, cm^{-1}): 3416 (s; ν(O–H)), 3222 (s; ν(N–H)), 1634 (s; ν(C=O--Tb)), 1558 (s; $\nu_{\text{amide II}}$ (N–H)), 1457 (m; ν(Py)). UV-vis (DMSO, λ_{max}, nm): 302 (C=O, n→π*), 291 (LMCT), 283 nm (LMCT). HRESIMS$^+$: calculated for $C_{36}H_{44}N_8TbO_4^{3+}$ 270.4241, found *m/z* 268.4232 $[M–3Cl]^{3+}$. Single crystals of $[Tb(BDCA)_2(H_2O)]Cl_3$ were grown from EtOH solution over a two-week period for XRD. Crystal lattice parameters: a = 11.2666(3), b = 15.2986(3), c = 14.2345(3); α = 90°, β = 106.335(3)°, γ = 90°; monoclinic, space group *P2/c* (13), temperature 100 K. Selected bond lengths (Å): Tb1–O1 2.390(2), Tb1–O2 2.3802(19), Tb1–

O3(H_2O) 2.445(3), Tb1–N1 2.512(2), Tb1–N3 2.517(2). Selected bond angles (°): O1–Tb1–N1 64.76(7), N1–Tb1–N3 62.65(8), O2–Tb1–N3 64.88(7), O1–Tb1–O3(H_2O) 70.18(5). CCDC number: 2215233.

3.2 Research methods

3.2.1 Spectroscopic and spectrometric methods of analysis

NMR spectra were recorded on a Bruker Avance III 400 spectrometer in $CDCl_3$ or DMSO-d_6 at room temperature (400 MHz for ^{1}H, 100 MHz for ^{13}C, and 80 MHz for ^{29}Si). The ^{13}C and ^{29}Si NMR spectra were recorded decoupled from ^{1}H. Chemical shifts are given in δ [ppm] and refer to residual signals from non-deuterated solvents: δ 7.26 (^{1}H) and 77.2 (13C) for $CHCl_3$ and δ 2.50 (^{1}H) and 39.5 (^{13}C) for DMSO. The following abbreviations were used to designate multiplicities: s = singlet, d = doublet, t = triplet, q = quartet, quint = quintet, m = multiplet, shir = wide, dd = doublet of doublets.

Solid state NMR spectra were obtained using a Bruker Avance III 400 MHz WB (three-channel solid state NMR spectrometer with magnetic resonance imaging and diffusion capability) operating at 400.23 MHz for ^{1}H (16 scans), 100.64 MHz for ^{13}C (2000 scans) and 79.51 MHz for ^{29}Si (2000 scans) while rotating the sample at a magic angle with a rotation frequency of approximately 12500 Hz. Solid-state ^{13}C and ^{29}Si NMR spectra were recorded by cross-polarization (typically with a delay of 2 s and a contact time of 2.0 ms) and direct excitation (typically with a delay of 5 s) decoupled from ^{1}H. Solid-state ^{1}H NMR spectra were obtained with direct excitation. The sample was ground into powder and placed in a special cuvette before measurement. Chemical shifts are given in δ [ppm] values relative to the external standard signal (pure tetramethylsilane).

IR spectra were recorded on a Shimadzu IRAffinity 1 IR-Fourier spectrophotometer. Before measurements, solid samples were crushed and pressed into a tablet with potassium bromide, and liquid samples were dissolved in carbon tetrachloride. The measurements were carried out at room temperature in the wavenumber range 4000–400 cm^{-1}. Classification of absorption bands according to intensity: s — strong, av — medium, w — weak.

Ultraviolet visible absorption spectra (UV view spectra) were recorded on a Shimadzu UV 1800 spectrophotometer. UV view spectra of low molecular weight compounds were obtained using their solutions. DMSO was used as solvents. The measurements were carried out at room temperature using a quartz cell 1 cm wide in the wavelength range of 250–800 nm. The UV spectra of silicone rubbers

were recorded using their polymer films, which were previously obtained by solution casting and crosslinking in quartz molds with a thickness of 12, 57, and 106 μm.

HRESIMS was carried out on a Bruker Maxis HRMS ESI QTOFspectrometer equipped with an electrospray ionization source. The analyzed samples were preliminarily dissolved in pure methanol for measurements of HRESIMS spectra. The instrument operated in the region of positive ions in the range m/z = 50–400. The most intense peak of the isotopic distribution is noted.

3.2.2 X-ray diffraction analysis

X-ray diffraction analysis of single crystals was carried out on Agilent Technologies "SuperNova" and Rigaku XtaLAB Synergy diffractometers using CuKα monochromatic radiation sources (λ = 1.5418 Å). The selected crystal was kept at 200 K during the acquisition. The unit cell parameters were refined by the least squares method. The crystal structure was solved using the ShelXT software package (with self-phasing) and refined by the full-matrix least squares method in F^2 in the anisotropic-isotropic approximation using the ShelXL software [125], included in the Olex2 software [126]. The CrysAlisPro software package (Agilent Technologies, 2012) used an empirical absorption correction with spherical harmonics implemented in the SCALE3 ABSPACK scaling algorithm. Hydrogen atoms were included in the refinement with fixed positional and temperature parameters. Additional crystallographic data for coordination compounds are available from the Cambridge Crystallographic Database under CCDC numbers 2215221, 2215232 and 2215233 and are available at www.ccdc.cam.ac.uk/data_request/cif.

3.2.3 Energy dispersive X-ray spectroscopy

A polymer sample (approximately 100 mg) was dissolved in a mixture of 1 mL 40% aqueous hydrofluoric acid and 4 mL concentrated nitric acid. The dissolution was performed in sealed PTFE tubes with an Ethos ONE microwave digestion system. The reaction mixture was stirred magnetically for 5 min at 80 °C to complete the reaction. The solution was centrifuged at 3000 rpm for 5 min after being cooled to RT and subsequently collected in a polypropylene film cup for EDX analysis on a Shimadzu EDX-800P spectrometer. The metal content in the solution was measured on a 41.54 keV (EuKα), 44.48 keV (TbKα) lines with signal accumulation for 100 s. The identification of the manifestation of oxidation was manifested by a linear calibration dependence using salts with a known use of metals ($EuCl_3$, $TbCl_3$,) soluble in the same acid mixture. In addition, a reference sample (a mixture

of 1 ml of 40% aqueous hydrofluoric acid and 4 ml of concentrated nitric acid) was measured to correct the baseline.

The metal content in the polymer was calculated using **equation 2**:

$$\omega_M, \% = \frac{C \cdot V}{1000000 \cdot m_{sample}} \cdot 100, \qquad (2)$$

where C — the measured M^{2+} content in solution, V = 5 mL — the volume of the solution, and m_{sample} — the mass of polymer sample, g.

3.2.4 Determination of cross-linking degree for polymers *via* swelling measurements

The *density* of a polymer was measured by the pycnometric method. First, the mass of an empty pycnometer, which was previously rinsed with distilled water and thoroughly dried, was determined. The pycnometer was filled with distilled water up to the volume mark, and the volume of water (m_1) in it was measured. The mass of a polymer pellet (m) (total weight of approximately 10 pieces of polymer) was determined. After the pieces were weighed, the polymer was immersed in the full pycnometer with water to avoid air bubbles remaining on thepieces. The excess water was removed using filter paper, thus bringing the water level down to the volume mark. Subsequently, the mass of the full pycnometer, with water and the polymer (m_2), was determined. The density of the polymer sample (ρ) was calculated using the **equation 3**:

$$\rho = \frac{m}{m_1 + m - m_2} \cdot \rho_0, \qquad (3)$$

where ρ_0 = 0.997 g mL^{-1} — the density of distilled water at RT.

The *swelling parameters* of a polymer were measured using a Soxhlet extractor. The initial dry weight of a polymer sample (a cylindrical disk of 10 mm diameter and 1 mm thickness) (m_{unex}) was established by weighing it. 125 mL of toluene was added to a round- bottom flask connected to the Soxhlet extractor with a reflux condenser. The polymer samples were loaded into the thimble, which was placed inside the Soxhlet extractor prior to the experiment. The process of swelling was carried out upon toluene refluxing for 2 h. The swelledpolymer sample was removed, gently wiped to remove the liquid solvent present on the sample surface, and it was immediately weighed (m_s). The swelling percentage (s) of the polymer sample was calculated using the **equation 4**:

$$s\ (\%) = \frac{m_s}{m_{unex}} \cdot 100, \qquad (4)$$

The polymer sample was then dried overnight at RT, dried at 100 °C under reduced pressure for 2 h, and finally reweighed (m_{ex}). The soluble fraction (sol fraction, w_{sol}) and the volume fraction of the polymer network in the swollen sample (gel fraction,) were calculated using **equations 5, 6**:

$$w_{sol}\,(\%) = \frac{m_{unex}-m_{ex}}{m_{unex}} \cdot 100, \quad (5)$$

$$v = \left[1 + \frac{m_s-m_{ex}}{m_{ex}} \cdot \frac{\rho_p}{\rho_s}\right]^{-1}, \quad (6)$$

where $\rho_s = 0.87$ g mL^{-1} and ρ_p — the toluene and polymer densities, respectively. The swelling experiments were carried out three times for each test.

The cross-linking degree ($_{cross}$) and the average molecular weight of the segment between the cross-links (M_c) were calculated for each polymer by the Flory-Rener equation [112] (**equation 7, 8**):

$$\rho_{cross} = -\frac{1}{V_s} \cdot \frac{\ln(1-v)+v+\chi v^2}{v^{\frac{1}{3}}-\frac{v}{2}}, \quad (7)$$

$$M_c = \frac{\rho_p}{\rho_{cross}}, \quad (8)$$

where V_s = 106.3 cm^3 mol^{-1} — the molar volume of toluene, $\chi = 0.465$ — the Flory-Hugginsparameter of the polymer–solvent interaction (PDMS–toluene [127]).

3.2.4.1 Calculation of a swelling mesuarment error

The non-excluded systematic error θ of the swelling measurement results for polymers (s, w_{sol} and v) has been calculated based on the systematic error of the digital analytical balance Shimadzu AUX 220 (I accuracy class, weighing capacity is 220 g) according to **equation 9** with the accepted confidence level $P = 0.95$ [128]:

$$\theta = 1.1 \cdot \overline{x} \cdot \sqrt{\sum_{i=1}^{n}\left(\frac{\Delta m}{m_i}\right)^2}, \quad (9)$$

where Δm=±0.3 mg — the systematic error of the analytical balance, m_i — the weight of the i^{th} sample (m_{unex}, m_s and/or m_{ex}), mg; $\overline{x}$ — the arithmetic mean of the determined parameter (s, w_{sol} or v).

Since each series included $n = 7$ polymer samples, the Student distribution has been used, and the Student's t-test has been chosen $t = 2.45$ to process the measurement results. The randomerror has been calculated *via* ϵ has been calculated *via* **equation 10** [129]:

$$\epsilon = t \cdot \frac{S_x}{\sqrt{n}} = t \cdot \sqrt{\frac{\sum_{j=1}^{n}(x_j - \overline{x})^2}{n(n-1)}}, \quad (10)$$

где S_x — the standard deviation of single measurement results, x_j — the j^{th} parallel measurement result of the sample in the series, $\overline{x}$ — the average value of the measurement results of the samples in the series.

The confidence interval for measurement error Δ has been determined using **equation 11** [128]:

$$\Delta = \sqrt{\theta^2 + \epsilon^2}, \quad (11)$$

3.2.5 Mechanical tensile tests

Mechanical tensile tests have been carried out on a Shimadzu EZ-L-5kN universal testing machine at RT. Tension tests have been carried out 7–9 times for each series of polymer samplesat a constant stretching rate of 10 mm·min^{-1}. The cyclic stress-strain tests have been implemented five times for the polymer samples at a constant stretching rate of 10 mm·min^{-1}.The manual screw flat grips Shimadzu SCG 5KNA CAP.5kN have been used to fix polymer samples. The polymer samples have been wrapped with two protective layers of blue 3M Temflex 1300 PVC insulating tape, preventing slipping and tearing of the studied soft materialsby the corrugated clamps' surface. The sample shape corresponded to ISO 37 type 3 (the working area was 16 mm × 4 mm × 1 mm), cut using a die cutter. The resulting stress-strain curves have been refined and averaged using the Origin Pro 2018 software. Polynomial interpolation smoothing was applied to the obtained averaged curves for a more visual representation in the figures.

The elongation at break ε has been determined according to **equation 12**:

$$\varepsilon = \frac{l_{break} - l}{l} \cdot 100, \quad (12)$$

where l_{break} — the length of the measured working area of a polymer sample at the moment of rupture, l — the initial length of the measured working area of a polymer sample.

The Young's modulus E was determined from a low strain region strain from ε_1 = 1% to ε_2 = 3–20%) and calculated *via* **equation 13**:

$$E = \frac{\sigma_2 - \sigma_1}{\varepsilon_2 - \varepsilon_1}, \quad (13)$$

where σ_1 and σ_2 — the stress values at strains ε_1 and ε_2.

The *self-healing efficiency* of polymers has been determined *via* tensile tests. A crosscutwas carefully made in the working area of a polymer strip using a thin razor blade to reproducethe "natural"

damage (a through-the-thickness crack) as much as possible. This procedure was conducted to prevent and minimize the distance between the sample halves without changing their position relative to each other. After cutting, self-healing of the strips was immediately carried out in aerobic conditions at RT or by heating to 100 °C in a thermostatic chamber for different time intervals (1, 2, 3, 24, 48, and 72 h). Following that, stress-strain tests of original and healed strips were conducted in the air at RT, in order to estimate their self-healing efficiency (η), which was calculated using the following **equation 14**:

$$\eta = \frac{\sigma_{max}}{\sigma_{max\,0}} \cdot 100, \qquad (14)$$

where σ_{max} and $\sigma_{max\,0}$ — the tensile strengths of healed and original strips.

3.2.5.1 Calculation of measurement error of mechanical properties

The measurement error of elongation at break. The non-excluded systematic error θ_ε of elongation at break has been calculated based on the instrument error of the crosshead position detector of the Shimadzu EZ-L-5kN testing machine (Δl_1 = 0.01 мм) and digital caliper (Δl_2 = 0.03 мм), used to measure the geometry of each sample. The calculations have been conducted according to **equation 15** with the accepted confidence level P = 0.95 [128]:

$$\theta_\varepsilon = 1.1 \cdot \overline{\varepsilon} \cdot \sqrt{\left(\frac{\Delta l_1}{l}\right)^2 + \left(\frac{\Delta l_2}{l}\right)^2}, \qquad (15)$$

where l — the initial length of the measured working area of a polymer sample, mm; $\overline{\varepsilon}$ — the arithmetic mean of elongation at break, %.

Since each series included n = 7–9 polymer samples, the Student distribution has been used, and the Student's t-test has been chosen t = 2.45, 2.37, and 2.31 (P = 0.95) for statistical sample n = 7, 8, and 9 to process the measurement results, respectively. The random error hasbeen calculated *via* **equation 16** [129]:

$$\epsilon_\varepsilon = t \cdot \frac{S_\varepsilon}{\sqrt{n}} = t \cdot \sqrt{\frac{\sum_{i=1}^{n}(\varepsilon_i - \overline{\varepsilon})^2}{n(n-1)}}, \qquad (16)$$

где S_ε — the standard deviation of single measurement results for elongation at break, ε_i — the i^{th} parallel measurement result of elongation at break for the sample in the series, $\overline{\varepsilon}$ — the average value of the measurement results of elongation at break for the samples in the series.

The confidence interval for measurement error Δ_ε (excluding ± sign) has been determined using **equation 17** [128]:

$$\Delta_\varepsilon = \sqrt{{\theta_\varepsilon}^2 + {\epsilon_\varepsilon}^2}, \qquad (17)$$

The measurement error of tensile strength and Young's modulus. The non-excluded systematic error $\theta_{\sigma,E}$ of tensile strength σ and Young's modulus E has been calculated based on the instrument error of the force sensor (ΔF of the measured force value according to the instrument specification, $\Delta F/F = 0.01$) crosshead position detector of the Shimadzu EZ-L-5kN testing machine ($\Delta l_1 = 0.01$ mm) and digital caliper ($\Delta l_2 = 0.03$ mm). Calculations were carried out according to **equation 18** with the accepted confidence probability P = 0.95 [128]:

$$\theta_{\sigma,E} = 1.1 \cdot \overline{x} \cdot \sqrt{(\frac{\Delta F}{F})^2 + (\frac{\Delta l_1}{l})^2 + (\frac{\Delta l_2}{l})^2 + (\frac{\Delta l_2}{d})^2 + (\frac{\Delta l_2}{h})^2}, \qquad (18)$$

где l — the initial length of the measured working area of a polymer sample, mm; d — the initial width of the measured working area of the polymer sample, mm; h — the initial thickness of the measured working area of the polymer sample, mm; $\overline{x}$ — the arithmetic mean of tensile strength and/or Young's modulus, MPa.

Since each series included n = 7–9 polymer samples, the Student distribution has been used, and the Student's t-test has been chosen t = 2.45, 2.37, and 2.31 (P = 0.95) for statistical sample n = 7, 8, and 9 to process the measurement results, respectively. The random error $\epsilon_{\sigma,E}$ has been calculated *via* **equation 19** [129]:

$$\epsilon_{\sigma,E} = t \cdot \frac{S_{\sigma,E}}{\sqrt{n}} = t \cdot \sqrt{\frac{\sum_{i=1}^{n}(x_i - \overline{x})^2}{n(n-1)}} \qquad (19)$$

where $S_{\sigma,E}$ — the standard deviation of single measurement results for tensile strength or Young's modulus, x_i — the i^{th} parallel measurement result of tensile strength or Young's modulus for the sample in the series, $\overline{x}$ — the average value of the measurement results of tensile strength or Young's modulus for the samples in the series.

The confidence interval for measurement $\Delta_{\sigma,E}$ (excluding ± sign) has been determined *via* **equation 20** [128]:

$$\Delta_{\sigma,E} = \sqrt{{\theta_{\sigma,E}}^2 + {\epsilon_{\sigma,E}}^2} \qquad (20).$$

3.2.6 Thermogravimetry

Polymer TG was carried out on a NETZSCH TG 209F1 Libra TGA209F1D 0024 analyzer in air and in an inert (argon) atmosphere. The samples were heated from 30 to 800°C at a heating rate of 10°C min^{-1}.

3.2.7 Scanning electron microscopy

SEM measurements have been carried out on a Carl Zeiss Supra 25 microscope on the basis of SPbAU RAS named after Zh.I. Alferova.

3.2.8 Photoluminescent properties study

PL spectra were recorded on a Horiba Fliorolog-3 spectrofluorimeter (Jobin Yvon Technology, Bensheim, Germany) at 21 °C. QY measurements were carried out using a Shimadzu RF-6000 spectrofluorimeter (Kyoto, Japan) with an integrating sphere (101 mm in diameter). Steady-state PL lifetime measurements were carried out using a Horiba Fliorolog-3 spectrofluorometer with a 150 W pulsed xenon lamp as the excitation source.

3.2.9 Growth of GaP NWs by molecular beam epitaxy

GaP NWs were synthesized through the self-catalyzed vapor-liquid-solid (VLS) growth mechanism by solid-source molecular beam epitaxy (MBE) on Si (111) substrate using Veeco GEN-III MBE machine. Si substrates were treated with the Shiraki cleaning procedure, ended by the wet-chemical oxidation in a boiling mixture of ammonia and hydrogen peroxide (NH_4OH:H_2O_2:H_2O with a ratio of 1:1:3). In further, the resulting thin surface oxide layer promotes the self-organized formation of Ga catalytic droplet and serves as a growth mask for NW nucleation Prior to the growth, oxidized Si (111) substrates were annealed in MBE chamber at 760 °C for 30 min order to promote the formation of pinholes in the oxide layer required for vertical NW growth.

The ratio of group-III and -V element fluxes, was controlled with conventional Bayard–Alpert vacuum gauge measuring their beam equivalent pressures. NWs were grown at the substrate temperature of 630 °C, Ga flux corresponding to the GaP equivalent planar growth rate of 190 $nm \cdot h^{-1}$, and V/III ratio of 20. NWs were intentionally doped with Si during the growth using a standard effusion cell as a Si

dopant source. Growth was initiated by simultaneous opening of Ga, P and Si shutters. It was shown, that despite the amphoteric nature of Si dopant in III–V compounds, it leads to predominantly n-type conductivity in VLS-grown III-phosphide alloy NWs. An in-situ analysis of the NW crystal structure by the reflection high energy electron diffraction (RHEED) demonstrates that NWs grow vertically along the Si [111], direction preserving GaP bulk zinc-blende structure. According to our observations, the introduction of Si flux does not perturb the VLS growth and NW morphology, and thus allows to obtain the epitaxial arrays of vertically oriented NWs with a height of about 8 μm and a diameter of about 185±40 nm.

3.2.10 $CsPbBr_3$ perovskite layer fabrication

PEO (10 mg·mL^{-1}) dimethyl sulfoxide (DMSO) solution and $CsPbBr_3$ (0.2 M) DMSO solution were mixed with 1.25:1 wt. ratio and stirred at room temperature for 1 h prior to thin film formation. The composite film was prepared via drop-casting and annealed at 60 °C for 5 min.

3.2.11 Synthesis of SWCNT layers

SWCNT layers were synthesized by an aerosol (floating catalyst) vapor deposition method. Carbon nanotubes were produced in a tubular quartz reactor by the Boudoir reaction using an Fe-based catalyst. The SWCNT aerosol was deposited on a HAWP nitrocellulose filter (Merck Millipore) with the formation of thin layers of a given thickness. Thin layers with a transparency of 90% (at a wavelength of 550 nm) on the filter were cut to a size of approximately 0.5 mm^2, and several contact pads were applied by dry transfer to both sides of the SSR25/n-GaP NWs/$CsPbBr_3$ membranes to create an ohmic contact.

3.2.12 Investigation of the adhesion properties of silicone rubbers

Adhesive properties were studied by analyzing AFM approach/retraction curves. AFM approach/retraction curves were measured and analyzed on a Bruker AFM using standard silicon cantilevers (TipsNano HA_CNC B, cantilever length 184 ± 2 μm, cantilever width 34 ± 3 μm). The cantilever "sticks" to the polymer layer due to van der Waals, capillary and other forces. The adhesion force significantly affects the interaction of the cantilever-polymer when the AFM probe is removed from the sample surface. This force causes the cantilever to bend until it lifts off the surface. An analysis of the approach/retraction curves from different polymer films under the same experimental conditions

makes it possible to estimate the adhesion forces. The influence of the cantilever shape on the results can be neglected by using the same probe in the study of a series of polymers. It is assumed that the decrease in the adhesion force to the Si AFM cantilever can be extrapolated to the adhesion of silicone to the Si substrate.

CONCLUSION

In this work, methods were developed and optimized for the production of silicone materials for flexible inorganic LEDs based on arrays of A3B5 NWs of compounds: *(i)* “styrene-containing” and “methyl methacrylate-containing” silicone rubbers with reduced adhesion to a growth Si substrate due to the substitution of side Si–H groups on phenylethyl and 2-methyl-3-methoxy-3-oxopropyl and *(ii)* luminescent polymer metal complexes of terbium(III) and europium(III) with 2,2-bipipridin-6,6'-dicarboxyamide-*co*-polydimethylsiloxanes, in which photoactive centers are also cross-links. The obtained SSR and MSR are optically transparent, mechanically strong, and have reduced adhesion to the growth silicon substrate. This allowed to employ them as a flexible supporting matrix in inorganic light-emitting devices based on A3B5 NW arrays synthesized on Si. The luminescent Eu–Bipy–PDMS and Tb–Bipy–PDMS obtained in this work exhibit the property of non-autonomous self-healing after mechanical damage. In this work, we demonstrate that the nature of the coordination center (Eu (III), Tb (III)) allows one to control the color of photoluminescence by applying thin silicone films containing various types of lanthanides. Due to the non-autonomus self-healing properties, superimposed thin films could be converted into monolithic systems by heating at 100°C. Such silicone "monoliths" have two photoluminescence colors, which are determined by the ratio and number of films of each type.

The developed low-adhesion (to silicon) silicone rubbers can be used as a flexible supporting matrix for light-emitting devices based on NW A3B5 arrays, in particular, LEDs with the SSR25/n-GaP NWs/$CsPbBr_3$/SWCNT architecture. The developed photoluminescent Eu–Bipy–PDMS and Tb–Bipy–PDMS can be used as photoluminescent coatings for flexible LEDs based on NW arrays, as well as self-healing protective coatings for smartphones, tablets, laptops, and smart watches.

Based on the work done, the following conclusions can be drawn:

1. S-PMHS and M-PMHS were synthesized by the reaction of catalytic hydrosilylation between polymethylhydrosiloxane and styrene or methyl methacrylate, respectively. Cross-linked SSR25, SSR50 and MSR25 (the content of phenylethyl and 2-methyl-3-methoxy-3-oxopropyl substituents is 25 and 50%) were obtained by catalytic hydrosilylation reaction between α,ω-di(trivinylsiloxy)polydimethylsiloxane and S-PMHS or M-PMHS. Using SS NMR spectroscopy, it was proved that the cross-linking occurs due to both catalytic hydrosilylation and catalytic dehydrocoupling reactions between unreacted Si–H groups.
2. It has been established that the SSR25 and MSR25 silicone rubbers have a uniform morphology, which was confirmed by SEM, and are optically transparent in the UV and visible regions of the spectrum. The values of adhesion to the growth silicon substrate for SSR25 and MSR25, obtained by analyzing the AFM approach/retraction curves, are

approximately two times lower than in the case of the commercially available Sylgard 184.

3. The degree of cross-linking of SSR25 (ρ_{cross} = 13.3 mmol·cm^{-3}) is higher than that of MSR25 and SSR50 (ρ_{cross} = 3.2 mmol·cm^{-3} and ρ_{cross} = 0.50 mmol·cm^{-3}, respectively) and is close to the values of Sylgard 184 (ρ_{cross} = 11.6 mmol·cm^{-3}), which makes SSR25 the most promising among the studied silicone rubbers. SSR25 is characterized by elongation at break (ε = 45%) and ultimate tensile strength (σ = 1.5 MPa), which is satisfactory for applications of flexible optoelectronics, as well as by a higher Young's modulus (E = 3.4 MPa), in contrast to Sylgard 184 (E = 1.1 MPa). SSR25 was used to obtain stronger and, at the same time, sufficiently flexible thin membranes (4 μm thick) with encapsulated NWs, which are separated from the silicon substrate without damage, in contrast to Sylgard 184
4. For the first time, a flexible LED with a new SSR25/n-GaP NWs/$CsPbBr_3$/SWCNT architecture has been created, demonstrating electroluminescence in the green region of the spectrum (538 nm) at an operating voltage of 5 V. The resulting PLED is able to maintain its operating characteristics after 30 bending cycles.
5. Eu–Bipy–PDMS and Tb–Bipy–PDMS polymer metal complexes based on 2,2'-bipyridine-6,6'-dicarboxamide-*co*-polydimethylsiloxanes (M_n = 5000 and 25000) and lanthanides (Tb^{3+} and Eu^{3+}) were synthesized. Using IR, UV spectroscopy, as well as XRD, HRESIMS and quantum-chemical calculations of model complexes $[Tb(BDCA)_2(H_2O)]Cl_3$ and $[Eu(BDCA)_2(H_2O)]Cl_3$ it was proved that the coordination cross-links in the obtained PMCs are carried out via lanthanide – N_{Bipy} and lanthanide – $O_{carboxyl}$.
6. Eu–Bipy–PDMS5000 and Tb–Bipy–PDMS5000 are characterized by higher values of tensile strength and Young's modulus (σ=1.5 MPa, E=3.6 MPa) compared to PMCs based on monopyridyl ligands (σ=0.45 MPa, E=1.39 MPa). The resulting Eu–Bipy–PDMS and Tb–Bipy–PDMS are characterized by high elasticity (in the case of Eu,Tb–Bipy–PDMS5000, the relative elongation at break is 185–188%, for Eu,Tb–Bipy–PDMS25000, it is 221–255%). Established Eu–Bipy–PDMS have the property of non-autonomus self-healing (90 % self-healing efficiency at 100°C) Eu–Bipy–PDMS and Tb–Bipy–PDMS are more heat-resistant silicone materials, the temperature of the onset of decomposition is 400°C, according to compared with PMCs based on monopyridyl ligands (300°C) [2].
7. At an excitation wavelength of 320–340 nm, Eu–Bipy–PDMS and Tb–Bipy–PDMS exhibit photoluminescence in the red and green spectral regions, respectively. Eu–Bipy–PDMS5000 and Tb–Bipy–PDMS5000 have the highest photoluminescence quantum yields of 10.5% and 18.5%, respectively. The possibility of controlling the color of photoluminescence by applying thin films (100 μm thick) containing different types of lanthanides is shown. Due

to the non-autonomous self-healing properties, superimposed films can be converted into monolithic systems by heating at 100°C. Such "monoliths" have different colors (from green to red) of photoluminescence, which are determined by the ratio and number of films of each type.

8. Eu–Bipy–PDMS and Tb–Bipy–PDMS were tested as photoluminescent layers for a flexible UV-LED (GaN/AlGaN) NWs/Sylgard 184/SWCNT. The resulting PCMs can be used as self-healing protective coatings for the screens of smartphones, tablets, laptops, and smart watches, as well as luminescent layers in flexible displays and light-emitting devices based on NWs arrays.

ACKNOWLEDGMENTS

The author expresses his deepest gratitude for the help in the preparation of the dissertation work to the supervisors – Assoc.Prof, Dr. of Science in Chem., Regina M. Islamova and Assoc.Prof, Dr. of Science in Phys. and Math., Ivan S. Mukhin.

The author is grateful to the laboratory of Prof, Dr. of Science in Phys. and Math., S.V. Makarov (Laboratory of hybrid nanophotonics and optoelectronics, ITMO University), in particular, research engineer M.G. Baeva for the synthesis of perovskite solutions and composites, as well as the development of a technique for applying a light-emitting perovskite layer and optimization of the hybrid green LED architecture.

The author is deeply grateful to Dr. F.M. Kochetkov (Laboratory of Renewable Energy Sources, St. Petersburg Academic University).

The author expresses her gratitude to Dr. A.S. Novikov (Department of Physical Organic Chemistry, Institute of Chemistry, St. Petersburg State University) for performing quantum chemical calculations and modeling spectra.

The author thanks Junior researcher A.M. Mozharov for conducting SEM measurements at St. Petersburg Academic University.

The work was carried out with the financial support of the Russian Science Foundation (grant 20-19-00256) and project of St. Petersburg State University (94124215) using the equipment of the resource centers of St. Petersburg State University "Magnetic resonance research centre", "Chemical analysis and materials research centre", " Centre for X-ray diffraction studies ", " Thermogravimetric and calorimetric research centre " and " Centre for optical and laser materials research ".

LIST OF ABBREVIATIONS

NW — nanowire;

PMC — polymer metal comlex;

Chemical compounds and substances

S–PMHS — poly(methylhydrosiloxane-co-methyl(2-phenylethyl)siloxane-*co*-methyl(1-phenylethyl)siloxane);

S–PMHS50 — poly(methylhydrosiloxane-co-methyl(2-phenylethyl)siloxane-*co*-methyl(1-phenylethyl)siloxane) with a molar content of phenylethyl units of 50%;

S–PMHS75 — poly(methylhydrosiloxane-co-methyl(2-phenylethyl)siloxane-*co*-methyl(1-phenylethyl)siloxane) with a molar content of phenylethyl units of 75%;

M–PMHS — poly(methyl(2-methyl-3-methoxy-3-oxopropyl)siloxane-co-methylhydrosiloxane);

SSR — phenylethyl-functionalized silicone rubber (styrene-containing silicone rubber);

SSR25 — phenylethyl-functionalized silicone rubber with 25 mol.% content of phenylethyl groups;

SSR50 — phenylethyl-functionalized silicone rubber with 50 mol.% content of phenylethyl groups;

MSR — 2-methyl-3-methoxy-3-oxopropyl-functionalized silicone rubber (methyl methacrylate-containing silicone rubber);

MSR25 — 2-methyl-3-methoxy-3-oxopropyl functionalized silicone rubber with 25 mole % 2-methyl-3-methoxy-3-oxopropyl groups;

n-GaP — n-doped gallium phosphide;

SWCNT — single-walled carbon nanotubes;

Bipy–PDMS — 2,2'-bipyridine-6,6'-dicarboxamide-*co*-polydimethylsiloxane

Eu–Bipy–PDMS — europium(III)-2,2'-bipyridine-6,6'-dicarboxamide-*co*-polydimethylsiloxane polymer metal complex;

Tb–Bipy–PDMS — terbium(III)-2,2'-bipyridine-6,6'-dicarboxamide-*co*-polydimethylsiloxane polymer metal complex;

Eu–Bipy–PDMS5000 — europium(III)-2,2'-bipyridine-6,6'-dicarboxamide-*co*-polydimethylsiloxane polymer metal complex with a number average molecular weight of 5000;

Tb–Bipy–PDMS5000 — terbium(III)-2,2'-bipyridine-6,6'-dicarboxamide-*co*-polydimethylsiloxane polymer metal complex with a number average molecular weight of 5000;

Eu–Bipy–PDMS25000 — europium(III)-2,2'-bipyridine-6,6'-dicarboxamide-*co*-polydimethylsiloxane polymer metal complex with a number average molecular weight of 25000;

Tb–Bipy–PDMS — terbium(III)-2,2'-bipyridine-6,6'-dicarboxamide-*co*-polydimethylsiloxane polymer metal complex with a number average molecular weight of 25000;

PDMS — polydimethylsiloxane;

PMMA — polymethyl methacrylate;

MOI — 2-(methacryloxy)methylisocyanate;

PDMS-*graft*-PSt— graft copolymer of PDMS and polystyrene;

EFSR — elastic ferrocenyl-containing silicone rubber;

$Zn(CF_3SO_3)_2$–PDMS — zinc(II)2,2'-bipyridine-5,5'-dicarboxyamide-*co*-PDMS polymer metal complex with $CF_3SO_3^-$ counterions;

Ni–Py–PDMS — nickel(II)-pyridine-2,6-dicarboxamide-*co*-polydimethylsiloxane;

Co–Py–PDMS — cobalt(II)-pyridine-2,6-dicarboxamide-*co*-polydimethylsiloxane;

Ln–Py–PDMS — lanthanide(III)-pyridine-2,6-dicarboxamide-*co*-polydimethylsiloxane

HPS — 1,1,2,3,4,5-heptaphenyl-1-hydrosilol;

D_4Vi — tetramethyl-tetravinyl-cyclotetrasiloxane;

D_4H — tetramethyl-tetrahydro-cyclotetrasiloxane;

PEDOT:PSS — poly(3,4-ethylenedioxythiophene)-polystyrenesulfonate;

AgNWs — silver nanowiers;

CuNWs — copper nanowiers;

v-PDMS — α,ω-di(dimethylvinylsiloxy)polydimethylsiloxane;

APDMS — *α,ω*-di(3-aminopropyldimethylsiloxy)polydimethylsiloxane;

BDCA — N^6,N^6– diisopropyl-2,2'-bipyridine-6,6'-dicarboxamide;

DMSO-d_6 — deuterated dimethyl sulfoxide;

PEO — polyethylene oxide;

PMHS — polymethylhydrosiloxane;

PTFE — polytetrafluoroethylene;

Research methods

NMR — nuclear magnetic resonance;

DFT — density functional theory;

EDX — energy-dispersive X-ray spectroscopy;

QTAIM — quantum theory of atoms in molecules;

IR — infrared spectroscopy (or spectrum);

HRESIMS — high-resolution electrospray ionization mass spectrometry;

XRD — single-crystal X-ray diffraction;

TG — thermogravimetry;

UV-vis — ultraviolet-visible spectroscopy (or spectrum);

SEM — scanning electron microscopy (scanning electron microscope);

AFM — atomic force microscopy (atomic force microscope);

I-V curve; — current-voltage curve;

EL — electroluminescence;

PL — photoluminescence;

Other abbreviations

OLED — organic ligth-emitting diode;

AMOLED — organic ligth-emitting diode;

LEPs — light-emitting polymers;

PLED — perovskite ligth-emitting diode;

ACEL — alternating-current electroluminescent devices;

DSSC — dye sensitized solar cells;

HOMO — highest occupied molecular orbital;

LUMO — lowest unoccupied molecular orbital;

HIL — hole injection layer;

EIL — electron injection layer;

HTL — hole transporting layer;

ETL — electron transporting layer;

Units and parameters

E — Young's modulus;

M_c — average molecular weight of the segment between the cross-links, calculated bythe swelling parameters;

M_n and M_w — number-average and mass-average molecular weights, respectively;

m_{unex}, m_s and m_{ex} — initial dry weight, weights of swollen and dried after swellingpolymer sample, respectively;

s — swelling percentage of a polymer;

T — temperature;

T_{mp} — melting point;

T_g — glass transition temperature;

υ — volume fraction of a dried polymer network in the swollen sample (gel fraction);

w_{sol} — mass percentage of the soluble fraction of a polymer (sol fraction);

δ — chemical shift in NMR spectroscopy;

ε — elongation at break;

η — self-healing efficiency;

λ — wavelength;

ρ — density;

ρ_{cross} — cross-linking degree;

σ — tensile strength, bulk conductivity;

$\sigma_{initial}$ and σ_{healed} — tensile strengths of initial and healed materials (after self-healing), respectively.

°C — degree Celsius;

mA — miliamper;

V — volt;

min — minute;

rpm — revolutions per minute;

ppm — parts-per-million;

Hz — herz;

kHz — kilohertz;

s — second;

h — hour;

nm — nanometr;

MPa — megapascal;

cSt — centiStokes;

mmol — millimol;

$S \cdot cm^{-1}$ — siemens per centimeter;

cm — centimeter;

S — siemens;

eV — electronvolt;

μm— micrometer;

Ω — Ohm;

Ω/□ — Ohm per square

cd/m^2 — candela per sq. meter.

REFERENCES

[1] Eliseeva, S.V. and Bünzli, J.-C.G. Lanthanide luminescence for functional materials and bio-sciences // Chemical Society Reviews. – 2009. – V. 39. –P. 189–227.

[2] Yang, J., Wang, T., Guo, R., Yao, D., Guo, W., Liu, S., Li, Zh, Wang, Y and Li, H. Self-healing material with reversible luminescence switch behavior // ACS Applied Materials & Interfaces. – 2020. – V. 12. –P. 54026–34.

[3] Kargin, V.A., Akutin, M.S., Efstratov, V.F., Enikolopyan, N.S., Kabanov, V.A., Korshak, V.V., Krenzel, B.A., Paksver, A.B., Smirnov, V.S., Slonimsky, G.S. and Yakubovich, S.V. Encyclopedia of polymers. // Soviet Encyclopedia V. 1. – 1972. –1224 p.

[4] Yilgör, E. and Yilgör, I. Silicone containing copolymers: Synthesis, properties and applications // Progress in Polymer Science. – 2014. – V. 39. –P.1165–95.

[5] Moretto, H.-H., Schulze, M. and Wagner, G. Silicones // B: Wiley-VCH Verlag GmbH & Co. KGaA, редактор. – Ullmann's Encyclopedia of Industrial Chemistry. – 2000. –P. a24_057.

[6] Hamdani, S., Longuet, C., Perrin, D., Lopez-cuesta, J.-M. and Ganachaud, F. Flame retardancy of silicone-based materials // Polymer Degradation and Stability. – 2009. – V. 94. –P. 465–95.

[7] Blanco, I. Polysiloxanes in theranostics and drug delivery: a review // Polymers. – 2018 г. – V. 10. –P. 755.

[8] McDonald, J.C., Duffy, D.C., Anderson, J.R., Chiu, D.T., Wu, H., Schueller, O.J. and Whitesides G.M. Fabrication of microfluidic systems in poly(dimethylsiloxane) // Electrophoresis. – 2000. – V. 21. –P. 27–40.

[9] Ren, Z. and Yan, S. Polysiloxanes for optoelectronic applications // Progress in Materials Science. – 2016. – V. 83. –P. 383–416.

[10] Yang, H., Liu, M.-X., Yao, Y.-W., Tao, P.-Y., Lin, B.-P., Keller, P., Zhang, X.-Q., Sun, Y. and Guo L.-X. Polysiloxane-based liquid crystalline polymers and elastomers prepared by thiol–ene chemistry // Macromolecules. – 2013. – V.46 –P. 3406–16.

[11] Ling, Q.-D., Liaw, D.-J., Zhu, C., Chan, D.S.-H., Kang, E.-T. and Neoh, K.-G. Polymer electronic memories: materials, devices and mechanisms // Progress in Polymer Science. – 2008. – V. 33. –P. 917–78.

[12] Monteiro, J.H.S.K. and de Bettencourt-Dias, A. Lanthanide ion emission in multicolor OLEDs (Ce 3+ , Pr 3+ , Tb 3+ , Dy 3+ , Tm 3+ , and white light Eu 3+ /Tb 3+ hybrid systems) and device characterization // Lanthanide-Based Multifunctional Materials. – 2018. –131 p.

[13] Grzegorczyk, W.J., Ganesan, P., Savenije, T.J., van Bavel, S., Loos, J., Sudhölter, E.J.R. Siebbeles, L.D.A. and Zuilhof, H. Photoconductance of bulk heterojunctions with tunable nanomorphology consisting of P3HT and naphthalene diimide siloxane oligomers // The Journal of Physical Chemistry C. – 2009. – V. 113. –P. 7863–9.

[14] Lee, S., Jeon, Y., Lim, Y., Hossain, Md.A., Lee, S., Cho, Y., Ju H. and Kim, W. A new siloxane containing imidazolium iodide as electrolyte for dye-sensitized solar cell // Electrochimica Acta. – 2013. – V. 107. – P. 675–80.

[15] Bae, J.-Y., Lim, D., Yun, H.-G., Kim, M., Jin, J. and Bae, B.-S. A quasi-solid-state dye-sensitized solar cell based on sol–gel derived in situ gelation of a siloxane hybrid electrolyte // RSC Advances. – 2012. – V. 2. – P. 5524–7.

[16] Lee, S.H., Lim, Y.D., Seo, D.W., Hossain, Md.A., Jang, H.H., Lee, H.C. and Kim, W.G. Novel cyclic sulfonium iodide containing siloxane high performance electrolyte for dye-sensitized solar cell // Journal of Industrial and Engineering Chemistry. – 2013. – V. 19. – P. 322–6.

[17] Mikkonen, R., Puistola, P., Jönkkäri, I. and Mäntysalo, M. Inkjet printable polydimethylsiloxane for all-inkjet-printed multilayered soft electrical applications // ACS Applied Materials & Interfaces. – 2020. – V. 12. – P.11990–7.

[18] Mark, J.E., Schaefer, D.W. and Lin, G. The Polysiloxanes //Oxford University Press, Oxford, UK. 2015 г. –296 с.

[19] Jung, H.-C., Moon, J.-H., Baek, D.-H., Lee, J.-H., Choi Y.-Y., Hong, J.-C. and Lee, S.-H. CNT/PDMS composite flexible dry electrodesfor long-term ECG monitoring // IEEE Transactions on Biomedical Engineering. – 2012. – V. 59. – C. 1472–9.

[20] Barshutina, M.N., Kirichenko, S.O., Wodolajski, V.A. and Musienko, P.E. Mechanisms of electrical conductivity in CNT/silicone composites designed for neural interfacing // Materials Letters. – 2019. – V. 236. – P. 183–6.

[21] Du, J., Wang, L., Shi, Y., Zhang, F., Hu, S., Liu, P., Li, A. and Chen, J. Optimized CNT-PDMS flexible composite for attachable health-care device // Sensors. – 2020. – V. 20. – P. 4523.

[22] Sharma, B., Kim, J.-S. and Sharma, A. AgNWs-graphene transparent conductor for heat and sensing applications // Materials Research Express. – 2019. – V. 6. – P. 066312.

[23] Liu, Y., Shi, J., Yang, Z., Wang, X., Guo, Z. and Ding, G. Graphene/PDMS composite microstructure for pressure sensor application by 3D printing // IOP Conference Series: Materials Science and Engineering. – 2019. – V. 490. – P. 072034.

[24] Li, B., Zhang, Y., Li, T., Yu, H., Guo, Q., Hu, M. and Yang, J. Multilayer graphene/PDMS composite gradient materials for high-efficiency photoresponse actuators // Macromolecular Materials and Engineering. – 2022. – V. 307. – P. 2100868.

[25] Ko, E.-H., Kim, H.-J., Lee, S.-M., Kim, T.-W. and Kim, H.-K. Stretchable Ag electrodes with mechanically tunable optical transmittance on wavy-patterned PDMS substrates // Scientific Reports. – 2017. – V.7. – P. 46739.

[26] Mia, R. and Sultana, S. Fabrication and properties of silver nanowires (AgNWs) functionalized fabric // Applied Sciences. – 2020 г. – V.2. – P. 2052.

[27] Wang, T., Wang, R., Cheng, Y. and Sun, J. Quasi in situ polymerization to fabricate copper nanowire-based stretchable conductor and its applications // ACS Applied Materials & Interfaces. – 2016. – V.8. – P. 9297−04.

[28] Wang, J., Yan, C., Chee, K.J. and Lee, P.S. Highly stretchable and self-deformable alternating current electroluminescent devices // Advanced Materials. – 2015. – V.27 – P. 2876–82.

[29] Wang, L., Xiao, L., Gu, H. and Sun, H. Advances in alternating current electroluminescent devices // Advanced Optical Materials. – 2019. – V.7. – P. 1801154.

[30] Cheng, S. and Zhong, H. What happens when halide perovskites meet with water? // The Journal of Physical Chemistry Letters. – 2022. – V.13. – P. 2281–90.

[31] Dai, X., Messanvi, A., Zhang, H., Durand, C., Eymery, J., Bougerol, C., Julien, F. H. and Tchernycheva, M. Flexible light-emitting diodes based on vertical nitride nanowires // Nano Letters. – 2015. – V.15. – P. 6958–64.

[32] Guan, N., Dai, X., Messanvi, A., Zhang, H., Yan, J., Gautier, E., Bougerol, C., Julien, F. H. and Durand, C. Flexible white light emitting diodes based on nitride nanowires and nanophosphors // ACS Photonics. – 2016. – V.3. – P. 597–603.

[33] Kochetkov, F.M., Neplokh, V., Mastalieva, V.A., Mukhangali, S., Vorob'ev, A.A., Uvarov, A.V., Komissarenko, F.E., Mitin, D.M., Kapoor, A., Eymery, J., Amador-Mendez, N., Durand, C., Krasnikov, D., Nasibulin, A.G., Tchernycheva, M. and Mukhin I.S. Stretchable transparent light-emitting diodes based on ingan/gan quantum well microwires and carbon nanotube films // Nanomaterials. – 2021. – V.11. – P. 1503.

[34] Neplokh, V., Fedorov, V., Mozharov, A., Kochetkov, F., Shugurov, K., Moiseev, E. Amador-Mendez, N., Statsenko, T., Morozova, S., Krasnikov, D., Nasibulin, A.G., Islamova, R.M., Cirlin, G., Tchernycheva, M. and Mukhin, I.S. Red GaPAs/GaP nanowire-based flexible light-emitting diodes // Nanomaterials. – 2021. – V.11. – P. 2549.

[35] Neplokh, V., Kochetkov, F.M., Deriabin, K.V., Fedorov, V.V., Bolshakov, A.D., Eliseev, I.E. Mikhailovskii, V. Yu., Ilatovskii, D.A., Tchernycheva, M., Cirlin, G.E., Nasibulin, A.G., Mukhin, I.S. and Islamova, R.M. Modified silicone rubber for fabrication and contacting of flexible suspended membranes of n-/p-GaP nanowires with a single-walled carbon nanotube transparent contact // Journal of Materials Chemistry C. – 2020. – V.8. – P. 3764–72.

[36] Miroshnichenko, A.S., Neplokh, V., Mukhin, I.S. and Islamova, R.M. Silicone Materials for Flexible Optoelectronic Devices // Materials. – 2022. – V.15. – P. 8731.

[37] SYLGARD™ 184 Silicone Elastomer Kit // www.dow.com.

[38] Cheng, J., Li, M., Cao, Y., Gao, Y., Liu, J. and Sun, F. Synthesis and properties of photopolymerizable bifunctional polyether-modified polysiloxane polyurethane acrylate prepolymer // Journal of Adhesion Science and Technology. – 2016. – V. 30. – P 2–12.

[39] Bao, H., Wu, Y., Liu, J., Hua, X., Lai, G. and Yang, X. Polyester–polysiloxane hyperbranched block polymers for transparent flexible materials // ACS Omega. – 2020. – V. 5. – P. 29513–9.

[40] Masloborodova, E.A., Kaganova, E.V., Gusakova, N.S., Agibalova, L.V., Maretina, E.Yu., Baranets, I.V. and Islamova, R.M. Effect of ferrocene on the synthesis of graft copolymers of vinylpolysiloxane and styrene // Russian Journal of General Chemistry. – 2017. – V.87. – P. 1038–46.

[41] Huang, B., Dai, L., Chen, Z., Zhao, Y., Gao, X., Wang, Q., Xie, Z. and Zhang, Z. Role of in-situ polymethyl-methacrylate in addition type silicone rubber with specific reference to adhesion and damping properties // Journal of Applied Polymer Science. – 2021. – V. 138. – P.50252.

[42] Sugimoto, H., Nishino, G., Koyama, H., Daimatsu, K., Inomata, K. and Nakanishi, E. Preparation and morphology of transparent poly(methyl methacrylate)–poly(dimethylsiloxane) hybrid materials using multifunctional silicone macromonomer // Journal of Applied Polymer Science. – 2012. – V.124. – P. 1316–22.

[43] Gregorio, G.L.D., Giannuzzi, R., Cipolla, M.P., Agosta, R., Grisorio, R., Capodilupo, A., Suranna, G.P., Giglicd, G. and Manca, M. Iodopropyl-branched polysiloxane gel electrolytes with improved ionic conductivity upon cross-linking // Chemical Communications. – 2014. – V.50. – P.13904–6.

[44] Miroshnichenko, A.S., Deriabin, K.V., Baeva, M., Kochetkov, F.M., Neplokh, V., Fedorov, V.V. Mozharov A.M., Koval, O.Yu., Krasnikov, D., Sharov, V.A., Filatov, N.A., Gets, D.S., Nasibulin, A.G., Makarov, S.V., Mukhin, I.S., Kukushkin, V.Yu., and Islamova, R.M. Flexible perovskite CsPbBr3 light emitting devices integrated with gap nanowire arrays in highly transparent and durable functionalized silicones // The Journal of Physical Chemistry Letters. – 2021. – V.12. – P. 9672–6.

[45] Kochetkov, F.M., Neplokh, V., Fedorov, V.V., Bolshakov, A.D., Sharov, V.A., Eliseev, I.E., Tchernycheva, M., Cirlin, G.E., Nasibulin, A.G., Islamova, R.M. and Mukhin, I.S. Fabrication and electrical study of large area free-standing membrane with embedded GaP NWs for flexible devices // Nanotechnology. – 2020. – V. 31. – P. 46LT01.

[46] Jeong, J., Jin, D.K., Choi, J., Jang, J., Kang, B.K., Wang, Q., Park, W.I., Jeong, M.S., Bae, B.-S., Yang, W.S., Kim, M.J. and Hong, Y.J. Transferable, flexible white light-emitting diodes of GaN p–n junction microcrystals fabricated by remote epitaxy // Nano Energy. – 2021. – V. 86. – P. 106075.

[47] Dong, J., Liu, Z., Feng, Y. and Zheng, C. Preparation, morphology, and mechanical properties of elastomers based on α,ω-dihydroxy-polydimethylsiloxane/poly(methyl

methacrylate) blends // Journal of Applied Polymer Science. – 2006. – V. 100. – P. 1547–53.

[48] Cheng, J., Cao, Y., Jiang, S., Gao, Y., Nie, J. and Sun, F. Synthesis and Performances of UV-Curable Polysiloxane–Polyether Block Polyurethane Acrylates for PVC Leather Finishing Agents // Industrial & Engineering Chemistry Research. – 2015. – V. 54. – P. 5635–42.

[49] Rao, Y.-L., Chortos, A., Pfattner, R., Lissel, F., Chiu, Y.-C., Feig, V., Xu, J., Kurosawa, T., Gu, X., Wang, C., He, M., Chung, J.W. and Bao, Z. Stretchable self-healing polymeric dielectrics cross-linked through metal–ligand coordination // Journal of the American Chemical Society. – 2016. – V. 138. – P 6020–7.

[50] Yu, D., Zhao, X., Zhou, C., Zhang, C. and Zhao, S. Room temperature self-healing methyl phenyl silicone rubbers based on the metal-ligand cross-link: synthesis and characterization // Macromolecular Chemistry and Physics. – 2017. – V. 218. – P. 1600519.

[51] Deriabin, K.V., Ignatova, N.A., Kirichenko, S.O., Novikov, A.S. and Islamova, R.M. Nickel(II)-pyridinedicarboxamide-co-polydimethylsiloxane complexes as elastic self-healing silicone materials with reversible coordination // Polymer. – 2021. – V. 212. – P. 123119.

[52] Deriabin, K.V., Ignatova, N.A., Kirichenko, S.O., Novikov, A.S., Kryukova, M.A., Kukushkin, V.Yu. and Islamova, R.M. Structural features of polymer ligand environments dramatically affect the mechanical and room-temperature self-healing properties of cobalt(II)-incorporating polysiloxanes // Organometallics. – 2021. – V. 40. – P. 2750–60.

[53] Tang, M., Li, Z., Wang, K., Jiang, Y., Tian, M., Qin, Y. Gong, Ye., Li, Z. and Wu, L. Ultrafast self-healing and self-adhesive polysiloxane towards reconfigurable on-skin electronics // Journal of Materials Chemistry A. – 2022. – V. 10. – P. 1750–9

[54] Wang, S. and Urban, M.W. Self-healing polymers // Nature Reviews Materials. – 2020. – V. 5. – P. 562–83.

[55] Schäfer, S. and Kickelbick, G. Self-healing polymer nanocomposites based on Diels-Alder-reactions with silica nanoparticles: the role of the polymer matrix // Polymer. – 2015. – V. 69. – P. 357–68.

[56] Fu, G., Yuan, L., Liang, G. and Gu, A. Heat-resistant polyurethane films with great electrostatic dissipation capacity and very high thermally reversible self-healing efficiency based on multi-furan and liquid multi-maleimide polymers // Journal of Materials Chemistry A. – 2016. – V. 4. – P. 4232–41.

[57] Gou, Z., Zuo, Y. and Feng, S. Thermally self-healing silicone-based networks with potential application in recycling adhesives // RSC Advances. – 2016. – V. 6. – P. 73140–7.

[58] Jo, Y.Y., Lee, A.S., Baek, K.-Y., Lee, H. and Hwang, S.S. Thermally reversible self-healing polysilsesquioxane structure-property relationships based on Diels-Alder chemistry // Polymer. – 2017. – V. 108. – P. 58–65.

[59] Jo, Y.Y., Lee, A.S., Baek, K.-Y., Lee, H. and Hwang, S.S. Multi-crosslinkable self-healing polysilsesquioxanes for the smart recovery of anti-scratch properties // Polymer. – 2017. – V. 124. – P. 78–87.

[60] Nasresfahani, A. and Zelisko, P.M. Synthesis of a self-healing siloxane-based elastomer cross-linked via a furan-modified polyhedral oligomeric silsesquioxane: investigation of a thermally reversible silicon-based cross-link // Polymer Chemistry. – 2017. – V. 8. – P. 2942–52.

[61] Zuo, Y., Gou, Z., Zhang, C. and Feng, S. Polysiloxane-based autonomic self-healing elastomers obtained through dynamic boronic ester bonds prepared by thiol-ene “click” chemistry // Macromolecular Rapid Communications. – 2016. – V. 37. – P. 1052–9.

[62] Zhang, B., Zhang, P., Zhang, H., Yan, C., Zheng, Z., Wu, B. and Yu, Y. A Transparent, highly stretchable, autonomous self-healing poly(dimethylsiloxane) elastomer // Macromolecular Rapid Communications. – 2017. – V. 38. – P. 1700110.

[63] Lv, C., Zhao, K. and Zheng, J. A. Highly Stretchable self-healing poly(dimethylsiloxane) elastomer with reprocessability and degradability // Macromolecular Rapid Communications. – 2018. – V. 39. – P. 1700686.

[64] Wu, X., Li, J., Li, G., Ling, L., Zhang, G., Sun, R. and Wong, C.-P. Heat-triggered poly(siloxane-urethane)s based on disulfide bonds for self-healing application // Journal of Applied Polymer Science. – 2018. – V. 135. – P. 46532.

[65] Li, C.-H., Wang, C., Keplinger, C., Zuo, J.-L., Jin, L., Sun, Y., Zheng, P., Cao, Yi., Lissel, F., Linder, C., You, X.-Z. and Bao, Z. A highly stretchable autonomous self-healing elastomer // Nature Chemistry. – 2016. – V. 8. – P. 618–24.

[66] Deriabin, K.V., Filippova, S.S. and Islamova, R.M. Self-Healing Silicone Materials: Looking Back and Moving Forward // Biomimetics. – 2023. – V. 8. –P. 286.

[67] Dobrynin, M.V., Sokolova, E.V., Kinzhalov, M.A., Smirnov, A.S., Starova, G.L., Kukushkin, V.Yu. and Islamova, R.M. Cyclometalated platinum(II) complexes simultaneously catalyze the cross-linking of polysiloxanes and function as luminophores // ACS Applied Polymer Materials. – 2021. – V. 3. – P. 857–66.

[68] Wang, X.-F., Wang, G.-G., Li, J.-B., Liu, Z., Zhao, W.-F.and Han, J.-C. Towards high-powered remote WLED based on flexible white-luminescent polymer composite films containing S, N co-doped graphene quantum dots // Chemical Engineering Journal. – 2018. – V. 336. – P. 406–15.

[69] Kovalchuk, A., Huang, K., Xiang, C., Martí, A.A. and Tour, J.M. Luminescent polymer composite films containing coal-derived graphene quantum dots // ACS Applied Materials & Interfaces. – 2015. – V. 7. – P. 26063–8.

[70] Saidzhonov, B.M., Zaytsev, V.B. and Vasiliev, R.B. Effect of PMMA polymer matrix on optical properties of CdSe nanoplatelets // Journal of Luminescence. – 2021. – V. 237. – P. 118175.

[71] Hu, M., Shu, Y., Kirillov, A., Liu, W., Yang, L. and Dou, W. Epoxy functional composites based on lanthanide metal–organic frameworks for luminescent polymer materials // ACS Applied Materials & Interfaces. – 2021. – V.13 – P. 7625–34.

[72] Kim, Y., Jang, G., Kim, D., Kim, J. and Lee, T.S. Fluorescence sensing of glucose using glucose oxidase incorporated into a fluorophore-containing PNIPAM hydrogel // Polymer Chemistry. – 2016. – V.7 – P. 1907–12.

[73] Calvino, C., Sagara, Y., Buclin, V., Haehnel, A.P., del Prado, A., Aeby, Yoan, C., Simon, C., Schrettl, S., and Weder, C. Mechanoresponsive, luminescent polymer blends based on an excimer-forming telechelic macromolecule // Macromolecular Rapid Communications. – 2019. – V.40 – P. 1800705.

[74] de Jesus, F.A., Santana, B.V., Bispo, G.F. da C., Filho, C.I. da S., Júnior, S.A., Valério, M.E.G., Caiut, G.M.A., Hugo, V., and Sarmento, V. Fine tuning of polymer content for enhanced structure and luminescent properties of Eu3+:siloxane–poly(methyl methacrylate) hybrids to be applied in photonics // Polymer. – 2019. – V. 181 – P. 121767.

[75] Jiang, L., Li, J., Xia, D., Gao, M., Li, W., Fu, D.-Y., Zhao, S. and Li, G. Lanthanide Polyoxometalate Based Water-Jet Film with Reversible Luminescent Switching for Rewritable Security Printing // ACS Applied Materials & Interfaces. – 2021. – V. 13. – P. 49462–71.

[76] Zhao, S., Gao, M. and Li, J. Lanthanides-based luminescent hydrogels applied as luminescent inks for anti-counterfeiting // Journal of Luminescence. – 2021. – V. 236.–P. 118128.

[77] Manzani, D., Nigoghossian, K., Iastrensk, M.F., Coelho, G.R., dos Santos, M.V., Maia, L.J.Q., Ribeiro, S.J.L. and Segatelli, M.G. Luminescent silicone materials containing Eu $^{3+}$ -complexes for photonic applications // Journal of Materials Chemistry C. – 2018. – V. 6 – P. 8258–65.

[78] Dobrynin, M.V., Kasatkina, S.O., Baykov, S.V., Savko, P.Y., Antonov, N.S., Mikherdov, A.S. и др. Deprotonated diaminocarbene platinum complexes for thermoresponsive luminescent silicone materials: both catalysts and luminophores // Dalton Transactions. – 2021 г. – The Royal Society of Chemistry. – V. 50. – P. 14994–9.

[79] Baranovskii, E.M., Khistiaeva, V.V., Deriabin, K.V., Petrovskii, S.K., Koshevoy, I.O., Kolesnikov, I.E., Grachova, E.V. and Islamova, R.M. Re(I) complexes as backbone substituents and cross-linking agents for hybrid luminescent polysiloxanes and silicone rubbers // Molecules. – 2021. – V. 26. – P. 6866.

[80] Bünzli, J.-C.G. and Eliseeva, S.V. Intriguing aspects of lanthanide luminescence // Chemical Science. – 2013. – V. 4 –P. 1939.

[81] Zhang, Y., Zuo, Y., Yang, T., Gou, Z. and Lin, W. Polysiloxane-based hyperbranched fluorescent materials prepared by thiol-ene “click” chemistry as potential cellular imaging polymers // European Polymer Journal. – 2019. – V. 112 – P. 515–23.

[82] Bünzli, J.-C.G. Benefiting from the unique properties of lanthanide ions // Accounts of Chemical Research. – 2006. – V. 39 – P. 53–61.

[83] Zhao, D., Yang, J., Tian, X., Wei, J., Li, Q. и Wang, Y. Self-healing metallo-supramolecular polymers showing luminescence off/on switching based on lanthanide ions and terpyridine moieties // Chemical Engineering Journal. – 2022. – V. 434. –P. 134806.

[84] Soheyli, E., Zargoush, S., Yazici, A.F., Sahraei, R. and Mutlugun, E. Highly luminescent ZnCdTeS nanocrystals with wide spectral tunability for efficient color-conversion white-light-emitting-diodes // Journal of Physics D: Applied Physics. – 2021. – V. 54. – C. 505110.

[85] Li, G., Qiu, Z., Wang, Y., Hong, Y., Wan, Y., Zhang, J., Yang, J., Wu, Z., Hong, W. and Guo, C.F. PEDOT:PSS/grafted-PDMS electrodes for fully organic and intrinsically stretchable skin-like electronics // ACS Applied Materials & Interfaces. – 2019. – V. 11. – P. 10373–9.

[86] Pionteck, J. and Wypych, G. Handbook of antistatics. 2 issue. // ChemTec Publishing, 2016. – 496 p.

[87] Hogan, T.E., Hergenrother, W.L. and DeTrano, M. Electrical conductivity of silica-filled rubber compositions using alkali metal salts dissolved in poly(alkylene oxide) compounds // patent US6399692B2, 2002.

[88] Fujiki, H., Matsubayashi, S., Kanto, K. and Suzuki, T. Curable antistatic organopolysiloxane composition and antistatic silicone film // patent US20150348670A1, 2015.

[89] Deriabin, K.V., Kirichenko, S.O., Lopachev, A.V., Sysoev, Y., Musienko, P.E. and Islamova, R.M. Ferrocenyl-containing silicone nanocomposites as materials for neuronal interfaces // Composites Part B: Engineering. – 2022. – V. 236. –P. 109838.

[90] Yin, H., Zhu, Y., Youssef, K., Yu, Z. and Pei, Q. Structures and Materials in Stretchable Electroluminescent Devices // Advanced Materials. – 2022. – V. 34. –P. 2106184.

[91] Liu, H.-S., Pan, B.-C. and Liou, G.-S. Highly transparent AgNW/PDMS stretchable electrodes for elastomeric electrochromic devices // Nanoscale. – 2017. – V. 9. –P. 2633–9.

[92] Amjadi, M., Pichitpajongkit, A., Ryu, S. and Park, I. Piezoresistivity of Ag NWs-PDMS nanocomposite // Proceedings of the IEEE International Conference on Micro Electro Mechanical Systems (MEMS) – 2014. –P.785–8.

[93] Zhang, B., Li, W., Yang, Y., Chen, C., Li, C.-F. and Suganuma, K. Fully embedded CuNWs/PDMS conductor with high oxidation resistance and high conductivity for stretchable electronics // Journal of Materials Science. – 2019. – V. 54. –P.6381–92.

[94] Huang, Q., Evmenenko, G.A., Dutta, P., Lee, P., Armstrong, N.R. and Marks, T.J. Covalently bound hole-injecting nanostructures. systematics of molecular architecture, thickness, saturation, and electron-blocking characteristics on organic light-emitting diode luminance, turn-on voltage, and quantum efficiency // Journal of the American Chemical Society. – 2005. – V. 127. –P. 10227–42.

[95] Kwak, S.-Y., Yang, S., Kim, N.R., Kim, J.H. and Bae, B.-S. Thermally stable, dye-bridged nanohybrid-based white light-emitting diodes // Advanced Materials. – 2011. – V. 6.–P. 5767–72.

[96] Zhao, Y., Wang, B., Hojaiji, H., Wang, Z., Lin, S., Yeung, C., Lin, H., Nguyen, P., Chiu, K., Salahi, K., Cheng, X., Tan, J., Cerrillos, B.A. and Emaminejad, S. A wearable freestanding electrochemical sensing system // Science Advances. – 2020. – V. 6. –P. eaaz0007.

[97] Hammock, M.L., Chortos, A., Tee, B.C.-K., Tok, J.B.-H. and Bao, Z. 25th anniversary article: the evolution of electronic skin (e-skin): a brief history, design considerations, and recent progress // Advanced Materials. – 2013. – V. 25. –P. 5997–6038.

[98] Nayeem, M.O.G., Lee, S., Jin, H., Matsuhisa, N., Jinno, H., Miyamoto, A., Yokata, T. and Someya, T. All-nanofiber–based, ultrasensitive, gas-permeable mechanoacoustic sensors for continuous long-term heart monitoring // Proceedings of the National Academy of Sciences. – 2020. – V. 117. –P.7063–70.

[99] Qu, C., Xu, Y., Xiao, Y., Zhang, S., Liu, H. and Song, G. Multifunctional displays and sensing platforms for the future: a review on flexible alternating current electroluminescence devices // ACS Applied Electronic Materials. – 2021. – V. 3. – P. 5188–210.

[100] Cho, S.H., Lee, S.W., Hwang, I., Kim, J.S., Jeong, B., Kang, H.S., Kim, E.H., Kim, K.L., Park, C. and Park, Ch. Shape-deformable self-healing electroluminescence displays // Advanced Optical Materials. – 2019. – V. 7. –P. 1801283.

[101] Chou, H.-H., Nguyen, A., Chortos, A., To, J.W.F., Lu, C., Mei, J., Kurosawa, T., Bae, W.-G., Tok, J.B.-H. and Bao, Z. A chameleon-inspired stretchable electronic skin with interactive colour changing controlled by tactile sensing // Nature Communications. – 2015. – V. 6. –P. 8011.

[102] Shi, X., Zuo, Y., Zhai, P., Shen, J., Yang, Y., Gao, Z., Liao, M., Wu, J., Wang, J., Xu, X., Tong, Q., Zhang, B., Wang, B., Sun, X., Zhang, L., Pei, Q., and Jin, D. Large-area display textiles integrated with functional systems // Nature. – 2021. – V. 591. –P. 240–5.

[103] Shin, H., Sharma, B.K., Lee, S.W., Lee, J.-B., Choi, M., Hu, L., Park, Ch., Choi, J.H., and Kim, T.-W. Stretchable electroluminescent display enabled by graphene-based hybrid electrode // ACS Applied Materials & Interfaces. – 2019. – V. 11. – P. 14222–8.

[104] Wager, J.F. and Keir, P.D. Electrical characterization of thin-film electroluminescent devices // Annual Review of Materials Science. – 1997. – V. 27. –P. 223–48.

[105] Neplokh, V., Messanvi, A., Zhang, H., Julien, F.H., Babichev, A., Eymery, J., Durand, C. and Tchernycheva, M. Substrate-free InGaN/GaN nanowire light-emitting diodes // Nanoscale Research Letters. – 2015. – V. 10. –P. 447.

[106] Miroshnichenko, A.S., Deriabin, K.V., Baranov, A.I., Neplokh, V., Mitin, D.M., Kolesnikov, I.E., Dobrynin, M.V., Parshina, E.K., Islamova, R.M. and Mukhin, I.S. Lanthanide(III)-incorporating polysiloxanes as materials for light-emitting devices // ACS Applied Polymer Materials. – 2022. – V. 4. –P. 2683–90.

[107] Clarson, S.J. Bogdan Marciniec, Hydrosilylation: A Comprehensive Review on Recent Advances // Silicon. – 2009 г. – V. 1. –P. 57–8.

[108] Deriabin, K.V., Lobanovskaia, E.K., Novikov, A.S. and Islamova, R.M. Platinum-catalyzed reactions between Si–H groups as a new method for cross-linking of silicones // Organic & Biomolecular Chemistry. – 2019. – V. 17. –P. 5545–9.

[109] Deriabin, K.V., Lobanovskaia, E.K., Kirichenko, S.O., Barshutina, M.N., Musienko, P.E. and Islamova, R.M. Synthesis of ferrocenyl-containing silicone rubbers via platinum-catalyzed Si–H self-cross-linking // Applied Organometallic Chemistry. – 2020. – V. 34. –P. e5300.

[110] Miroshnichenko, A.S., Deriabin, K.V., Mukhin, I.S. and Islamova, R.M. Low-adhesive silicone rubbers for flexible light-emitting devices // St. Petersburg State Polytechnical University Journal. Physics and Mathematics. 2022. – V. 15. –P. 320–325.

[111] Borók, A., Laboda, K. and Bonyár, A. PDMS bonding technologies for microfluidic applications: a review // Biosensors. – 2021. – V. 11. –P. 292.

[112] Sperling, L.H. Introduction to Physical Polymer Science. 1th ed. //Wiley, USA, 2005. – 878 p.

[113] Delebecq, E., Hamdani-Devarennes, S., Raeke, J., Lopez Cuesta, J.-M. and Ganachaud, F. High Residue Contents Indebted by Platinum and Silica Synergistic Action during the Pyrolysis of Silicone Formulations // ACS Applied Materials & Interfaces. – 2011. – V. 3. –P. 869–80.

[114] Deriabin, K.V., Yaremenko, I.A., Chislov, M.V., Fleury, F., Terent'ev, A.O. and Islamova, R.M. Similar nature leads to improved properties: cyclic organosilicon triperoxides as promising curing agents for liquid polysiloxanes // New Journal of Chemistry. – 2018. – V. 42. –P. 15006–13.

[115] Islamova, R.M., Dobrynin, M.V., Vlasov, A.V., Eremina, A.A., Kinzhalov, M.A., Kolesnikov, I.E., Zolotarev, A.A., Masloborodova, E.A., and Luzyanin, K.V. Iridium(III)-catalysed cross-linking of polysiloxanes leading to the thermally resistant luminescent silicone rubbers // Catalysis Science & Technology. – 2017. – V. 7. –P. 5843–6.

[116] Fedorov, V.V., Koval, O.Yu., Ryabov, D.R., Fedina, S.V., Eliseev, I.E., Kirilenko, D.A., Pidgayko, D.A., Bogdanov, A., Zadiranov, Yu.M., Goltaev, A.S., Ermolaev, Georgy, A.A., Arsenin, A.V., Makarov, S.V., Samusev, A.K., Volkov, V.S. and Mukhin, I.S. Nanoscale Gallium Phosphide Epilayers on Sapphire for Low-Loss Visible Nanophotonics // ACS Applied Nano Materials. – 2022. – V. 5. –P. 8846–58.

[117] Mitin, D., Berdnikov, Y., Vorobyev, A., Mozharov, A., Raudik, S., Koval, O., Neplokh, V., Moiseev, E., Ilatovskii, D., Nasibulin, A.G. and Mukhin, I.S. Optimization of Optoelectronic Properties of Patterned Single-Walled Carbon Nanotube Films // ACS Applied Materials and Interfaces. – 2020. – V. 12. –P. 55141–7.

[118] Sharma, D.K., Hirata, S. and Vacha, M. Single-particle electroluminescence of CsPbBr3 perovskite nanocrystals reveals particle-selective recombination and blinking as key efficiency factors // Nature Communications. – 2019. – V. 10. –P. 1–5.

[119] Mannino, G., Deretzis, I., Smecca, E., La Magna, A., Alberti, A., Ceratti, D and Cahen, D. Temperature-dependent optical band gap in CsPbBr3, MAPbBr3, and FAPbBr3 single crystals // Journal of Physical Chemistry Letters. – 2020. – V. 11. –P. 2490–6.

[120] Miroshnichenko, A.S., Deriabin, K.V., Rashevskii, A.A., Suslonov, V.V., Novikov, A.S., Mukhin, I.S. and Islamova, R.M. Structural features of Eu3+ and Tb3+-bipyridinedicarboxamide complexes // Polymers. – 2022. – V. 14. –P. 5540.

[121] Pilmé, J., Renault, E., Bassal, F., Amaouch, M., Montavon, G. and Galland, N. QTAIM analysis in the context of quasirelativistic quantum calculations // Journal of Chemical Theory and Computation. – 2014. – V. 10. –P. 4830–41.

[122] Zhang, F., Ju, P., Pan, M., Zhang, D., Huang, Y., Li, G. и and Li. X. Self-healing mechanisms in smart protective coatings: A review // Corrosion Science. – 2018. – V. 144. –P. 74–88.

[123] Wang, X., Bodunov, E.N. and Nau, W.M. Fluorescence quenching kinetics in short polymer chains: Dependence on chain length // Optics and Spectroscopy. – 2003. – V. 95. –P. 560–70.

[124] Grenier, V., Finot, S., Valera, L., Eymery, J., Jacopin, G. and Durand, C. UV-A to UV-B electroluminescence of core-shell GaN/AlGaN wire heterostructures // Applied Physics Letters. – 2022. – V. 121. –P. 131102.

[125] Sheldrick, G.M. Crystal structure refinement with SHELXL // Acta Crystallographica Section C Structural Chemistry. – 2015. – V. 71. –P. 3–8.

[126] Dolomanov, O.V., Bourhis, L.J., Gildea, R.J., Howard, J.A.K. and Puschmann, H. OLEX2: a complete structure solution, refinement and analysis program // Journal of Applied Crystallography. – 2009. – V. 42. –P. 339–41.

[127] Mark, J.E. The Polymer Data Handbook. Second Edition. // Oxford University Press, Oxford. 2009. – 1294 p.

[128] Rodinkov, O.V., Bokach, N.A. and Bulatov, A.V. Fundamentals of metrology of physical and chemical measurements and chemical analysis: textbook // VVM Publishing House, St. Petersburg. 2010. – 136 p.

[129] Zhukov, V.K. Theory of errors in technical measurements: a textbook // Publishing house of the Tomsk Polytechnic University, Tomsk. 2009. – 180 p.